The Mount Manengouba, a complex volcano of the Cameroon Line: Volcanic history, petrological and geochemical features

André Pouclet, Armand Kagou Dongmo, Jacques-Marie Bardintzeff, Pierre Wandji, Pulchérie Chakam Tagheu, D. Nkouathio, Hervé Bellon, Gilles Ruffet

The Mount Manengouba, a complex volcano of the Cameroon Line: Volcanic history, petrological and geochemical features

André Pouclet[a,*], Armand Kagou Dongmo[b], Jacques-Marie Bardintzeff[c], Pierre Wandji[d], Pulchérie Chakam Tagheu[e], David Nkouathio[b], Hervé Bellon[f], Gilles Ruffet[g]

[a] *1383, rue de la Source, 45160 Olivet, France , retired of the "Institut des Sciences de la Terre de l'Université d'Orléans", Orléans, France*

[b] *Department of Earth Sciences, University of Dschang, BP 67, Dschang, Cameroon*

[c] *Laboratory of Petrography-Volcanology and Planetology Team, UMR IDES 8148 CNRS, University of Paris-Sud, 91405 Orsay Cedex, France and ESPE, University of Cergy-Pontoise, 95000 Cergy-Pontoise, France*

[d] *Laboratory of Geology, Ecole Normale Supérieure, University of Yaounde-1, BP 47, Yaoundé, Cameroon*

[e] *Department of Earth Sciences, University of Yaoundé-1, BP 812, Yaoundé, Cameroon*

[f] *Laboratory of Geochronology, University of Bretagne Occidentale, CS 93637, 29238 Brest Cedex 3, France*

[g] *CNRS (CNRS/INSU) UMR 6118, Géosciences Rennes, 35042 Rennes Cedex, and Université de Rennes I, Géosciences Rennes, 35042 Rennes Cedex, France*

* Corresponding author.

E-mail address: andre.pouclet@sfr.fr

Keywords: Cameroon Volcanic Line, Manengouba volcano, alkaline magmatism, Quaternary volcanism, K/Ar and $^{40}Ar/^{39}Ar$ age dating, Caldera collapse, Olivine and pyroxene thermobarometry, Sr- Nd- Pb-isotopes, Mantle source components

ABSTRACT

The volcanic story of Mount Manengouba is related to four chronological stages: 1) forming of the early Manengouba shield volcano between 1.55 and 0.94 Ma, 2) building of the Eboga strato-cone between 0.94 and 0.89 Ma, 3) caldera collapse and silicic extrusions of the

Elengoum Complex between 0.89 and 0.70 Ma, and 4) intra-caldera and flank activity between 0.45 and 0.11 Ma. The volume of the volcano is calculated at 320 km^3 ± 5%. The volcanic rocks are attributed to two magmatic outputs. The first and main magma generation produced the shield volcano, the strato-cone, and the syn- to post-caldera extrusions, displaying a complete series from basanites to trachytes (magmatic Group 1). The second magma generation is limited to the late and flank activity evolving from basanites to trachy-phonolite (magmatic Group 2). Both magmatic groups belong to the under-saturated alkaline sodic series. Petrological calculations locate the magmatic reservoir between 37 and 39 km in the upper mantle for the Group 1 lavas, and between 42 and 44 km for the Group 2 lavas. Trachytes were generated in a secondary crustal reservoir. Magmatic series evolve with medium to low pressure fractional crystallization of olivine, pyroxene, oxides, feldspar, and apatite. Significant crustal assimilation is evidenced in trachytes. The magma of Group 1 was generated with 3 to 6% of partial melting of a moderately enriched source containing 3 to 7% of garnet. Melting took place in the spinel to garnet transition zone located at 70 to 90 km and around 25 kb. The magma of Group 2 resulted from a slightly higher partial melting from a less garnet-rich source that indicates uprising of the melting column in the upper part of transition zone. Sr, Nd, and Pb isotope data of the Manengouba rocks and neighbouring lavas are analyzed and compared with those of the mafic lavas of the CVL. Three source components are distinguished: a depleted component originated from the asthenospheric swell, a radiogenic component linked to the contaminated lithosphere of the Neoproterozoic mobile belt, and an enriched component or the lithosphere possibly related to pre-rifting magmatic processes.

1. Introduction

Mount Manengouba is one of the great continental volcanoes of the Cameroon Line, consisting of the Mts Cameroon, Bambouto, Bamenda, and Oku (**Fig. 1**). The Cameroon Line is a transtensional passive rift, showing an alternation of volcanic horsts and grabens (Moreau et al., 1987; Meyers et al., 1988; Déruelle et al., 2007). Tectonic extension caused lithospheric thinning, asthenospheric upwelling and the formation of a magmatic hot line, trending N30°E. An important volcanic activity took place along the Line, from the Eocene to recent times (Déruelle et al., 1991). Present activity is restricted to Mount Cameroon (Wandji et al., 2009) and Bioko Island, but numerous Quaternary eruptions have occurred in the volcanic areas of Tombel, Manengouba, Bambouto, Noun, and Oku (Déruelle et al., 1991, 2000; Kagou

Dongmo et al., 2001; Nkouathio et al., 2002; Suh et al., 2003; Itiga et al., 2004; Wotchoko et al., 2005; Kagou Dongmo et al., 2010).

The Mount Manengouba is located 120 km north-east of Mount Cameroon, between 09°42' to 10°10' E, and 4°49' to 5°15' N (**Fig. 2**). It mainly consists of a shield volcano overlain by a stratovolcano that culminates at 2411 m and covers 500 km^2. It is set up on a volcano-tectonic height trending N30°E above the uplifted granite basement and crosscut by N 0°, N 30° to 50°E and N 140°E faults. Along this height, there is an alternation of horst and graben structures. The Manengouba volcano emplaced at the northern end of the Tombel graben in the sedimentary Manjo and Mbo plains limited by two N 30°E trending normal faults: the Tombel Fault to the west and the Nlonako Fault to the east (Fig. 1B).

Since Gouhier et al. (1974), Tchoua (1974), Dunlop (1983), and Fitton and Dunlop (1985), a volcanological pattern has been assumed for the Manengouba building. The Mount Manengouba was built between 1.55 Ma and 0 Ma during three stages (Kagou Dongmo, 1998, 2006; Kagou Dongmo et al., 2001). The first stage, from 1.55 to 0.7 Ma, corresponds to the formation of a basaltic shield volcano evolving to a stratovolcano named Elengoum, which was capped by trachyte domes and flows. The second stage, between 0.7 and 0.56 Ma, points to the collapse of the Elengoum summit that created a large caldera which opened to the west. The third stage, from 0.56 Ma to recent time, includes the building-up of a new stratovolcano named Eboga inside the caldera. Then the collapse of the Eboga summit formed the Eboga caldera enclosed in the former caldera of Elengoum. Finally, since 0.48 Ma, numerous flank eruptions, mainly basaltic, supplied lava flows on the Manengouba slopes. The volcanic rocks belong to the alkaline sodic series, evolving from basanite to trachyte.

Conducting new mapping, we established geological contradictions with the commonly accepted history of the volcanic activity. New sample analyses were done and new ages were obtained by K/Ar and $^{40}Ar/^{39}Ar$ methods. These data led to a complete revision of the conventional Manengouba history. Petrological and magmatic features are documented from mineral and chemical analyses. Trace elements and Sr, Nd, and Pb isotopes are used to constrain the magma source composition.

2. The Manengouba volcano, reappraisal of the volcanic history

The geological pattern of the volcano has been reviewed. A new map is drawn, using recent aerial photographs, suitable satellite imagery and field work surveys. The reduced map is given on Figure 2 and detailed on **Figures 3 and 4**.

102

103 *2.1. The pre-Manengouba formations*

104 The lavas of the basal shield volcano overflowed the Cretaceous and Quaternary lacustrine
105 and fluvial sediments of the northern end of the Tombel Graben. The Precambrian granite
106 basement is exposed on the SW, S, E, and NE sides. The south-eastern border was intruded by
107 a small syenite intrusion and associated rocks, the Mount Nlonako (Fig. 2), in middle Eocene
108 between 43-46 Ma according to K-Ar age geochronology by Tchoua (1974) and Cantagrel et
109 al. (1978). A similar intrusion, the Mount Koupé took place to the south-west of the
110 Manengouba area (Fig. 1) and is dated at 53 Ma (Rb/Sr isotopic age in Lamilen, 1989). These
111 intrusions belong to the Cretaceous to Eocene alkaline complex alignment from the Gulf of
112 Guinea to the Lake Chad and betray the initial magmatic activity of the Cameroon tectonic
113 line (Moreau et al., 1987; Déruelle et al., 1991). The north-western area exhibits thick
114 ignimbritic flows and abundant extrusive domes of phonolite and trachyte that built Mounts
115 Bakossi and Ekomane on both sides of the Bangem breach. Similar lavas are disseminated as
116 small outcrops to the north and south of the Manengouba area. Previous dating of a trachyte
117 dome of Ekomane yields a Middle Miocene age (Dunlop, 1983). These volcanic products can
118 be related to the Miocene acidic activity of Mount Bambouto, north of Mount Manengouba
119 (Youmen et al., 2005; Kagou Dongmo et al., 2010). A noticeable sight of this work is the
120 discovery of old mafic lavas preserved along the western base of the Nlonako hill by means of
121 tectonic uplift. The first flows of Manengouba came into contact with these pre-Manengouba
122 lavas while the youngest flows from flank cones covered some parts of them. These later
123 young lavas include 5 to 10 cm sized angular xenoliths of the old mafic lavas, indicating that
124 these old lavas are set beneath Mount Manengouba. A new age dating is provided.

125

126 *2.2. The Manengouba formations*

127 Taking into account the piling up of different volcanic formations of Mount Manengouba,
128 we distinguished four main chronological units and formational stages from the early shield
129 volcano to the late flank lavas.

130

131 1) The early Manengouba shield volcano

132 The oldest lavas crop out all around the main building on the middle and low slopes. They
133 consist of stacked lava flows of ankaramite, basalt and hawaiite. Spectacular stacking of these
134 lavas can be seen in the canyon of the Nkam river, at the Ekom Nkam water fall, north-east of
135 the Manengouba field (Fig. 2). These lavas belong to a large shield volcano that was the

primary Manengouba building. They are capped by more evolved lavas of the upper volcanic edifice and overlain by numerous parasitic cones and their lava flows.

2) The Eboga stratovolcano

The upper mountain is a stratovolcano named Eboga and made of alternating, more evolved lavas flows and pyroclastic deposits. The lava composition is dominated by mugearites though hawaiites and benmoreites also occur. The northern and north-eastern upper flanks are covered by benmoreite flows. The summit of the edifice collapsed in a roughly circular caldera, averaging 4 km in diameter (Fig. 3). An arc-shaped scarp to the north-eastern upper slope is attributed to this collapse event and not to a former caldera because the scarp plan crosscut the Eboga flows that have outpoured from the initial crater. The caldera was filled with basaltic flows contemporaneously with the late flank volcanic activity until its north-western breach. Thus, the extent of the sinking event is unknown as well as the height of the initial crater rim. The present day height of the caldera wall reaches 200 m.

The formation of the Eboga cone is the continuation of the activity of the early shield volcano assuming a magmatic evolution from fluid mafic lavas to more viscous differentiated lavas.

3) The Elengoum Extrusive Complex

The Eboga south-eastern upper slope is overlapped by thick trachyte pyroclastic flows and benmoreite to trachyte domes which constitute the Elengoum Extrusive Complex (EEC). Numerous bodies of similar composition extruded the summit part of the Eboga, and particularly the caldera wall in using the circular faults of the caldera and the north-eastern arc-shaped fault (Fig. 3). Consequently it is obvious that the formation of the EEC postdates the formation of the Eboga cone. Definitely, the Elengoum cannot be attributed to a pre-Eboga volcanic stage. One may assume that the Elengoum trachytic lava withdrawal of the magma chamber was linked to the Eboga caldera collapse. The tectonic location of the EEC is controlled by the major SW-NE trending fracture system (Fig. 2).

A singular acidic dome, the Ekom rhyolite extrusion, seems to intrude the basalt flows of the early Manengouba shield at the north-eastern lower slope. The meaning of this activity is questionable.

4) Flank cones and flows

All around the main cone but also on the upper flanks and inside the caldera, ca. one hundred parasitic and monogenetic cones are set up along short fractures, mainly trending SW-NE and WSW-ENE. The cones resulted from common strombolian activities and supplied lava flows of one to ten kilometres in length. In addition, three maar volcanoes are pointed out: one on the eastern upper flank and two inside the caldera (DS, LF and LH in Figure 3). The intra-caldera maars were emplaced along a SW-NE fracture, formerly used by the C2 strombolian cone, and two trachytic extrusions of the caldera wall. Indeed, they postdate the two strombolian cones C1 and C2, because their volcaniclastic debris covered the cones. In addition, a plug-dome named Mboriko extruded the caldera floor along a short SSW-NNE fracture. A significant amount of cones took place in the eastern upper slope, namely the supra-caldera strombolian volcanic complex (SCSV, Fig. 3) and the strombolian cone set above the caldera edge that is the summit of Mount Manengouba at 2,411 m. Most of the lavas are basanites and hawaiites, whilst mugearites are also common.

Assuming that Mount Manengouba rests above the granitic substratum that crops out to the west, south, and east, the total volume of the volcano is calculated at 320 km^3 ± 5%.

On the base of the features of volcanic activities, the mafic to evolved lavas of the early shield volcano (Eboga volcano and Elengoum Complex) may belong to a single magmatic series. In return, the activity of flank cones requires a new magma supply. Compared to the volcano main building (stages 1 to 3), the volume of late flank lavas (stage 4) is very weak and estimated between 1.5 to 2 km^3.

3. Chronological data

A total of eight lavas are dated by the K/Ar method and six by the $^{40}Ar/^{39}Ar$ method (**Table 1**). All these new age data as well as the previous ones are located on Figures 2, 3, and 4. The $^{40}Ar/^{39}Ar$ plateau ages are plotted in **Figure 5**. The complete available geochronological data for the Manengouba area are given in **Table 2**.

The oldest ages are devoted to volcanic rocks emplaced before the formation of the Manengouba volcano. They concern trachyte and phonolite extrusions related to a thick acidic volcanic pile at the north-western border of the Manengouba area. Two new Miocene ages, 13.56 ± 0.39 and 7.55 ± 0.18 Ma, are provided for a trachyte extrusion of the Ekomane Mounts and for a phonolite extrusion of the Bakossi Mounts, respectively (Fig. 4). A slightly younger age, 11.82 ± 0.47 Ma, was obtained by K/Ar method for a trachyte of the Ekomane

area (Table 2; Dunlop, 1983). In addition, a few old mafic lava flows are preserved at the western lower flanks of the Eocene syenite intrusion of Nlonako, which is the south-eastern border of the Manengouba. One of these flows of hawaiite composition is dated at 9.37 ± 0.05 Ma (Fig. 3).

A particular volcanic activity occurred at the eastern edge of the Manengouba field close to Ekom. It consists of a rhyolite extrusion a few hundred metres wide (Fig. 2) that we dated at 1.02 ± 0.03 Ma. Relationships with the surrounding basalts are unknown.

The oldest Manengouba lava that we analyzed is a trachyte extrusion of the Elengoum Extrusive Complex, eastern upper flank of Manengouba. It is dated at 0.89 ± 0.02 Ma (Fig. 3). This age is consistent with that of an Elengoum trachyte formerly dated at 0.70 ± 0.01 Ma (Table 2; Kagou Dongmo et al., 2001) but geological study demonstrates that the Elengoum extrusions are late activities of Mount Manengouba. Older ages have been measured for basaltic lavas constituting the lower flanks of Manengouba and belonging to the early shield volcano. These basalts are dated at 1.55 ± 0.10 and 0.94 ± 0.06 Ma, south-west of Nkongsamba in the south-eastern Manengouba field (Table 2; Gouhier et al., 1974; Dunlop, 1983). These basalts are overlain by the Elengoum trachyte flows.

All the other and younger ages concern the flank volcanic activity. According to both new and previous age dating, this activity began at the north-western and northern slopes with the hawaiite eruptions of Mboassoum and Melong dated at 0.45 ± 0.07 and 0.45 ± 0.04 Ma respectively (Figs. 2 and 4). It continued with the mugearite eruption of Nyam at 0.40 ± 0.23 Ma, north-western slope, the basanite eruption of Njinjo at 0.40 ± 0.04 Ma (northern slope), the alkaline basalt eruption of the cone of Manengouba-village at 0.22 ± 0.10 Ma (southern flank), the hawaiite eruption at 0.20 ± 0.10 Ma on the south-eastern flank, and the basanite eruption of Ekoh at 0.11 ± 0.03 Ma (eastern flank) (Figs. 2, 3 and 4). A singular extrusive trachy-phonolite activity at the north-western slope is dated at 0.21 ± 0.02 Ma. In the same time, hawaiite eruptions occurred inside the Eboga caldera with the formation of two groups of strombolian cones to the south-east (C1) and the west (C2) and the covering of the caldera floor (Fig. 3). The C1 flow is dated at 0.36 ± 0.13 and 0.33 ± 0.02 Ma, and the C2 flow is dated at 0.16 ± 0.07 Ma. This strombolian activity was followed by two phreatomagmatic explosions that created two maars named “lac de la femme” and “lac de l’homme” (LF, LH, Fig. 3), and by the Mboriko plug-dome extrusion.

In summary, the volcanic story of Mount Manengouba is written in four chronological stages that are sketched in a schematic WNW-ESE cross-section of the volcano in **Figure 6**.

Stage 1) The early Manengouba shield volcano was initiated between 1.55 and 0.94 Ma with piling-up of basaltic lava flows. Few data are available concerning these lavas because they have been neglected in the field studies at the benefit of the more attractive strombolian cones and flows at the flanks.

Stage 2) Building of the Eboga central volcano took place between 0.94 and 0.89 Ma. The stratovolcano was fed by evolved magma from the main reservoir, in a continuation of the shield volcano activity.

Stage 3) Draining of the reservoir and caldera collapse were linked to benmoreitic and trachytic extrusions from 0.89 to 0.70 Ma. Most of the extrusions were emplaced in a SW-NE trending fracture zone of the south-eastern upper slope, namely the Elengoum Extrusive Complex. Some extrusive activities were drained by the caldera sink faults and by the associated sub-circular fault at the north-eastern flank. The total volume of acidic deposits is estimated ca. 20 km^3.

The meaning of the Ekom rhyolite extrusion dated at 1.02 Ma is unknown. It is impossible to relate this highly evolved product to any Eboga activity. More field work is needed and the age dating must be improved.

Stage 4) Renewal of the volcanic activity began at 0.45 Ma and lasted until 0.11 Ma. Lava poured out along flank fractures and inside the caldera. It can be assumed that the main conduit of the initial crater was blocked up by the collapsed rocks of the caldera and acidic intrusions. A small volume of lava reached the caldera but most of the lavas were drained by middle to lower slope fractures. The magma composition evolved from basanites to mugearites and few trachy-phonolites. No time or space distribution of the different rock compositions can be evidenced. Such a volcanic activity requires a renewal of the magma production and the tectonic stress after the emptying of the Eboga reservoir with the extrusion of the last evolved products.

Obviously this story is a rough draft of more than one million years of volcanic activity. Very few data are known of the primary shield. No precise dating is available for the Eboga cone building. Relationships between the two collapses of the north-east fault scarp and of the caldera are not clear. It is not sure that the acidic extrusions of Elengoum Complex and the caldera rim are contemporaneous. However, it is clear that the caldera belongs to the Krakatoan or plate/piston type (Cole et al., 2005) and was due to a single main collapse event. According to Acocella (2007), the north-eastern curved scarp can be interpreted as an outer ring fault of the stage four of the evolution of caldera collapse. Regarding the post-caldera activity with extrusion of acidic domes at the caldera rim and further setting of mafic vents on

the floor that was covered with basaltic flows, the caldera is classified as type-MS and type-L of Geyer and Marti (2008). We assume that this caldera resulted from the collapse of a strato-cone that culminated circa 2,500 m according to a crater diameter of 1 km (Fig. 6). The depth of the collapse is unknown. For calderas of the same size, measured diameter/subsidence (d/s) ratios range from 5 to 10 (Acocella, 2007). An average value of 7.5 is best estimated referring to many volcanoes of Galapagos, Azores, Canaries, and Cape Verde of similar size and shape (Mitchell-Thomé, 1980; Munro and Rowland, 1996; Caldera Data Base of Geyer and Marti, 2008). The initial floor of the caldera was thus ca. 530 m below the present rim. It is doubtful that the acidic domes of the caldera margins took place at such a low level. Owing to their shapes, their bases are less than 50 m deep below the present basaltic floor. These domes probably extruded at the final stage of an acidic activity that has supplied ignimbrite flows filling the caldera (Fig. 6, Stage 3b). The calculated volume of the acidic caldera filling could be estimated between 1.5 and 2 km^3.

4. Composition of volcanic rocks

In agreement with the volcanic story, the volcanic rocks of Manengouba can be attributed to two successive magmatic outputs. The first magma generation produced the primary shield volcano, the Eboga stratovolcano, and the syn- to post-caldera extrusions. It yields the magmatic **Group 1**, displaying a complete series from basanite to trachyte. The second generation was responsible for the formation of the flank cones and flows. It corresponds to the magmatic **Group 2**, evolving from basanite to mugearite and trachy-phonolite. The pre-Manengouba volcanic rocks consist of trachytes and phonolites to the western side, and of hawaiites and mugearites to the eastern side.

The mineral compositions have been analyzed with electron probe microanalyzers Cameca SX50 at the University of Orléans and the University of Paris-VI (France). The main results are summarized in **Table 3A and 3B**. Selected analyses of minerals are listed in **Tables 4A to 4G**. The rocks have been analyzed by ICP-AES and ICP-MS at the analytical laboratory of CRPG-CNRS of Nancy (France). The **Table 5** displays the complete set of chemical analyses. Most of the petrographical data have been acquired during the work for the Ph. D. theses of Kagou Dongmo (1998) and Chakam Tagheu (2006), and were completed in the Professoral thesis of Kagou Dongmo (2006).

4.1. Chemical nomenclature

Both magmatic groups belong to the under-saturated, alkaline sodic series, although the intermediate terms overlap with the sodic-potassic limit and the acidic terms are fairly potassic. In the TAS diagram (La Bas et al., 1986), the Group 1 displays a continuous trend from basanites to trachytes (**Fig. 7**). The Group 2 evolves from basanites to basaltic trachy-andesites or mugearites, though one trachy-phonolite dome is pointed out. We use the nomenclature of the common sodic series and chemical cut based on the Differentiation Index (DI) of Thornton and Tuttle (1960). This system has the double benefit of regularly dividing the series and easily naming rocks according to chemical analyses. The mafic rocks evolve from basanites or alkaline basalts (limit at ± 5% of normative nepheline) to hawaiites. A few mafic lavas are enriched in cumulative olivine and clinopyroxene phenocrysts and are termed ankaramites. The intermediate lavas are composed of mugearites and benmoreites with no compositional gap. The more evolved lavas consist of oversaturated trachytes.

4.2. Petrographical features of Group 1 lavas

The petrographical features of Group 1 lavas are displayed in Table 3A. The more mafic lavas consist of ankaramites, basanites and alkaline basalts. Their textures are hyalo-microlitic and more or less porphyritic with 10 to 15 vol.% of olivine, pyroxene, and plagioclase phenocrysts or microphenocrysts, and magnetite microphenocrysts, sometimes included in clinopyroxene. The same minerals crystallized in the groundmass in addition with apatite and ilmenite in a vitreous matrix. The hawaiites have similar textures with varying abundance of phenocrysts. They are characterized by a higher amount of plagioclase. The mugearites are hyalo-microlitic and more or less rich in microphenocrysts of olivine, clinopyroxene, and plagioclase plus Ti-rich amphibole and rare phlogopite. The benmoreites contain few microphenocrysts of olivine and clinopyroxene, but abundant laths of sodic plagioclase. Clots of olivine, clinopyroxene, plagioclase, and oxides are frequent. The trachytes show a common trachytic texture with laths of anorthoclase and microphenocrysts of clinopyroxene.

The mineral compositions commonly evolve from mafic to acidic rocks with increasing Fe/Fe+Mg and Na/Na+Ca ratios. Hereafter, we investigate the composition of the main magmatic mineral phases. The minerals are depicted following the crystallization order in the mafic rocks.

Olivine

Olivine phenocrysts of basanites and alkaline basalts are moderately zoned. Their Fo contents range from 81.7 to 77.1, from core to rim. The Fo 78.4-74.1 compositions of microcrysts share alike the phenocryst rim compositions. Phenocrysts of hawaiites are also zoned Fo 79.0-69.0, and have the composition of the basalt microcrysts. Microcrysts show significant iron enrichment: 70.5-57.9. The same pattern is recorded with the phenocrysts of mugearites and benmoreites having Fo 68.7-65.2 and Fo 67.5-58.3, respectively, and with their microcrysts having Fo59.6-55.0 and Fo55.0-51.3. This is consistent with a continuous differentiation of a batch of magma involving drastic decrease of the Mg content as a result of olivine fractionation.

A few xenocrysts are recorded in basanites. Their Fo (85.2-84.5) and CaO (0.30-0.25 wt.%) contents indicate that they are inherited from melt rather than entrained mantle xenocrysts. They probably crystallized in the more primitive magma. Xenocrysts are frequent in hawaiites. Their Fo (84.5-83.2) and CaO (0.28-0.23 wt.%) contents also indicate that they are inherited from melt. They have the same composition as the xenocrysts and phenocrysts of basanites. They then were fractionated from the previous more primitive batch of magma that has generated the basanites and alkali basalts of the basal shield volcano. Similarly, mugearites enclose xenocrysts Fo 77.4-74.8 that may have been extracted from the hawaiite magma. The benmoreites also contain xenocrysts Fo 68.5-66.5 originated from the mugearite magma. However we cannot discard a post-olivine crystallization modification of the liquid by crustal assimilation and Mg# decrease (see Geochemical Chapter). We assume that xenocrysts were removed from the walls of the main magma reservoir where olivines precipitated with decreasing temperature, causing differentiation of the inner magma continuously depleted in magnesium.

Compositions of olivines are plotted in a Fo% vs. CaO (wt.%) diagram (**Fig. 8A**). Phenocrysts, microcrysts, as well as xenocrysts crystallized from a related suite of magmas. The diagram showing the Mg# of lava vs. Fo contents of olivine (**Fig. 9**) allows to distinguish xenocrysts, phenocrysts and microcrysts. The olivine-liquid equilibrium temperature is calculated using the equation (4) of Putirka et al. (2007). The temperature decreases from 1300°C for the initial basaltic composition to 1250°C, 1180°C, and 1080°C, while the inner residual batch of magma evolves from hawaiite to mugeanite, and benmoreite composition. The liquid temperature calculated after the equation (15) of Putirka (2008) decreases from 1230°C to 1190°C, 1100°C, 1085°C, 1070°C, and 1025°C, from basanite to benmoreite.

Magnetite and ilmenite

Magnetite phenocrysts of basanites and alkali basalts are titaniferous and rich in magnesium and aluminium but poor in chromium. The mole content is dominated by magnetite, Mg-magnetite or Mg-ferrite and ulvöspinel. The spinel component is limited by the Al amount. Exceeding Mg substitutes to Fe^{2+} in magnetite. From alkaline basalts to benmoreites, spinel mole decreases and ulvöspinel slightly increases. Magnetite mole increases in hawaiites but decreases in benmoreites. Mg-ferrite evolves reversely. Microcrysts of trachytes are pure Ti-magnetite, devoid of aluminium and magnesium.

In **Figure 10**, magnetite compositions display a positive correlation of Ti / (Ti+Al+Cr) and Fe^{2+}/ (Fe^{2+}+Mg) ratios from basalts to trachytes due to decreasing Al and Mg contents in the evolved magmas.

Ilmenites are rare in the basaltic rocks. They constitute of more or less abundant microphenocrysts and microcrysts in hawaiites, mugearites, and benmoreites of the Eboga middle and upper slopes. From hawaiites to benmoreites, they display a decreasing amount of the ilmenite component ($0.95 < X'_{ilm} < 0.87$), calculated after Stormer (1983), and a concomitant increasing amount of the hematite phase and the Fe^{3+}/Fe^{2+} ratio value ($0.12 < Fe^{3+}/Fe^{2+} < 0.34$). Ilmenites are limited to few crystals in benmoreites and trachytes of the Elengoum extrusions and show a composition close to pure ilmenite.

Coexisting magnetites and ilmenites have been analyzed in hawaiites, mugearites and benmoreites. The oxygen fugacity f_{O2} is estimated from the mole fraction of ulvöspinel X'_{Usp} in magnetite and of ilmenite X'_{Ilm} in ilmenite, calculated after Stormer (1983), and using the parameters of Andersen and Lindsley (1988). In hawaiites, $\log f_{O2}$ averages -13.7 ± 0.5 close to the $\log f_{O2}$ (FMQ) value ($\Delta \log f_{O2}$ (FMQ) = 0). In mugearites, $\log f_{O2}$ ranges from -13.5 to 12.1 with $\Delta \log f_{O2}$ (FMQ) = 0. In benmoreites, $\log f_{O2}$ ranges from -10.8 to 10.5 with $\Delta \log f_{O2}$ (FMQ) = + 0.5. These results are consistent with an increase of the oxygen fugacity fairly above the fayalite-magnetite-quartz buffer.

Clinopyroxene

A large set of Group 1 pyroxenes have been analyzed in fourteen samples of basanites to trachytes including xenocrysts, phenocrysts and microcrysts. To illustrate the various types of analyzed crystals, pyroxenes are plotted in the temperature vs. K_D(Fe-Mg) diagram of Putirka et al. (2003; Figure 5), using the liquid temperature as calculated after equation (15) of Putirka (2008) and consistent with the olivine-liquid equilibrium temperature (**Fig. 11**). There is a continuous range of composition of phenocrysts from basanites to benmoreites. Xenocrysts are rare in basanites but frequent in hawaiites, mugearites, and benmoreites. The

analyzed pyroxenes of the more evolved mugearites and of benmoreites are mainly glomerocrysts from aggregates of olivine, magnetite, and feldspar. The test for equilibrium of Putirka et al. (2003) and Putirka (2008) (observed pyroxene compositions compared to calculated compositions) indicates that pyroxenes of the more evolved benmoreites and trachytes can be phenocrysts.

Conventional pyroxene compositions are shown in the Mg-Ca-Fet+Mn diagram (**Fig. 12**). Two broadly separated clusters are found, one for basanite to benmoreite rocks and one for trachyte. The first cluster overlaps the diopside-calcic augite boundary. Details of the composition ranges of the various types of crystals are given in Table 3A. There is a limited evolutionary trend from phenocrysts of basanite to microcrysts of mugearite with a moderate decrease in Mg and Ca. The more magnesian crystals are xenocrysts of basanite and hawaiite. Owing to their Mg-Fe contents, these xenocrysts were inherited from a melt rather than the mantle. They probably crystallized in the more primitive magma. Most of the phenocrysts of the less evolved benmoreite are glomerocrysts. One may note that xenocrysts and glomerocrysts of this benmoreite have the same composition like phenocryts of hawaiite and mugearite. This feature reinforces the assumption also given by the olivines that the xenocrysts were removed from the margins of the main magma reservoir where liquids differentiated.

Pyroxenes of trachytes display a sharply different composition while plotting in the hedenbergite to calcic augite area. They contain low amount of Na_2O (0.7–1.6 wt.%) despite belonging to the quadrilateral pyroxenes (100 Di+Hd/Jd+Ac = 86-94). Taking into account the large compositional gap between the basanites and benmoreite pyroxenes, it can be concluded that the trachytes were not generated in the main magma reservoir.

Additional compositional data of the pyroxenes are given with the Al^{IV} vs.. Al^{VI}, Ti vs.. Al^{VI}, and Ti vs.. Na diagrams (**Fig. 13**). First, there are no pyroxenes inherited from mantle peridotites. Xenocrysts as well as phenocrysts and microcrysts crystallized from magmas in the course of the differentiation. Al^{IV}, Al^{VI}, and Ti decrease from basanites to benmoreite in relationship to the decreasing content of jadeite, esseneite, and Ti-tschermakite at the benefit of ferrosilite. The Ca-tschermakite mole does not play a significant role. The Ti-Na diagram indicates that pyroxenes of trachytes crystallized in a distinct batch enriched in Na.

To provide clues to the depth of crystallization of the magma, we applied the clinopyroxene-liquid thermobarometer of Putirka et al. (2003). The barometer is based on jadeite crystallization and jadeite-diopside + hedenbergite exchange equilibria and is temperature dependent. It is appropriate for volatile-bearing lava compositions. Here, we used

442 the FeO calculated contents and not the total FeO for rocks and pyroxenes because ferric iron
443 cannot be neglected in natural samples. The less porphyritic mafic lavas are considered,
444 discarding cumulate rocks to avoid hazardous subtraction of the olivine phase. We selected
445 analyses of the core of phenocrysts, yielding a K_D (Fe-Mg) in equilibrium with the lava when
446 close to the initial liquid composition (0.275; Putirka et al., 2003). Xenocrysts and mantled or
447 rimed phenocrysts are thus eliminated. Equations of Model A (pressure) and Model B
448 (temperature) are solved simultaneously. Satisfying results are achieved when both models
449 yield similar values, with the temperature estimation close to the calculated liquid temperature
450 according to Putirka (2008). Calculated pressures range from 10.5 to 11.3 ± 1.7 kbars.
451 Iterative calculations yield somewhat lower P estimations of 9.4 to 10.6 kbars, but with a
452 temperature 30°C below the calculated liquid temperature. In the continental Cameroon
453 Volcanic Line, the crustal thickness averages 35.5 km using 1-D shear wave velocity models
454 (Tokam et al., 2010). In the Manengouba area (station CM15 of Tokam et al., 2010) a more
455 precise value of 33 km is calculated. With this crustal thickness, the pyroxene barometer
456 allows locating the crystallization depth between 37 and 39 km in the upper mantle for the
457 accurate temperature calculation, or between 33.5 and 37 km slightly below the Moho, for the
458 iterative calculation.
459
460 **Amphibole and mica**
461 Amphiboles are limited to mugearites of the Eboga upper slopes as phenocrysts and
462 microphenocrysts. They consist of edenite or kaersutite, depending on their increasing content
463 of TiO_2. Their $Mg/Mg+Fe^{2+}$ ratios and TiO_2 contents are ranging from 0.86-0.89 and 2.1-2.2
464 wt.% for edenite, and from 0.66-0.77 and 5.6-6.2 for kaersutite. The Ti-rich amphiboles are
465 phenocrysts of the more evolved mugearitic lavas.
466 Biotites occur in mugearites and benmoreites of the Eboga upper slopes and comply with a
467 Ti-rich phlogopite composition ($0.79 < Mg/Mg+Fe^{2+} < 0.83$; $3.5 < TiO_2$ wt % < 3.9).
468
469 **Feldspar**
470 Phenocrysts and microcrysts of plagioclases are common phases and display a complete
471 calcic to sodic compositional trend from basanites to evolved lavas. Phenocrysts of basanites
472 and alkaline basalts are zoned An_{66-60} and microcrysts have the An_{60-51} composition close to
473 the phenocryst rim. Some lavas contain corroded xenocrysts An_{51-40}, which are inherited
474 from a former, evolved magma. In the compositional range of hawaiites, phenocrysts vary
475 from An_{60} to An_{51} and microcrysts from An_{53} to An_{46}. Frequent xenocrysts An_{62-59} originated

476 from a more mafic magma. The same features are depicted in the mugearite and benmoreite
477 evolutionary trend with An_{52-38} and An_{45-39} phenocrysts, An_{40-28} and An_{41-26} microcrysts, and
478 An_{61-60} and An_{52-50} xenocrysys. In addition, K-rich microcrysts are discerned in mugearites
479 (An_{22-15}, Or_{9-11}) and benmoreites (An_{25-14}, Or_{9-16}). In trachytes, phenocrysts and microcrysts
480 are undistinguishable and consist of anorthoclase Or_{30-36}.
481
482
483 *4.3. Petrographical features of Group 2 lavas*
484
485 The petrographical features of Group 2 lavas are shown in Table 3B. This group is limited
486 to basanites, alkali basalts, hawaiites, mugearites, and rare trachy-phonolites, sharing similar
487 features with equivalent lavas of Group 1, pending more abundant amphiboles and micas. A
488 sub-holocrystalline, intergranular texture is observed in the ponded lavas and in the Mboriko
489 plug-dome of the caldera. Mineral compositions are close to those of the Group 1 lavas.
490
491 **Olivine**
492 Olivine phenocrysts are zoned from 83.0 to 78.1. The microcrysts Fo 78.7-72.2 evolve
493 from the phenocryst rim to slightly iron enriched composition. The phenocrysts of hawaiites
494 Fo 78.7-70.5 exhibit the composition of the basalt microcrysts. Hawaiite microcrysts are iron
495 enriched: 71.2-65.8. The mugearites show the same trend with the phenocrysts having Fo
496 77.1-64.4, and the microcrysts: Fo62.9-54.0. This is consistent with a continuous
497 differentiation of a batch of magma involving drastic decrease of the Mg content as a result of
498 olivine fractionation.
499 Xenocrysts are also recorded in basanites-alkali basalts (Fo 87.0-86.5) and inherited from a
500 more primitive magma, hawaiites (Fo 85.0-82.5), inherited from the basanites magma, and
501 mugearites (Fo 77.9-77.3), inherited from the hawaiite magma. As for Group 1, it is suspected
502 that xenocrysts were removed from the walls of the main magma reservoir where olivines
503 precipitated with decreasing temperature, causing differentiation of the residual magma.
504 Compositions of olivines are plotted in a Fo% vs. CaO (wt.%) diagram (Fig. 8B).
505 Phenocrysts, microcrysts, as well as xenocrysts, crystallized from a related suite of magmas.
506 In the Mg number vs. Fo diagram (Fig. 9), the olivine-liquid equilibrium temperature
507 decreases from 1310°C for basanite to 1110°C for mugearite. The liquid temperature
508 decreases from 1260°C to 1085°C.
509

Magnetite and ilmenite

The Group 2 magnetites share similar mineralogical features with those of Group 1. They consist of microphenocrysts, which are rare in basaltic lavas but common in evolved lavas, and abundant microcrysts. Compositions are similar to those of Group 1, except for the chromium content that may reach 12wt % of Cr_2O_3 in basanite microphenocrysts. The mole content is dominated by magnetite, Mg-magnetite or Mg-ferrite, and ulvöspinel. The spinel component is limited by the Al amount. Exceeding Mg substitutes to Fe^{2+} in magnetite. From basanite and alkaline basalt to mugearite, spinel mole decreases and ulvöspinel increases. Magnetite mole increases in hawaiite but decreases in mugearite. Mg-ferrite evolves inversely.

In Figure 10, magnetite compositions display positive correlation of Ti / (Ti+Al+Cr) and Fe^{2+}/ (Fe^{2+}+Mg) ratios from basalt to mugearite due to decreasing Al, Mg, and also Cr contents in evolved magmas.

Ilmenites appear as microphenocrysts and microcrysts in basanites to mugearites. With evolving lava composition, they display a moderate enrichment in the hematite mole component (X'_{ilm} = 0.96 to 0.94 and Fe^{3+}/Fe^{2+} ratio = 0.09 to 0.13).

Rare coexisting magnetites and ilmenites have been analyzed in hawaiites. The log f_{O2} averages -12.5 ± 0.5 slightly below the log f_{O2} (FMQ) value (Δ log f_{O2} (FMQ) = - 0.4). This agrees with the scarcity of early magnetites in mafic magmas.

Pyroxene

Group 2 pyroxenes have been analyzed in five basanites and olivine basalts, seven hawaiites, and four mugearites. As for Group 1 pyroxenes, xenocrysts are rare in basanites, frequent in hawaiites and abundant in mugearites (Fig. 11). In the Mg-Ca-Fet+Mn diagram (**Fig. 14**), a very limited trend is displayed from basanites phenocrysts to mugearite microcrysts with weak decreasing of Mg and increasing of Fe from phenocrysts and xenocrysts to microcrysts. As explained for the Group 1 pyroxenes before, xenocrysts, phenocrysts and microcrysts crystallized from magmas (**Fig. 15A**). They are only concerned with Ti-Tchermak, Ca-Tschermak and esseneite mole substitutions. However, the basanite phenocrysts show an unusual range of composition with either Mg-rich composition (type a) or apparent Mg-depletion and Ca-enrichment (type b*)*. In the Mg-Ca-Fe ternary diagram, the enrichment of Ca relative to Mg and Fe (the fassaitic feature) is a consequence of the contribution of the Tshermak moles to the pyroxene composition. The type b pyroxenes display higher contents in Ti, Al and Fe^{3+}. They plot in a Ti-enriched area in the Fe^{2+} vs. Ti

diagram (**Fig. 15B**), where most of the pyroxenes define a common trend with Fe^{2+} enrichment from mafic phenocrysts and xenocrysts to evolved microcrysts. The high-Ti and low-Ti pyroxenes are discriminated in the Al vs. Ti diagram (**Fig. 15C**). The Ti and Fe activities in the magma are controlled by the Ti-magnetite crystallization, depending on the oxygen fugacity. In the mafic lavas, magnetites and pyroxenes crystallize in the same thermobarometric range. In most of the cases for the vapor-rich alkaline magmas, magnetite crystallizes first (high fO_2). Then, the pyroxenes are moderately titaniferous. In the case of poor magnetite crystallization (lower fO_2), the pyroxenes are enriched in titanium. The various types of pyroxenes are located at different flank eruptive centres. It is suggested that these centres were supplied from different magma batches with varying oxygen fugacities. One may conclude that the late parasitic volcanic activity was originated from separated reservoirs.

According to the clinopyroxene-liquid thermobarometer of Putirka et al. (2003), calculated pressure ranges from 12.1 to 12.8 ± 1.7 kbars. Assuming a crustal thickness of 33 km (Tokam et al., 2010), the crystallization depth is located between 42 and 44 km in the upper mantle. Iterative calculations give temperature values 20°C below the calculated liquid temperature values, and 11.3 to 12.2 kbars, that is to say 39 to 42 km in depth. In both cases, the crystallization depth is below the crystallization zone determined for the Group 1 pyroxenes.

Amphibole and mica

Amphiboles are common in Group 2 lavas from basanites to mugearites, in being more abundant in the evolved rocks. Their composition evolves from edenite to kaersutite with $Mg/Mg+Fe^{2+}$ ratios and TiO_2 contents ranging from 0.74 to 0.79 and 2.6 to 3.5 wt.% for edenite and from 0.67 to 0.79 and 4.6 to 5.8 for kaersutite. They are frequently highly oxidized in basanites.

Biotites coexist with amphibole in displaying a Ti-rich phlogopite composition ($0.76 < Mg/Mg+Fe^{2+} < 0.80$; $4.4 < TiO_2$ wt % < 5.9).

Feldspar

As for Group 1 lavas, phenocrysts and microcrysts show a common compositional trend from basanites to mugearites. Phenocrysts of basanites and alkaline basalts are An_{66-60} and microcrysts An_{62-52}. A few rounded xenocrysts An_{43-39} originated from a more evolved magma are reported in some lavas. Plagioclases of hawaiites and mugearites are An_{60-50} and An_{55-43} for phenocrysts, and An_{55-45} and An_{47-32} for microcrysts, respectively. Again, rounded

xenocrysts An_{28-22} originated from a more evolved unknown magma are analyzed in some lavas. Additional K-rich microcrysts An_{11-6} and Or_{32-46} crystallized in the doleritic facies of the caldera late extrusion.

4.4. Petrographical features of the pre-Manengouba lavas

The pre-Manengouba volcanic rocks are on one hand, the phonolites and trachytes of Mounts Bakossi and Ekomane, and on the other hand, a hawaiite and a mugearite flow of the Nlonako area (Fig. 7).

Phonolites and trachytes display a common trachytic texture with laths of sodic feldspars and microphenocrysts of pyroxenes.

The hawaiite is hyalo-microlitic porphyritic with 15% of phenocrysts and microphenocrysts of abundant plagioclase, olivine Fo_{64-68}, diopside, phlogopite, magnetite and rare ilmenite. The mineral composition is close to that of the Manengouba lavas except for the occurrence of phlogopite that is rare in Manengouba hawaiites. Magnetite is titaniferous and moderately aluminous and magnesian ($18.0 < TiO_2$ wt.% < 19.3; $2.9 < Al_2O_3$ wt.% < 4.5; $3.2 <$ MgO wt.% < 4.1; $0.56 < X'_{Usp} < 0.58$).

The mugearite is hyalo-microlitic porphyritic rich in phenocrysts of plagioclase in addition with xenocrysts of olivine Fo_{86-77} and phenocrysts and microphenocrysts of diopside ($41.9 <$ XMg% < 44.0; $14.0 <$ XFet+Mn% < 15.4; $41.3 <$ XCa% < 43.2), phlogopite, Ti-magnetite ($19.6 < TiO_2$ wt.% < 22.4). $2.3 < Al_2O_3$ wt.% < 4.2; $3.7 <$ MgO wt.% < 4.7; $1.1 < Cr_2O_3$ wt.% < 1.4; $0.61 < X'_{Usp} < 0.67$), and ilmenite ($X'_{Ilm} = 0.91$; $Fe^{3+}/Fe^{2+} = 0.23$). The xenocrystic olivine is inherited from a more mafic magma. Coexisting magnetite and ilmenite indicate a $\log f_{O2}$ ranges from -11.1 to 9.9 with $\Delta \log f_{O2}$ (FMQ) = - 0.1.

According to the clinopyroxene-liquid thermobarometer of Putirka et al. (2003), calculated pressure ranges from 6.0 to 5.2 kbars, locating the crystallization level in the lower to middle crust.

5. Geochemistry

5.1. Geochemical features

A total of 29 analyses have been carried out for the magmatic Group 1, 42 for the Group 2, and 2 for the Ekom rhyolite. Four analyses concern the western pre-Manengouba acidic lavas, and four the eastern pre-Manengouba mafic lavas.

The Group 1 lavas display a complete differentiation trend from basanite to trachyte. The Group 2 lavas evolve from basanite to trachy-phonolite. Both groups display similar trends on the MgO wt.% vs. oxides covariation diagrams (**Fig. 16A**). Decrease of MgO and increase of all the oxides in the more mafic lavas are related to olivine fractionation. Below 8 MgO wt.%, additional fractionation of clinopyroxene in alkali basalt and hawaiite is evidenced by decreases of CaO and FeO. The decreasing TiO_2 in hawaiite indicates fractionation of Ti-bearing oxides. The sudden decrease of Al_2O_3 in mugearite points to plagioclase fractionation. Possible fractionation of apatite may have occurred in benmoreite according to P_2O_5 loss. In the minor element covariation diagrams (**Fig. 16B**), the compatible elements Cr and Ni display heavy depletion from mafic to evolved rocks due to Mg-Fe phase fractionation. Vanadium decreases in hawaiites, like titanium, indicating an oxide fractionation. Strontium exhibits a wide range of contents betraying the heterogeneity of Group 2 lavas of the late magmatic activity. However, Sr-decreases in hawaiite and mugearite are linked to plagioclase fractionation. The incompatible elements Rb, Ba, Ga, Zr, Hf, Nb, Ta, Y, Pb, Th, U, and the REE exhibit common enrichments from basanite to trachyte, while some trachytes and the rhyolite are depleted by volatile transfer. Again, variations in the Zr, Hf, Nb, Ta, and the light rare earth element contents in basalt and hawaiite indicate a somewhat heterogeneity of primitive magmas.

The incompatible element signatures are illustrated with the chondrite-normalized and MORB-normalized diagrams (**Figs. 17 and 18**). The stages 1 and 2 lavas display rare earth element (REE) enriched patterns with $(La/Yb)_N$ ratios ranging from 9.6 to 24.5 and 163 to 332 rare earth amounts. Compared to MORB, these lavas point to increasingly enriched trends from high field strength to large ion lithophile elements, except Sr and K which are poorly enriched. But the heavy rare earth elements are depleted indicating a different source than the MORB one.

The stage 3 evolved lavas are similarly enriched ($10.8 < (La/Yb)_N < 23.3$), except the rhyolite ($3.0 < (La/Yb)_N < 7.3$) with 259 to 589 rare earth element amounts. The trachytes exhibit significant negative Eu anomalies ($0.8 < Eu/Eu^* < 0.1$). The MORB normalized patterns show higher amounts of incompatible trace elements compared to mafic lavas, and significant negative anomalies resulting from fractional crystallization that increases in importance from benmoreite to trachyte. The Ti and P negative anomalies are due to

644 fractional crystallization of oxides and apatite, respectively. Ba, Sr, in addition with Eu
645 negative anomalies in trachyte comply with feldspar fractionation.
646 The stage 4 lavas (Group 2) display the same patterns as the stages 1 and 2 lavas. From
647 basanite to trachy-phonolite, the $(La/Yb)_N$ ratios range from 9.5 to 25.6, and rare earth
648 abundances from 117 to 379. They are poorly enriched in Sr and K, and depleted in the heavy
649 rare earth elements. The lava with the lowest enrichment in incompatible elements is an
650 olivine and pyroxene-rich basanite (CT110) of a thick flow that ponded inside the caldera in
651 form of a temporary lava lake. This relative depletion is due to olivine and pyroxene
652 cumulation. The basanite to trachy-phonolite evolved patterns are compatible with fractional
653 crystallization as shown by the major element covariation diagrams (Fig. 16). Most of the
654 mugearites exhibit moderate P and Ti negative anomalies denoting apatite and oxides
655 fractionation. A few mugearites have weak positive anomalies of Ba and Eu, compatible with
656 feldspar cumulation. The trachy-phonolite is enriched in incompatible elements but depleted
657 in Eu, Ba, P, and Ti. These features denote fractional crystallization of feldspar, apatite and
658 oxides.
659 The pre-Manengouba mafic lavas share close geochemical compositions with the lavas of
660 Manengouba. The hawaiites show positive anomalies of Eu and Ba due to feldspar
661 accumulation. The trachytes and phonolites show signs of fractional crystallization of
662 feldspar, apatite and oxides as evidenced by negative anomalies of Eu, Ba, P, and Ti. In
663 addition, the phonolites are depleted in the middle rare earth elements (MREE) and Ta that
664 may suggest an amphibole fractionation because amphibole has a greater compatibility of the
665 MREE (Zack at al., 1997).
666 The Manengouba mugearites and benmoreites contain a few biotite and amphibole that
667 may have played in the differentiation processes. To test this effect, Rb, Ba, K, and Sr
668 covariation diagrams have been drawn, as well as a Ba/Rb vs. Rb/Sr diagram as suggested by
669 Furman et al. (2006). The differentiation trends for these elements are dominated by the
670 feldspar fractionation. Indeed, the lithophile element variations indicate a limited role or no
671 role for biotite and amphibole. In return, Th and Pb contents in many trachytes attest for a
672 crustal contribution. Lower Ce/Pb is typical of crustal assimilation. A Ce/Pb value lower then
673 20 is commonly retained (Rogers et al., 1992; Furman et al., 2007). In the Th/Pb vs. Ce/Pb
674 diagram (**Fig. 19**), all the trachytes plot below this value, as well as the Bakossi phonolites.
675
676 *5.2. Source characteristics and degree of partial melting*
677

678 The mafic lava compositions are used to determine the parental magma composition and
679 the mantle source characteristics, excluding cumulate facies. The closest rocks to primary
680 mantle melts are CT46 and EB20 for the Manengouba main cone building (Stages 1 and 2,
681 magmatic Group 1) and for the late activity (Stage 4; magmatic Group 2) owing to their MgO
682 and Ni contents (**Fig. 20**). CT46 is a basal thick flow of the early shield volcano cropping out
683 at the lower southern flank. EB20 is an intra-caldera flow that filled the caldera basin before
684 the ultimate explosive maar activity. We retain the mafic lavas of magmatic Group 1 (5
685 analyses) and of Group 2 restricted to MgO greater than 6 wt.% (15 analyses). Two
686 neighbouring olivine fractionation trends can be defined from the partial melting area drawn
687 after Class et al. (1994). The primary melt composition averages 9 to 10 wt.% of MgO and
688 250 to 290 ppm of Ni.
689 The MORB normalized trace element diagram of the selected mafic lavas show that the
690 Manengouba profiles are identical to that of the average OIB of Sun and McDonough (1989)
691 (**Fig. 21**). A similar enriched mantle source can be assumed, as shown by the Ta/Yb vs.
692 Th/Yb diagram (**Fig. 22A**). However, distinct Zr/Hf and Nb/Ta ratios (**Fig. 22B**) prove that
693 the sub-Manengouba mantle source is different of that of OIBs, and also of MORBs and
694 continental basalts. This source is suspected to have high Zr/Hf ratio of 46.2 and low Nb/Ta
695 ratio of 13.75 averaging the CT46 and EB20 values. Considering the set of mafic lavas,
696 Nb/Ta remains constant with variable Zr/Hf, a feature of OIB and MORB fields that is usually
697 explained by pyroxene fractionation (Pfänder et al., 2007 and 2012). However, the
698 petrographical relationships show that the Zr/Hf ratio decreases with Zr from mafic to
699 evolved lavas. Such a trend cannot be explained by pyroxene fractionation. Similar high
700 Zr/Hf ratios are known from the eastern and western branches of the East African rift, but
701 with high Nb/Ta ratios as in the Kenya rift (Rogers et al., 2006). Nevertheless, lavas of the
702 Virunga area, north of the Lake Kivu, display Nb/Ta ratios close to those of the Manengouba,
703 as well as high Zr/Hf ratios (Rogers et al., 1992, 1998; Platz et al., 2004; Chakrabarti et al.,
704 2009). The Zr/Hf trend can be due to enrichment of the source region by metasomatic fluid as
705 suggested by Dupuy et al. (1992) or to infiltration of carbonatite-rich fluids according to
706 Rudnick et al. (1993).
707 The rare earth element abundances and ratios are commonly used to constrain the mantle
708 source characteristics. The relative heavy rare earth element depletion with a $(Tb/Yb)_N$ ratio
709 lower than 1.8 is indicative of a garnet-bearing source at the melting zone (e.g. Rooney et al.,
710 2010). The higher ratio for CT46 (23.48) compare to EB20 (2.17) indicates a more amount of
711 garnet in the source that must be deeper. The same result is given by the $(Dy/Yb)_N$ ratio

712 compared to the La/Yb_N ratio used by Rogers et al. (2006) to calculate the garnet content of
713 the melting primitive mantle. In that case, the garnet content is 8% for CT46 and 4% for
714 EB20. If the source is enriched, contents are slightly lowered. Mineral composition and
715 degree of partial melting can be approached with La/Sm and Sm/Yb values. On the one hand,
716 the La/Sm ratio is a function of the degree of melting and provides information on the source
717 chemical composition. On the other hand, the Sm/La ratio discriminates the spinel or garnet-
718 bearing source, and provides an estimation of the degree of melting once the La/Sm ratio is
719 defined. In the La vs. La/Sm and La/Sm vs. Sm/Yb diagrams (**Fig. 23**), melt curves are drawn
720 for spinel-lherzolite, garnet-lherzolite, and a 50:50 mixture of spinel- and garnet-lherzolite.
721 Modal compositions of spinel-lherzolite (olivine 53%, OPX 27%, CPX 17%, spinel 3%) and
722 garnet-lherzolite (olivine 60%, OPX 20%, CPX 10%, garnet 10%) are after Kinzler (1997)
723 and Walter (1998). Mineral/melt partition coefficients for basaltic liquids are after the
724 compilation of Rollinson (1993). The mantle array is defined by the depleted MORB mantle
725 (DMM composition from Salters and Stracke, 2004) and primitive mantle (PM after Sun and
726 McDonough, 1989) trend. In the La vs. La/Sm diagram (Fig. 23A), the mafic lavas plot in the
727 melting trends between 2% and 5% of partial melting. The trends deal with an enriched
728 source and a La/Sm ratio value between 2 and 2.5. A more precise composition of the source
729 is calculated by the inversion method. However, we know the precision of such calculation is
730 illusive whatever the used formulae and the batch melting scenarios, because of the
731 uncertainty of the bulk partition coefficients that highly control the results (notwithstanding
732 the heterogeneity of the source). In the La/Sm vs. Sm/Yb diagram (Fig. 23B), the lavas plot
733 slightly above (CT46) or close (EB20) to the 50:50 spinel-garnet lherzolite melting trend.
734 Partial melting degrees average 3% for CT46 and 6% for EB20. On the base of the estimated
735 enriched source composition, the garnet content of the source could be 7% for CT46 and 3%
736 for EB20 according the $(Dy/Yb)_N$ ratio compared to the La/Yb_N ratio (Rogers et al., 2006).
737 Assuming a 6 to 8 times enrichment of chondritic abundances suggested by the La/Sm and
738 Sm/Yb ratios and a La value averaging 2.2, the melting degrees are calculated on the base of
739 the above indicated data. Unrealistic values were obtained due to excess garnet in the source.
740 A second calculation was done with the garnet peridotite composition and bulk partition
741 coefficients of Salters and Longhi (1999), and Salters et al. (2002). Partial melting degrees of
742 3% for CT46 and of 6% for EB20 agree with the La/Sm-Sm/Yb diagram.
743 It can be concluded that melting took place in the spinel to garnet transition zone located at
744 70 to 90 km and around 25 kb at the melt temperature values (O'Neill, 1981; Schilling et al.
745 2005). The less abundant garnet and the higher partial melting degree in the late and parasitic

volcanic activity (EB20, Stage 4) indicate uprising of the melting column to the upper part of transition zone. It has been noted that the magmatic signature is sodic (Fig. 7) and poor in potassium. Rb is moderately enriched and the Ba/Rb and Rb/Sr ratios are low. These chemical features are compatible with an amphibole-bearing source rather than with a mica-bearing source. Limit of the stability fields of amphibole and phlogopite locates around 25 to 30 kb in the lithospheric mantle (e.g. Class and Goldstein, 1997). It is consistent with the location of the Manengouba magma source in the spinel-garnet transition zone and in the amphibole field. The existence of an amphibole-bearing upper mantle beneath the CVL is supported by the sampling of amphibole-spinel-garnet ultramafic xenoliths in volcanoes of Ngaoundéré, Lake Nyos, Oku, and Mount Cameroon (Lee et al. 1996; Temdjim et al., 2004; Matsukage and Oya, 2010; Temdjim, 2012). After Marzoli et al. (2000), trace element patterns agree with an amphibole-bearing source for Sr-rich mafic rocks of the Bambouto volcano. Moreover, an amphibole-bearing lherzolite composition is advocated by Yokoyama et al (2007) for the lithospheric mantle beneath Mt Cameroon on the base of U-series disequilibria relationships. It is straightforward to postulate that the same lithospheric mantle locates beneath Mt Manengouba.

5. 3. Isotopic data

A total of nine samples of Manengouba have been analyzed by Halliday et al. (1988; 1990) for Sr, Nd, and Pb isotope ratios. Most of these samples are basaltic lavas from the flank cones. One basalt belongs to the old shield. The ratio variations between old and recent lavas are in the range of the analytical reproducibility. In addition to these data, we analyzed seven samples of Manengouba including the Ekom rhyolite and the trachy-phonolite of the late north-western flank activity, and three samples of the north-western Essom trachyte, the Bakossi phonolite, and the eastern basaltic substratum (**Table 6**). A representative mafic lava of Manengouba, the rhyolite, the trachy-phonolite and the Essom trachyte have been selected for lead isotope analyses.

In the Manengouba lavas, initial $^{87}Sr/^{86}Sr$ ratios display a restricted range from 0.7030 to 0.7032 with low radiogenic Sr values close to the Enriched Depleted MORB Mantle in **Figure 24A** (E-DMM of Workman and Hart, 2005). Initial $^{143}Nd/^{144}Nd$ ratios expressed as εNd are from +4.4 to +6.8, the lowest value pertaining to the trachy-phonolite. The values of the late Miocene hawaiite of the substratum are close to those of the Manengouba and may have originated from similar source. As it is common, trachyte, phonolite, and rhyolite are

780 enriched in radiogenic Sr resulting from crustal assimilation as shown by the chemical data.
781 In return, such process has not affected the trachy-phonolite that simply derived from mafic
782 parent by fractional crystallization. The Pb isotopic compositions of Manengouba are
783 radiogenic with 19.6 < $^{206}Pb/^{204}Pb$ < 20.2, 15.6 < $^{207}Pb/^{204}Pb$ < 15.7, and 39.3 < $^{208}Pb/^{204}Pb$ <
784 39.9. They straddle to the FOZO component redefined by Stracke et al. (2005) and plot near
785 the NHRL (Northern Hemisphere Reference Line at 1.77 Ga; Hart, 1984) with a Th/U ratio
786 averaging 4 (**Fig. 24B and C**). The Ekom rhyolite and the Essom trachyte, thought to be
787 contaminated by continental crustal material are less radiogenic. It should be noted that the
788 rhyolite was fractionated in U and Pb (Th/U = 21).
789 The Manengouba shares same geochemical and isotopic features with all the Cenozoic
790 volcanoes of the Cameroon Volcanic Line (CVL), and particularly the high $^{208}Pb/^{204}Pb$ ratio
791 commonly related to the HIMU component. Along the CVL, one distinctive isotopic feature
792 is reported with slightly higher $^{206}Pb/^{204}Pb$ ratio for the continental-ocean boundary (cob)
793 volcanoes (Mount Cameroon, Etinde, Bioko) compared to the continental sector and the
794 oceanic sector (Halliday et al., 1988). The Manengouba isotope values are similar to those of
795 the continental part.
796
797 *5.4. Search for the source components*
798
799 The Cameroon Volcanic Line is characterized by depleted values of the Sr and Nd isotopic
800 ratios with Pb isotopic radiogenic enrichments. There are no prominent geochemical
801 discrepancies between the recent lavas of both the continental and oceanic sectors. On these
802 bases, it was suggested that the lavas have been derived from sub-lithospheric sources which
803 were contaminated by melts of an (HIMU) enriched fossil plume head emplaced during
804 continental breakup in the present Gulf of Guinea area (Halliday et al., 1990; Lee et al., 1994).
805 Alternatively, the lead isotope peculiarities may be explained by contamination of primary
806 asthenospheric melts by melting of sub-continental mantle hosted the FOZO component
807 (Rankenburg et al., 2005). For addressing these models to the Manengouba magmatic sources,
808 we collected the Sr, Nd, and Pb isotopic values of the CVL from Halliday et al. (1988; 1990),
809 Lee et al. (1994), Marzoli et al. (2000), Rankenburg et al. (2005), Yokoyama et al. (2007),
810 Nkouandou et al. (2008), Nkouathio et al. (2008), Wandji et al. (2009), Mbassa et al. (2012)
811 and Kamgang et al. (2013). We limited the data set to mafic lavas and recalculated the initial
812 ratios. Plotted results are outlined in $^{87}Sr/^{86}Sr$ vs. $^{143}Nd/^{144}Nd$, $^{206}Pb/^{204}Pb$ vs. $^{207}Pb/^{204}Pb$, and
813 $^{206}Pb/^{204}Pb$ vs. $^{208}Pb/^{204}Pb$ diagrams (Fig. 24A, B and C).

Lavas of the CVL are distributed in six groups bearing on distinct isotopic features (Fig. 1): 1) Biu and Mandara lavas in the northern end display both the highest depleted and the highly radiogenic terms. They also show a wide compositional range to enriched and less radiogenic terms. Rankenburg et al. (2005) explain these features with two contamination processes of the primary magmas: addition of an "enriched" (they mean "radiogenic") sub-continental lithospheric melts and addition of bulk continental crust. 2) Ngaoundéré lavas in the north-eastern faulted branch are moderately enriched and moderately radiogenic with an enrichment trend. 3) Lavas of the middle continental sector of the CVL (Oku, Bamenda, Bambouto, Manengouba and Tombel) share similar moderately enriched and moderately radiogenic isotope composition, but with a significant enrichment trend suggesting an EM1 contribution according to Sr/Nd and lead isotope covariation diagrams (Fig. 24). 4) Towards the continent-ocean boundary (COB), lavas of Mount Cameroon, Etinde, and Bioko Island are characterized by high radiogenic lead isotope ratios that are due to young fractionation in U/Pb within the upper mantle according to correlatives with Sr, Nd, Pb, and Hf isotopic values (Ballentine et al., 1997). They are fairly enriched with low Nd isotopic ratios 5) At the islands of Principe and São Tomé, lavas are quite similar with highly to moderately radiogenic lead isotopes and significantly depleted terms. 6) The Pagalu Island lavas point out unradiogenic lead ratios and somewhat enriched terms.

The salient isotopic features are best discriminated in the Sr vs.. $^{208}Pb/^{204}Pb$ diagram (**Fig. 24D**). The data fields are explained by varying contribution of three components. First, two components: a depleted component (DC) and a radiogenic component (RC) define the primary magmas, because they are prominent in the most primitive lavas. DC and RC resemble the 'A' and 'B' components of Rankenburg et al. (2005). Then, the different primary magmas evolve along orthogonal paths owing to increasing contribution of an enriched component (EC) that could be the 'CC' component of Rankenburg et al. (2005).

The geochemical data reveal that there are no doubts that **the depleted component** originated from asthenospheric upwelling that occurred all along the CVL as shown by swell elevation related to thermal thinning (Poudjon-Djomani et al., 1995, 1997; Meyers et al., 1998). **The radiogenic component** was suspected to belong to a plume head. One main plume (St Helena type) or several small plumes (Halliday et al., 1988; Lee et al. 1994, 1996) have fed the upper mantle in the past and contaminated the magmatic sources with the HIMU component. However, the highest radiogenic composition of the cognate magmatic megacrysts reflecting the source composition may be representative of the radiogenic end-member after Rankenburg et al. (2005). This end-member is more enriched than the HIMU

848 end-member (higher Sr ratio and lower Nd ratio) and is close to the richest Nd and Pb ratio
849 domain of the FOZO compositional field (Stracke et al., 2005). In the African plate Cenozoic
850 volcanism, FOZO is ubiquitous in the continental part: Hoggar-Aïr, Darfur, Ethiopia, Kenya,
851 and Tanzania (Paslick et al., 1995; Franz et al., 1999; Aït-Hamou et al., 2000; Rogers et al.,
852 2000; Kieffer et al., 2004; Furman et al., 2006; Pik et al., 2006) as well as in the oceanic part:
853 Canary, Madeira, and Cape Verde (Gerlach et al., 1988; Hoernle et al., 1991; Halliday et al.,
854 1992; Millet et al., 2008). The continental sectors are located in the Mesoproterozoic and
855 Neoproterozoic mobile belts where many ocean plate subduction and collision processes have
856 taken place. It can thus be inferred that the continental lithosphere, unlike the oceanic
857 lithosphere, registered multiple metasomatic events and not only a single Mesozoic
858 enrichment from a hypothetical mantle plume. Consequently, we assume that the radiogenic
859 component is a common feature of the African continental lithosphere particularly in the Pan-
860 African belts. This radiogenic orogenic-related source is more realistic than the plume source
861 unless to invoke numbers of plume and unsustainable plume tracks. No plume trail can be
862 evidenced below the CVL (Pasyanos and Nyblade, 2007). Late Pliocene to present day
863 volcanic activities emplaced simultaneously all along the CVL, from Biu to the middle
864 continental sector, the Mount Cameroon, and the Pagalu Island (Fitton and Dunlop, 1985: Lee
865 et al., 1994; Kagou Dongmo et al., 2010).
866 **The enriched component** resembles the 'CC' component of Rankenburg et al. (2005)
867 deriving either from the sub-continental lithospheric mantle (SCLM) or the continental crust,
868 both being characterized by high Sr isotope ratio and low Nd and Pb isotope ratios (Fig. 24).
869 On the base of osmium isotope values, Rankenburg et al. (2005) promote the contamination
870 with continental crust for Biu lavas. Similar isotopic trends are shown by mafic lavas of the
871 middle continental CVL, namely in the Bambouto and Bamenda volcanoes (Nkouathio et al.,
872 2008; Kamgang et al., 2013). These volcanoes and the Manengouba have produced abundant
873 evolved lavas, phonolites, trachytes, and rhyolites. These acidic lavas display geochemical
874 evidences of crustal contamination, as shown for the Manengouba trachytes (this work, Fig.
875 19). In return, no clear geochemical witnesses of crustal assimilation are seen in the mafic
876 lavas. Except for the Os isotope ratio (after Rankenburg et al., 2005), the commonly used
877 isotope ratios (Sr, Nd, Pb) are unable do discriminate alone between the crust and the
878 enriched mantle contributions. In the lack of crustal-related geochemical arguments, we
879 support the hypothesis that enriched trends to EC in mafic lavas are due to the contribution
880 either of an EM1-like inherent component of the sub-continental lithosphere or to any recent
881 enrichment linked to pre-rifting processes. Indeed, clear evidences of sub-continental

882 lithosphere enrichment are given by the numerous Cretaceous to Eocene alkaline volcano-
883 plutonic complexes distributed all along the CVL from the Atlantic coast to the Lake Chad
884 (Déruelle et al., 1991; Vicat et al., 2002) and emplaced before the Miocene to present-day
885 volcanoes.
886 A latent question is how the lavas of the oceanic portion of the CVL can be so enriched in
887 continental lithosphere source component if both the radiogenic and the enriched components
888 (RC and EC) belong to the sub-continental lithospheric mantle? The oceanic localization
889 would favour asthenospheric origin of the source components. Indeed, the Pagalu lavas are
890 unradiogenic but significantly enriched (Fig. 24D). Many authors have invoked the
891 entrainment of delaminated continental fragments in the oceanic domain during the
892 continental breakup (e.g. Rankenburg et al., 2005). First, we must specify that the CVL
893 oceanic volcanoes straddle NE-SW fracture zones in the continuation the continental fault
894 network predating the breakup (Meyers et al., 1998). Second, these faults have fed a
895 continental margin volcanic activity: the Pointe Gombé volcano and the Banc du Loiret lava
896 plateau (Cornen et al., 1993). This activity was contemporaneous with the early activity of the
897 São Tomé and Pagalu volcanoes and shares the same petrographical, chemical, and isotopic
898 composition (Cornen et al., 1993). Third, these faults are associated with post-Pan-African
899 late Neoproterozoic intrusions of alkaline syenites and carbonatites that give evidences of
900 metasomatic enrichment of the sub-continental mantle. The São Tomé volcano straddles the
901 Kribi fracture zone that joints the on-land northern Kribi Fault. The Pagalu volcano straddles
902 the Fang fracture zone that extends the Kribi Fault. The Fang fracture zone has fed the Pointe
903 Gombé and Banc du Loiret volcanics in the time of the Pagalu volcano building. The Kribi
904 Fault is linked to the Kribi alkaline syenite recently investigated and dated at 590 Ma (Nsifa et
905 al., 2013). Giving all these consistent volcano-tectonic relationships, there is no doubt that
906 magmas of the CVL oceanic volcanoes merely originated from the metasomatized sub-
907 continental mantle. The source of Pagalu is limited to DC+EC (Fig. 24D) and is located in the
908 Congo Craton margin lithospheric mantle and outside the Pan-African realm that may explain
909 its unradiogenic composition.
910
911 **6. Conclusion**
912
913 The Mount Manengouba is a great volcano of the middle continental sector of the
914 Cameroon Volcanic Line (CVL). It culminates at 2411 m and covers 500 km^2. It emplaced in

915 a graben between two N 30°E trending normal faults. It straddles a N 50°E fracture zone
916 suggesting a right-lateral transtensional setting.
917 New mapping of the volcanic formations led to distinguish four chronological units from
918 the early shield volcano to the late flank lavas. The volume of the volcano is calculated at 320
919 km^3 ± 5%. The final flank activity volume is weak and estimated between 1.5 to 2 km^3. The
920 four chronological stages dated by 5 published K/Ar ages and 11 new K/Ar and $^{40}Ar/^{39}Ar$
921 measurements are as follow: 1) piling-up of the early Manengouba shield volcano between
922 1.55 and 0.94 Ma, 2) building of the Eboga stratovolcano between 0.94 and 0.89 Ma, 3)
923 caldera collapse and acidic Elengoum extrusions between 0.89 and 0.70 Ma, and 4) intra-
924 caldera and flank activity between 0.45 and 0.11 Ma. New K/Ar ages are also provided for
925 pre-Manengouba volcanic activities: 13.56 Ma and 7.55 Ma for a trachyte and a phonolite of
926 the western border, and 9.37 Ma for a hawaiite of the south-eastern substratum of the
927 Manengouba shield.
928 The Eboga caldera belongs to the Krakatoan or plate-piston type and resulted from a single
929 collapse. It is classified in the type-Ms and type-L of Geyer and Marti (2008).
930 The volcanic rocks are attributed to two magmatic outputs. The first and main magma
931 generation produced the shield volcano, the stratovolcano, and the syn- to post-caldera
932 extrusions, displaying a complete series from basanites to trachytes (magmatic Group 1). The
933 second magma production is limited to the late intra-caldera and flank activity evolving to
934 basanites to trachy-phonolite (magmatic Group 2). Olivine and pyroxene thermobarometers
935 locate the magmatic reservoir between 37 and 39 km in the upper mantle for the Group 1
936 lavas, and between 42 and 44 km for the Group 2 lavas. Similar depth, 35 to 44 km, has been
937 obtained with the same method for the magma chamber of basanites of Mount Cameroon by
938 Wandji et al. (2009). Trachytes were generated in a secondary crustal reservoir because of the
939 large gap in the pyroxene composition. Magmatic series evolve with medium to low pressure
940 fractional crystallization of olivine, pyroxene, oxides, feldspar, and apatite. Significant crustal
941 assimilation is evidenced in trachytes. The parental magma composition is estimated close to
942 the average OIB composition. But, distinct Zr/Hf and Nb/Ta ratios prove that the magma
943 source registered a distinct metasomatic enrichment event. The magma of the main volcano
944 was generated with 3 to 6% of partial melting of a moderately enriched source (6 to 8 times
945 enrichment of chondrite abundances) containing 3 to 7% of garnet. Melting of the
946 Manengouba source took place in the spinel to garnet transition zone located at 70 to 90 km
947 and around 25 kb at the melt temperature values. The magma of the late flank activity resulted
948 from a slightly higher partial melting from a less garnet-rich source that indicates uprising of

the melting column to the upper part of transition zone. The low Rb contents and low Ba/Rb and Rb/Sr ratios are compatible with an amphibole-bearing source.

Some Sr, Nd, and Pb isotope new data of the Manengouba rocks and neighbouring lavas complete the data of Halliday et al. (1988, 1990). They comply with those of the middle continental sector of the CVL. Sr and Nd isotope values plot near the enriched depleted MORB mantle source with a moderate enrichment. Pb isotope values are somewhat radiogenic in plotting in the FOZO compositional field, close to the NHRL, and show a short enrichment trend. The evolved lavas are unradiogenic and registered crustal assimilation. Review of the isotope data of mafic lavas of the whole CVL led to discriminate three source components: a depleted component related to the asthenospheric upwelling, a radiogenic component that we attributed to the lithosphere of the Neoproterozoic mobile belt contaminated during orogenic events, and an enriched component or the lithosphere possibly related to pre-rifting magmatic processes linked to the Cretaceous to Eocene intrusions of alkaline volcano-plutonic complexes distributed all along the CVL.

Aknowledgements

This work has been supported by the SCAC (Service de Coopération et d'Action Culturelle de la France au Cameroun) and EGIDE (Centre français pour l'accueil et les échanges internationaux) of the French Government. Mineral analyses are indebted to the Institut des Sciences de la Terre of the University and CNRS of Orléans (France), and to the Faculty of Sciences of the University of Orsay (France). Special thanks are due to Daniel Demaiffe of the Laboratory of isotope geochemistry of the Open University of Bruxelles, Belgium, for providing the Sr-, Nd-, and Pb-measurements. We are grateful to two anonymous reviewers who provided useful critiques of this contribution.

This paper is dedicated to Pr. Pierre Wandji who has leaved our world in April 2014. Pierre Wandji managed many volcanological studies of the Cameroon Line and was the director of Armand Kagou Dongmo, Pulchérie Chakam Tagheu and David Nkouathio.

References

Acocella, V., 2007. Understanding caldera structure and development: An overview of analogue models compared to natural calderas. Earth-Science Reviews 85, 125-160.

Aït-Hamou, F., Dautria, J.M., Cantagrel, J.M., Dostal, J., Briqueu, L., 2000. Nouvelles données géochronologiques et isotopiques sur le volcanisme cénozoïque de l'Ahaggar

983 (Sahara algérien) : des arguments en faveur de l'existence d'un panache. C. R. Acad. Sci.
984 Paris, Sciences de la Terre et des planètes, 330, 829-836.
985 Andersen, D.J., Lindsley, D.H., 1988. Internally consistent solution models for Fe-Mg-Mn-Ti
986 oxides: Fe-Ti oxides. Am. Mineralogist 73, 714-726.
987 Ballentine, C.J., Lee, D.-C., Halliday, A.N., 1997. Hafnium isotopic studies of the Cameroon
988 line and new HIMU paradoxes. Chemical Geology 139, 111-124
989 Cantagrel, J.-M., Jamond, C., Lasserre, M., 1978. Le magmatisme alcalin de la "Ligne du
990 Cameroun" au Tertiaire inférieur : données géochronologiques K/Ar. C. R. Som. Soc.
991 Géol. France, 6, 300-303.
992 Chakam Tagheu, P.J., 2006. Le volcanisme quaternaire des régions du stratovolcano
993 Manengouba (Ligne du Cameroun). Thèse de 3ème cycle Univ. Yaoundé I, Cameroon,
994 155p.
995 Chakrabarti, R., Basu, A.R., Santo, A.P., Tedesco, D., Vaselli, O., 2009. Isotopic and
996 geochemical evidence for a heterogeneous mantle plume origin of the Virunga volcanics,
997 Western rift, East African Rift system. Chemical Geology 259, 273-289.
998 Cole, J.W., Milner, D.M., Spinks, K.D., 2005. Calderas and caldera structures: a review.
999 Earth-Science Reviews 69, 1-26.
1000 Class, C., Altherr, R., Volker, F., Eberz, G., McCulloch, M.T., 1994. Geochemistry of
1001 Pliocene to Quaternary alkali basalts from the Huri Hills, northern Kenya. Chemical
1002 Geology 113, 1-22.
1003 Class, C., Goldstein, S.L., 1997. Plume-lithosphere interactions in the ocean basins:
1004 constraints from the source mineralogy. Earth Planet. Sci. Lett. 150, 245-260.
1005 Cornen, G., Bellon, H., Joron, J.-L., 1993. Le volcan de Pointe Gombé (Gabon) et ses
1006 relations avec le Golfe de Guinée. C. R. Acad. Sci. Paris, t. 317, Série II, 919-926.
1007 Déruelle, B., Moreau, C., Nkoumbou, C., Kambou, R., Lissom, J., Njongfang, E., Ghogomu,
1008 R.T., Nono, A., 1991. The Cameroon Line: a review. In: Kampunzu, A.B., Lubala, R.T.
1009 (Eds.), Magmatism in extensional structural settings. The Phanerozoic African Plate.
1010 Springer, Berlin, pp. 274-327.
1011 Déruelle, B., Bardintzeff, J.-M., Cheminée, J.-L., Ngounouno, I., Lissom, J., Nkoumbou, C.,
1012 Etame, J., Hell, J.V., Tanyileke, G., N'ni, J., Ateba, B., Ntepe, N., Nono, A., Wandji, P.,
1013 Fosso, J., Nkouathio, D.G., 2000. Eruptions simultanées de basalte alcalin et de hawaiite
1014 au mont Cameroun (28 mars-17 avril 1999). C.R. Acad. Sci. Paris, Sér IIa 331, 8, 525-
1015 531.

1016 Déruelle, B., Ngounouno, I., Demaiffe, D., 2007. The « Cameroon Hot Line » (CHL): A
1017 unique example of active alkaline intraplate structure in both oceanic and continental
1018 lithospheres. C.R. Geoscience 339, 589-600.
1019 Dunlop, H.M., 1983. Strontium isotope geochemistry and potassium-argon studies on
1020 volcanic rocks from the Cameroon line, West Africa. PhD. thesis Univ. Edinburgh, Great
1021 Britain, 347p.
1022 Dupuy, C., Liotard, J.M., Dostal, J., 1992. Zr/Hf fractionation in intraplate basaltic rocks:
1023 Carbonate metasomatism in the mantle source. Geochim. Cosmichim. Acta 56, 2417-2423.
1024 Fitton, J.G., Dunlop, H.M., 1985. The Cameroon line, West Africa, and its bearing on the
1025 origin of oceanic and continental alkali basalt. Earth Planet. Sci. Lett. 72, 23-38.
1026 Franz, G., Steiner, G., Volker, F., Pudlo, D., Hammerschmidt, K., 1999. Plume related
1027 alkaline magmatism in central Africa-the Meidob Hills (W Sudan). Chemical Geology
1028 157, 27-47.
1029 Furman, T., Graham, D., 1999. Erosion of lithospheric mantle beneath the East African Rift
1030 system : geochemical evidence from the Kivu volcanic province. Lithos 48, 237-262.
1031 Furman, T., Kaleta, K.M., Bryce, J.G., Hanan, B.B., 2006. Tertiary mafic lavas of Turkana,
1032 Kenya: Constraints on East African plume structure and the occurrence of high-μ
1033 volcanism in Africa. J. Petrology 47, 1221-1244.
1034 Gerlach, D.C., Cliff, R.A., Davies, G.R., Norry, M., Hodgson, N., 1988. Magmas sources of
1035 the Cape Verdes archipelago: Isotopic and trace element constraints. Geochim.
1036 Cosmochim. Acta 52, 2979-2992.
1037 Geyer, A., Marti, J., 2008. The new worlwide collapse caldera database (CCDB): A tool for
1038 studying and understanding caldera processes. J. Volcanol. Geotherm. Res. 175, 334-354.
1039 Gouhier, J., Nougier, J., Nougier, D., 1974. Contribution à l'étude volcanologique du
1040 Cameroun (« Ligne du Cameroun »-Adamawa). Ann. Fac. Sci. Univ. Yaoundé Cameroun
1041 17, 3-48.
1042 Haggerty, S.E., 1976. Opaque mineral oxides in terrestrial igneous rocks. In: Rumble, D. III
1043 (Ed.) Reviews in mineralogy. Miner. Soc. Amer. Washington 3, pp. 101-300.
1044 Halliday, A.N., Dickin, A.P., Fallick, A.E., Fitton, J.G., 1988. Mantle dynamics: a Nd, Sr, Pb
1045 and O isotopic study of the Cameroon Line Volcanic Chain. J. Petrology 29, 181-211.

1046 Halliday, A.N., Davidson J.P., Holden, P., DeWolf, C., Lee, D.-C., Fitton, J.G., 1990. Trace-
1047 element fractionation in plumes and the origin of HIMU mantle beneath the Cameroon
1048 line. Nature 347, 523-528.

1049 Halliday, A.N., Davies, G.R., Lee, D.-C., Tommasini, C.R., Paslick, J.G., Fitton, J.G., James,
1050 D.E., 1992. Lead isotope evidence for young trace element enrichment in the oceanic
1051 upper mantle. Nature 359, 623-627.

1052 Hart, S.R., 1984. A large-scale isotope anomaly in the southern hemisphere mantle. Nature
1053 309, 753-757.

1054 Hoernle, K., Tilton, G., Schmincke, H.-U., 1991. Sr-Nd-Pb isotopic evolution of Gran
1055 Canaria: evidence for shallow enriched mantle beneath the Canary Islands. Earth Planet.
1056 Sci. Lett. 106, 44-63.

1057 Itiga, Z., Chakam Tagheu, P.J., Wotchoko, P., Wandji, P., Bardintzeff, J.-M., Bellon, H.,
1058 2004. La ligne du Cameroun : Volcanologie et géochronologie de trois régions (mont
1059 Manengouba, plaine du Noun et Tchabal Gangdaba). Géochronique 91, 13-16.

1060 Kagou Dongmo, A., 1998. Etude volcanologiquer, pétrographique et géochimique d'un
1061 volcan polygénique de la Ligne du Cameroun : le Mont Manengouba. Thèse 3ème cycle,
1062 Univ. Yaoundé I, Cameroon, 197p.

1063 Kagou Dongmo, A., 2006. Le mont Manengouba : évolution volcanologique, caractères
1064 magmatologiques et risques naturels; comparaison avec les monts Bambouto et Bamenda
1065 (Ligne du Cameroun). Thèse d'Etat, Univ. Yaoundé I, Cameroon, 239p.

1066 Kagou Dongmo, A., Wandji, P., Pouclet, A., Vicat, J.-P., Cheilletz, A., Nkouathio, D.G.,
1067 Alexandrov, P., Tchoua, F., 2001. Evolution volcanologique du mont Manengouba (Ligne
1068 du Cameroun), nouvelles données pétrographiques, géochimiques et géochronologiques.
1069 C. R. Acad. Sci. Paris, Sér IIa 333, 155-162.

1070 Kagou Dongmo, A., Nkouathio, D., Pouclet, A., Bardintzeff, J.-M., Wandji, P., Nono, A.,
1071 Guillou, H., 2010. The discovery of late Quaternary basalt on Mount Bambouto:
1072 Implications for recent widespread volcanic activity in the southern Cameroon Line. J.
1073 Afr. Earth Sci. 57, 96-108.

1074 Kamgang, P., Chazot, G., Njonfang, E., Ngongang, N.B., Tchoua, F., 2013. Mantle sources
1075 and magma evolution beneath the Cameroon Volcanic Line: Geochemistry of mafic rocks
1076 from the Bamenda Mountains (NW Cameroon). Gondwana Res. 24, 727-741.

1077 Kieffer, B., Arndt, N., Lapierre, H., Bastien, F., Bosch, D., Pecher, A., Yirgu, G., Ayalew, D.,
1078 Weis, D., Jerram, D.A., Keller, F., Meugniot, C., 2004. Flood and schield basalts from
1079 Ethiopia: Magmas from the African Superswell. J. Petrology 45, 793-834.
1080 Kinzler, R.J., 1997. Melting of mantle peridotite at pressures approaching the spinel to garnet
1081 transition: application to mid-ocean ridge basalt petrogenesis. J. Geophys. Res. 102, 853-
1082 874.
1083 Lamilen, B.D., 1989.Contribution à l'étude du complexe anorogénique du mont Koupé : un
1084 exemple de série alcaline incomplète. Thèse 3ème cycle, Univ. Yaoundé I, Cameroon,
1085 169p.
1086 Le Bas, M.J., Le Maitre, R.W., Streckeisen, A., Zanettin, B., 1986. A chemical classification
1087 of volcanic rocks based on the Total Alkali-Silica diagram. J. Petrology 27, 745-750.
1088 Lee, D.-C., Halliday, A.N., Fitton, J.G., Poli, G., 1994. Isotopic variations with distance and
1089 time in the volcanic islands of the Cameroon line: evidence for a mantle plume origin.
1090 Earth Planet. Sci. Lett. 123, 119-138.
1091 Lee, D.-C., Halliday, A.N., Davies, G.R., Essene, E.J., Fitton, J.G., Temdjim, R., 1996. Melt
1092 enrichment of shallow depleted mantle: a detailed petrological, trace element and isotopic
1093 study of mantle-derived xenoliths and megacrysts from the Cameroon Line. J. Petrology
1094 37, 415-441.
1095 Marzoli, A., Piccirillo, E.M., Renne, P.R., Bellieni, G., Iacumin, M., Nyobe, J.B., Tongwa,
1096 A.T., 2000. The Cameroon volcanic line revisited: Petrogenesis of continental basaltic
1097 magmas from lithospheric and asthenospheric mantle source. J. Petrology 41, 87-109.
1098 Matsukage, K.N., Oya, M., 2010. Petrological and chemical variability of peridotite xenoliths
1099 from the Cameroon volcanic line, West Africa: an evidence for plume emplacement. J.
1100 Miner. Petrol. Sci. 105, 57-69.
1101 Mbassa, B.J., Njonfang, E., Benoit, M., Kamgang, P., Grégoire, M., Duchene, S., Brunet, P.,
1102 Ateba, B, Tchoua, F., 2012. Mineralogy, geochemistry and petrogenesis of the recent
1103 magmatic formations from Mbengwi, a continental sector of the Cameroon Volcanic Line
1104 (CVL), Central Africa. Miner. Petrol. 106, 217-242.
1105 McDonough, W.F., Sun, S.-s., 1995. The composition of the Earth. Chemical Geology 120,
1106 223-253.
1107 Meyers, J.B., Rosendahl, B.R., Harrison, C.G.A., Ding, Z.-D., 1998. Deep-imaging seismic
1108 and gravity results from the offshore Cameroon Volcanic Line, and speculation of African
1109 hotlines. Tectonophysics 284, 31-63.

1110 Millet, M.-A., Doucelance, R., Schiano, P., David, K., Bosq, C., 2008. Mantle plume
1111 heterogeneity vs. shallow-level interactions: A case study, the São Nicolau Island, Cape
1112 Verde archipelago. J. Volcanol. Geotherm. Res. 176, 265-276.
1113 Mitchell-Thomé, R.C., 1980. The calderas of Macaronesia. Boletim do Museu Municipal do
1114 Funchal 33 (141), 5-43.
1115 Moreau, C., Regnoult, J.-M., Déruelle, B., Robineau, B., 1987. A new tectonic model for the
1116 Cameroon line, Central Africa. Tectonophysics 139, 317-334.
1117 Münker, C., Pfänder, J.A., Weyer, S., Büchl, A., Kleine, T., Mezger, K., 2003. Evolution of
1118 planetary cores and the Earth-Moon system from Nb/Ta systematics. Science 301, 84-87.
1119 Munro, D.C., Rowland, S.K., 1996. Caldera morphology in the western Galapagos and
1120 implications for volcano eruptive behaviour and mechanism of caldera formation. J.
1121 Volcanol. Geotherm. Res. 72, 85-100.
1122 Nkouandou, O.F., Ngounouno, I., Déruelle, B., Ohnenstetter, D., Montigny, R., Demaiffe, D.,
1123 2008. Petrology of the Moi-Pliocene volcanism to the North and East of Ngaoundéré
1124 (Adamawa, Cameroon). C. R. Geoscience 340, 28-37.
1125 Nkouathio, D.G., Ménard, J.-J., Wandji, P., Bardintzeff, J.-M., 2002. The Tombel graben
1126 (West Cameroon): a recent monogenetic volcanic field of the Cameroon Line. J. Afr.
1127 Earth Sci. 35, 285-300.
1128 Nkouathio, D.G., Kagou Dongmo, A., Bardintzeff, J.-M., Wandji, P., Bellon, H., Pouclet, A.,
1129 2008. Evolution of volcanism in graben and horst structures along the Cenozoic
1130 Cameroon Line (Africa): implications for tectonic evolution and mantle source
1131 composition. Miner. Petrol. 94, 287-303.
1132 Nsifa Nkonguin, E., Tchameni, R., Nédélec, A., Siqueira, R., Pouclet, A., Bascou, J., 2013.
1133 Structure and petrology of Pan-African nepheline syenites from the South West
1134 Cameroon; Implications for their emplacement mode, petrogenesis and geodynamic
1135 significance. J. Afr. Earth Sci. 87, 44-58.
1136 O'Neill, H.St.C., 1981. The transition between spinel lherzolite and garnet lherzolite and its
1137 use as a geobarometer. Contrib. Mineral. Petrol. 77, 185-194.
1138 O'Nions, R.K., Hamilton, P.J., Evensen, N.M., 1977. Variations in $^{143}Nd/^{144}Nd$ and $^{87}Sr/^{86}Sr$
1139 in oceanic basalts. Earth Planet. Sci. Lett. 34, 13-22.
1140 Paslick, C., Halliday, A., James, D., Dawson, J.B., 1995. Enrichment of the continental
1141 lithosphere by OIB melts: Isotopic evidence from the volcanic province of northern
1142 Tanzania. Earth Planet. Sci. Lett. 130, 109-126.

1143 Pasyanos, M.E., Nyblade, A.A., 2007. A top to bottom lithospheric study of Africa and
1144 Arabia. Tectonophysics 444, 27-44.
1145 Pik, R. Marty, B., Hilton, D.R., 2006. How many plumes in Africa? The geochemical point of
1146 view. Chemical Geology 226, 100-114.
1147 Pfänder, J.A., Münker, C., Stracke, A., Mezger, K., 2007. Nb/Ta and Zr/Hf in ocean island
1148 basalts – Implications for crust-mantle differentiation and the fate of niobium. Earth
1149 Planet. Sci. Lett. 254, 158-172.
1150 Pfänder, J.A., Jung, S., Münker, C., Stracke, A., Mezger, K., 2012. A possible high Nb/Ta
1151 reservoir in the continental lithospheric mantle and consequences on the global Nb budget
1152 – Evidence from continental basalts from Central Germany. Geochim. Cosmochim. Acta
1153 77, 232-251.
1154 Platz, T., Foley, S.F., André, L., 2004. Low-pressure fractionation of the Nyiragongo volcanic
1155 rocks, Virunga Province, D.R. Congo. J. Volcanol. Geotherm. Res. 136, 269-295.
1156 Poudjom Djomani, Y.H., Nnange, J.M., Diament, M., Ebinger, C.J., Fairhead, J.D., 1995.
1157 Effective elastic thickness and crustal thickness variations in west-central Africa inferred
1158 from gravity data. J. Geophys. Res. 100, 22047-22070.
1159 Poudjom Djomani, Y.H., Diament, M., Wilson, M., 1997. Lithospheric structure across the
1160 Adamawa plateau (Cameroon) from gravity studies. Tectonophysics 273, 317-327.
1161 Putirka, K., 2008. Thermometers and barometers for volcanic systems. In: Putirka, K.,
1162 Tepley, F. (Eds.) Minerals, inclusions and volcanic processes. Review in mineralogy and
1163 geochemistry, Miner. Soc. Am. 69, pp. 61-120.
1164 Putirka, K.D., Mikaelian, H., Ryerson, F., Shaw, H., 2003. New clinopyroxene-liquid
1165 thermobarometers for mafic, evolved, and volatile-bearing lava compositions, with
1166 applications to lavas from Tibet and the Snake River Plain, Idaho. Am. Mineralogist 88,
1167 1542-1554.
1168 Putirka, K.D., Perfit, M., Ryerson F.J., Jackson, M. G., 2007. Ambient and excess mantle
1169 temperatures, olivine thermometry, and active vs.. passive upwelling. Chemical Geology
1170 241, 177-206.
1171 Rankenburg, K., Lassiter, J.C., Brey, G., 2005. The role of continental crust and lithospheric
1172 mantle in the genesis of Cameroon Volcanic Line lavas: Constraints from isotopic
1173 variations in lavas and megacrysts from the Biu and Jos Plateaux. J. Petrology 46, 169-
1174 190.
1175 Roeder, P.L., Emslie, R.F., 1970. Olivine-liquid equilibrium. Contrib. Mineral. Petrol. 29,
1176 275-289.

1177 Rogers, N.W., De Mulder, M., Hawkesworth, C.J., 1992. An enriched mantle source for
1178 potassic basanites: evidence from Karisimbi volcano, Virunga volcanic province, Rwanda.
1179 Contrib. Mineral. Petrol. 111, 543-556.
1180 Rogers, N.W., James, D., Kelley, S.P., De Mulder, M., 1998. The generation of potassic lavas
1181 from the Eastern Virunga Province, Rwanda. J. Petrology 39, 1223-1247.
1182 Rogers, N.W., Macdonald, R., Fitton, J.G., George R., Smith M., Barreiro, B., 2000. Two
1183 mantle plumes beneath the East African Rift system: Sr, Nd and Pb isotope evidence from
1184 Kenya rift basalts. Earth Planet. Sci. Lett. 176, 387-400.
1185 Rollinson, H., 1993. Using geochemical data: Evaluation, presentation, interpretation.
1186 Longman Group UK Limited, 352 pp.
1187 Rudnick, R.L., McDonough, W.F., Chappell, B.W., 1993. Carbonatite metasomatism in the
1188 northern Tanzanian mantle: petrographic and geochemical characteristics. Earth Planet.
1189 Sci. Lett. 114, 463-475.
1190 Rudnick, R.L., Gao, S., 2003. Composition of the continental crust. In: Holland, H.D.,
1191 Turekian, K.K. (Eds.) Treatise on geochemistry, Vol. 3 The crust, pp 1-64, Elsevier-
1192 Pergamon, Oxford, 683p.
1193 Salters, V.J.M., Longhi, J., 1999. Trace element partitioning during the initial stages of
1194 melting beneath mid-ocean ridges. Earth Planet. Sci. Lett. 166, 15-30.
1195 Salters, V.J.M., Longhi, J.E., Bizimis, M., 2002. Near mantle solidus trace element
1196 partitioning at pressure up to 3.4 GPa. Geochem. Geophys. Geosyst. 3.
1197 doi:10.1029/2001GC000148.
1198 Salters, V.J.M., Stracke, A., 2004. Composition of the depleted mantle. Geochem. Geophys.
1199 Geosyst. 5, 27. doi:10.1029/2003GC000597, Q05004.
1200 Schilling, M., Conceição, R.V., Mallmann, G., Koester, E., Kawashita, K., Hervé, F., Morata,
1201 D., Motoki, A., 2005. Spinel-facies mantle xenoliths from Cerro Redondo, Argentine
1202 Patagonia: Petrographic, geochemical, and isotopic evidence of interaction between
1203 xenoliths and host basalt. Lithos 82, 485-502.
1204 Steiger, R.H., Jäger, E., 1977. Subcommission on geochronology: convention on the use of
1205 decay constants in geo- and cosmochronology. Earth Planet. Sci. Lett. 36, 359-362.
1206 Stracke, A., Hofmann, W., Hart, S.R., 2005. FOZO, HIMU, and the rest of the mantle zoo.
1207 Geochem. Geophys. Geosyst. 6, Q05007, doi:10.1029/2004GC000824.
1208 Stormer, J.C., 1983. The effects of recalculation on estimates of temperature and oxygen
1209 fugacity from analyses of multicomponent iron-titanium oxides. Am. Mineralogist 68,
1210 586-594.

1211 Suh, C.E., Sparks, R.S.J., Fitton, J.G., Ayonghe, S.N., Annen, C., Nana, R., Luckman, A.,
1212 2003. The 1999 and 2000 eruptions of Mount Cameroon: eruption behaviour and
1213 petrochemistry of lava. Bull. Volcanol. 65, 267-281.
1214 Sun, S.S., McDonough, W.F., 1989. Chemical and isotopic systematics of oceanic basalts:
1215 implications for mantle composition and processes. In: Saunders, A.D., Norry, M.J. (Eds.)
1216 Magmatism in ocean basins. Geol. Soc. London, Special Publication 42, pp 313-345.
1217 Tchoua, F., 1974. Contribution à l'étude géologique et pétrologique de quelques volcans de la
1218 «Ligne du Cameroun» (Monts Manengouba et Bambouto). Thèse 3ème cycle, Univ.
1219 Clermont-Ferrand, France.
1220 Temdjim, R., 2012. Ultramafic xenoliths from Lake Nyos area, Cameroon volcanic line,
1221 West-central Africa: Petrography, mineral chemistry, equilibration conditions and
1222 metasomatic features. Chemie der Erdre 72, 39-60.
1223 Temdjim, R., Boivin, P., Chazot, G., Robin, C., Rouleau, E., 2004. L'hétérogénéité du
1224 manteau supérieur à l'aplomb du volcan de Nyos (Cameroun) révélée par les enclaves
1225 ultrabasiques. C. R. Geoscience 336, 1239-1244.
1226 Thornton, C.P., Tuttle, O.F., 1960. Chemistry of igneous rocks. I, differentiation index. Am.
1227 J. Sci. 258, 664-684.
1228 Tokam, A.P.K., Tabod, C.T., Nyblade, A.A., Julia, J., Wiens, D.A., Pasyanos, M.E., 2010.
1229 Structure of the crust beneath Cameroon, West Africa, from the joint inversion of
1230 Rayleigh wave group velocities and receiver functions. Geophysical Journal International
1231 183, 1061-1076.
1232 Vicat, J.-P., Pouclet, A., Bellion, Y., Doumnang, J.-C., 2002. Les rhyolites hyperalcalines
1233 (pantellérites) du lac Tchad. Composition et signification tectonomagmatique. C. R.
1234 Géoscience 224, 885-891.
1235 Wandji. P., Tsafack, J.P.F., Bardintzeff, J.M., Nkouathio, D.G., Kagou Dongmo, A., Bellon,
1236 H., Guillou, H., 2009. Xenoliths of dunites, wehrlites and clinopyroxenites in the
1237 basanites from Batoke volcanic cone (Mount Cameroon, Central Africa): petrogenetic
1238 implications. Miner. Petrol. 96, 81-98.
1239 Walter, M.J., 1998. Melting of garnet peridotite and the origin of komatiite and depleted
1240 lithosphere. J. Petrology 39, 29-60.
1241 Workman, R.K., Hart, S.R., 2005. Major and trace element composition of the depleted
1242 MORB mantle (DMM). Earth Planet. Sci. Lett. 231, 53-72.

1243 Wotchoko, P., Wandji, P., Bardintzeff, J.-M., Bellon, H., 2005. Données pétrologiques et
1244 géochronologiques nouvelles sur le volcanisme alcalin néogène à récent de la rive ouest
1245 du Noun (plaine du Noun, Ligne du Cameroun). Review Bulgarian Geol. Soc. 66, 97-105.

1246 Yokoyama, T., Aka, F.T., Kusakabe, M., Nakamura, E., 2007. Plume-lithosphere interaction
1247 beneath Mt. Cameroon volcano, West Africa: Constraints from ^{238}U-^{230}Th-^{226}Ra and Sr-
1248 Nd-Pb isotope systematics. Geochim. Cosmochim. Acta 71, 1835-1854.

1249 Youmen, D., Schmincke, H.-U., Lissom, J., Etame, J., 2005. Données géochronologiques :
1250 mise en évidence des différentes phases volcaniques au Miocène dans les monts
1251 Bambouto (Ligne du Cameroun). Sci. Technol. Dev. 11, 49-57.

1252 Zack, T., Foley, S.F., Jenner, G.A., 1997. A consistent partition coefficient set for
1253 clinopyroxene, amphibole and garnet from laser ablation microprobe analysis of garnet
1254 pyroxenites from Kakanui, New Zealand. Neues Jahrbuch für Mineralogie, Abh. 172, 23-
1255 41.

1256 Zindler, A., Hart, S.R., 1986. Chemical geodynamics. Ann. Rev. Earth Planet. Sci. 14, 493-
1257 571.

1258
1259 **Caption**

1260

1261 **Fig. 1.** A) The Mount Manengouba and the great volcanoes in the Cameroon Line. B) Main
1262 structural features of the Mt Manengouba are on a Digital Elevation Model (Image Landsat 7
1263 ETM Satellite Imagery, data set: SRTM, Producer: USGS/GLCF, Date 2000, ID 045-76
1264 Cameroon). Nk, Nkongsamba town. N, Nlonako, and K, Koupé, Eocene syenitic alkaline
1265 intrusions.

1266

1267 **Fig. 2.** Geological map of the Manengouba. Main units of the volcano: 1) stacked lavas of the
1268 middle and low slopes of the shield, 2) the Eboga stratovolcano, 3) the Elengoum Extrusive
1269 Complex, and 4) the flank cones and flows of the late parasitic activity.

1270

1271 **Fig. 3.** Detailed map of the Eboga caldera, Elengoum complex and south-eastern low flank
1272 showing the pre-Manengouba flows preserved along the Nlonako syenite massif. Most of the
1273 age data locate in this area. DS, phreatomagmatic crater of Djeu Sey; LF, maar of the “Lac de
1274 la femme”; LH, maar of the “Lac de l’homme”; MB, plug-dome of Mbouroukou; SCSV,
1275 supra-caldera strombolian volcanic complex.

Fig. 4. Detailed map of the north-western low slope showing the age data of flank activity and of the pre-Manengouba trachy-phonolite extrusions of Ekomane and Bakossi.

Fig. 5. Ar/Ar plateau ages.

Fig. 6. Sketch of the four stages of the volcanic activities.

Fig. 7. Nomenclature of the Manengouba lavas. A, SiO_2 vs. $Na_2O + K_2O$ diagram after Le Bas et al. (1986). B, DI vs. normative quartz or nepheline diagram displaying the under-saturation of the series. DI, Differentiation Index of Thornton and Tuttle (1960).

Fig. 8. Fo% vs. CaO (wt.%) diagram of olivines: A) Group 1; B) Group 2. In both groups, phenocrysts, microcrysts, as well as xenocrysts crystallized from a related suite of magmas.

Fig. 9. Mg# vs. Fo diagram of whole rock and olivine compositions. The Mg number is calculated assuming a wt.% Fe_2O_3/FeO ratio of 0.15. The olivine-liquid equilibrium temperature is calculated after the equation (4) of Putirka et al. (2007). The liquid temperature is calculated after the equation (15) of Putirka (2008). The pressure of the main magma chamber is estimated at 1 GPa according to the clinopyroxene-liquid thermobarometer of Putirka et al. (2003) and Putirka (2008). Distribution coefficient K_D = (XOl/FeO)/(XLiq/FeO) x (XLiq/MgO)/(XOl/MgO) of Roeder and Emslie (1970). Same symbols as for Figure 8.

Fig. 10. Fe^{2+}/ (Fe^{2+}+Mg) vs. Ti / (Ti+Al+Cr) diagram of Ti-magnetites of Groups 1 and 2. Projections from the multicomponent spinel prism (Haggerty, 1976). From basanite to hawaiite, magnetites display decreasing Ti and Fe^{2+} ratios due to decreasing Al and Mg contents in Group 1, and decreasing Cr, Al and Mg contents in Group 2. Mugearite and benmoreite phenocrysts are similar to those of hawaiite, while microcrysts are depleted in Al and Mg. Trachyte microcrysts only contain Fe and Ti.

Fig. 11. 10^4/T(K) vs. ln (K_D^{Fe-Mg}) of pyroxenes, according to Putirka et al. (2003), for illustrating the distribution of phenocrysts in equilibrium with liquids, microcrysts of the evolved groundmasses, and xenocrysts inherited from more mafic magmas crystallized in the magma chamber. Pyroxenes of the more differentiated benmoreites and trachytes could be

either xenocrysts or phenocrysts of a liquid that was disturbed by post-pyroxene crystallization processes. K_D is calculated assuming a wt.% Fe_2O_3/FeO ratio of 0.15 for liquids and using the pyroxene calculated FeO contents.

Fig. 12. Mg-Ca-Fet+Mn diagram of Group 1 pyroxenes.

Fig. 13. Al^{IV} vs. Al^{VI}, Ti vs. Al^{VI}, and Ti vs. Na diagrams. Symbols as for Figure 12.

Fig. 14. Mg-Ca-Fet+Mn diagram of Group 2 pyroxenes.

Fig. 15. Al^{IV} vs. Al^{VI}, Fe^{2+} vs. Ti, and Al vs. Ti diagrams. Symbols as for Figure 14.

Fig. 16 A and B. MgO wt.% vs. major and minor elements covariation diagrams. Symbols as for Figure 7.

Fig. 17. Chondrite normalized rare earth element patterns for A) stages 1 and 2 lavas, B) stage 3 lavas, C) stage 4 lavas, and D) pre-Manengouba lavas. Normalizing values after McDonough and Sun (1995).

Fig. 18. N-MORB normalized incompatible trace element patterns for A) stages 1 and 2 lavas, B) stage 3 lavas, C) stage 4 lavas, and D) pre-Manengouba lavas. Normalizing values after Sun and McDonough (1989).

Fig. 19. Th/Pb vs. Ce/Pb diagram showing the crustal assimilation in the Manengouba trachytes and in the Bakossi phonolites. Bulk continental crust after Rudnick and Gao (2003).

Fig. 20. Covariation of MgO and vs. Ni for Group 1 (Stages 1 and 2) and Group 2 (Stage 4) mafic lavas. Partial melting area of primitive mantle drawn after Class et al. (1994). CT46 and EB20 are close to the primitive mantle melts with, respectively Mg# of 60 and 63 and Ni (ppm) of 222 and 238. Parental magmas may average 9 to 10 wt.% of MgO and 250 to 290 ppm of Ni in resulting from about 5% of partial melting. The two almost similar fractional trends of the two magmatic groups extend until 15 to 20% of olivine fractionation.

Fig. 21. N-MORB normalized incompatible trace element patterns restricted to mafic lavas of the Manengouba main building (Group 1, stages 1 and 2) and of the late parasitic activity (Group 2, stage 4). OIB pattern after Sun and McDonough (1989).

Fig. 22. A) Ta/Yb vs. Th/Yb diagram. **B)** Zr/Hf vs. Nb/Ta diagram.
PM, N-MORB, E-MORB, and OIB from Sun and McDonough (1989); DMM from Salters and Stracke (2004); chondritic values from Münker et al. (2003); MORB, OIB, and continental basalts fields after Pfänder et al. (2007); Kenya rift and Virunga fields drawn with the data of Rogers et al. (1992, 1998, 2006), Platz et al. (2004), and Chakrabarti et al. (2009).

Fig. 23. A) La vs. La/Sm and **B)** La/Sm vs. Sm/Yb diagrams for determining the enrichment of the source and the partial melting degrees of the mantle source. The La vs. La/Sm diagram suggests a source enrichment similar to that of the E-MORB and a degree of partial melting between 2% and 5% on the lherzolite melt curves. Once this source is admitted, the La/Sm vs. Sm/Yb diagram suggests a spinel-garnet lherzolite source composition with a 50:50 mixture of spinel and garnet. Modal compositions of spinel-lherzolite (olivine 53%, OPX 27%, CPX 17%, spinel 3%) and garnet-lherzolite (olivine 60%, OPX 20%, CPX 10%, garnet 10%) are after Kinzler (1997) and Walter (1998). Mineral/melt partition coefficients for basaltic liquids are after the compilation of Rollinson (1993). Primitive Mantle (PM), N-MORB, and E-MORB compositions are from Sun and McDonough (1989). Depleted MORB mantle (DMM) from Salters and Stracke (2004).

Fig. 24. A, B, and C, $^{86}Sr/^{87}Sr$ vs. $^{143}Nd/^{144}Nd$, $^{206}Pb/^{204}Pb$ vs. $^{207}Pb/^{204}Pb$, and $^{206}Pb/^{204}Pb$ vs. $^{208}Pb/^{204}Pb$ diagrams (time corrected values) for the Manengouba and pre-Manengouba lava analyses of this study completed by the Manengouba mafic lava analyses of Halliday et al. (1988 and 1990). These data are compared with the whole data for mafic lavas of the Cameroon Volcanic Line plotted in six fields from north to south: Biu-Mandara, Ngaoundéré, middle continental shields (Oku, Bamenda, Bambouto, Manengouba, and Tombel), continent-ocean boundary (Mt Cameroon, Etinde, Bioko), Principe-São Tomé, and Pagalu. See text for the references. DMM, HIMU, PREMA, BSE, EM1, and EM2 after O'Nions et al. (1977), Zindler and Hart (1986), Rollinson (1993); FOZO after Stracke et al. (2005); EDMM after Workman and Hart (2005).

D, $^{86}Sr/^{87}Sr$ vs. $^{206}Pb/^{204}Pb$ diagram for showing the three theoretical components of magmatic sources of the Cameroon Volcanic Line. DC, depleted component; RC, radiogenic component; EC, enriched component. Explanation of the trends, see text.

Table 1. New radiochronological data. K/Ar analyses were done by H. Bellon at the Laboratory of Geochronology of the "Université de Bretagne Occidentale", Brest, France. Ar/Ar analyses were done by G. Ruffet at the Laboratory of Geochronology of the "Université de Rennes 1", Rennes, France. CNRS (CNRS/INSU) UMR 6118, Géosciences Rennes, 35042 Rennes Cedex, and Université de Rennes I, Géosciences Rennes, 35042 Rennes Cedex, France. Age calculation was carried on using the constants of Steiger and Jäger (1977). Data, parameters used for Ar/Ar calculations (isotopic ratios measured on K, Ca and Cl pure salts; mass discrimination; atmospheric argon ratios; J parameter; decay constants) and reference sources are available in the supplementary data repository.

Table 2. Report of the available chronological data for the Manengouba area distributed in age groups.

Table 3. Petrographical composition of Group 1 (A) and Group 2 (B) lavas.
X'USP, apparent mole fraction of ulvöspinel according to Stormer (1983).

Table 4. Representative chemical analyses of minerals: A, Olivine; B, Magnetite; C, Ilmenite. D, Clinopyroxene; E, Amphibole; F, Mica; G, Feldspar.
Alk-B, alkaline basalt; Ank, ankaratrite; Bn, benmoreite; Bs, basanite; Na-Bs, sodic basanite; H, hawaiite; M, mugearite; Tr, trachyte.

Table 5. Chemical analyses of the rocks. Petrographical facies as for Table 4 plus Na-H, sodic hawaiite; Ph, phonolite; Rh, rhyolite; Tr-Ph, trachy-phonolite. DI (Differentiation Index) after Thornton and Tuttle (1960). Analyses by ICP-AES (major elements) and ICP-MS (minor and trace elements) at the Centre de Recherches Pétrographiques et Géochimiques (CRPG, CNRS) of Nancy, France.

Table 6. Sr, Nb, and Pb isotope data. MS measurements (VG Sector 54 TIMS) at the Université libre of Bruxelles (Belgium)**.** Analyst: Daniel Demaiffe.

KPB-Table 1

K/Ar analyses

			K_2O (wt%)	$^{40}Ar^*$ %	$^{40}Ar^*$ /g (10^{-7} cm^3)	^{36}Ar Exp (10^{-9} cm^3)	Age (Ma) ± 1 σ
CT107	Tr	Essom peak	5.31	86.5	23.29	1.24	13.56 ± 0.39
CT103	Ph	W-Bangem	5.26	82.5	12.82	0.93	7.55 ± 0.18
CT155	Rh	Ekom	4.46	41.6	1.46	0.7	1.02 ± 0.03
CT108	H	Mboassoum (flank activity)	1.25	6.1	0.18	0.94	0.45 ± 0.07
CT47	H	Melong (flank activity)	1.38	9.55	0.2	0.51	0.45 ± 0.04
CT52	M	Nyam-Enyandong (flank activity)	2.19	1.6	0.28	6.27	0.40 ± 0.23
CT105	T-P	W-Bangem (flank activity)	4.12	11.9	0.28	0.71	0.21 ± 0.02
CT55	Bs	Ekoh (flank activity)	1.7	3.5	0.059	1.662	0.11 ± 0.03

$^{40}Ar/^{39}Ar$ analyses

				Plateau Age ± 1 σ	Isochron Age ± 1 σ	MSWD	$(^{40}Ar/^{36}Ar)_i$ ± 1 σ
KBT5	H	Nkongsamba, NE-Nlonako		9.37 ± 0.05	9.31 ± 0.63	1.24	305.8 ± 13.9
PTE6	Tr	Elengoum		0.89 ± 0.02	0.88 ± 0.05	1.2	305.7 ± 5.6
KEB19	H	Eboga caldera SE floor	flow from cone # 1	0.46 ± 0.05	0.36 ± 0.13	0.05	301.5 ± 4.0
KEB32	H	Eboga caldera SE floor	flow from cone # 1	0.33 ± 0.02	0.34 ± 0.03	0.99	292.7 ± 6.1
KTC1	B	W-Ndougué	flank activity	0.24 ± 0.07	0.22 ± 0.10	2.68	284.4 ± 5.1
KEB33	H	Eboga caldera NW floor	flow from cone # 2	0.14 ± 0.04	0.16 ± 0.07	0.49	291.5 ± 4.8

KPB-Table 2

Pre-Manengouba volcanic rocks				
Northwestern and eastern borders				
Extrusions of trachyte and phonolite and mafic lava flows				
CT107	Tr	13.56 ± 0.39	Essom peak	K4
C54	Tr	11.82 ± 0.47	Ekomane	K2
KBT5	H	9.37 ± 0.05	Nkongsamba	A1
CT103	Ph	7.55 ± 0.18	W-Bangem	K4

MANENGOUBA				
Mafic shield volcano and strato-volcano building (Early Manengouba and Eboga) (stages 1				
x	B	1.55 ± 0.10	Nkongsamba area	K1
C55	B	0.94 ± 0.06	Ndoungué	K2

Acidic extrusions (Elengoum Extrusive Complex) (stage 3)				
CT155	Rh	1.02 ± 0.03	NE-Ekom	K4
PTE6	Tr	0.89 ± 0.02	Central Elengoum	A1
PT3	Tr	0.70 ± 0.01	South Elengoum	K3

Post-caldera and flank activities (stage 4)				
CT108	H	0.45 ± 0.07	Mboassoum	K4
CT47	H	0.45 ± 0.04	Melong	K4
CT52	M	0.40 ± 0.23	Enyandong	K4
C52	B	0.40 ± 0.04	Njinjo	K2
KEB19	H	0.36 ± 0.13	Eboga caldera	A1
KEB32	H	0.33 ± 0.02	Eboga caldera	A1
KTC1	B	0.22 ± 0.10	W-Ndouguè	A1
CT105	TP	0.21 ± 0.02	W-Bangem	K4
SP5	H	0.20 ± 0.10	SE-Nkongsamba	K3
KEB33	H	0.16 ± 0.07	Eboga caldera	A1
CT55	Bs	0.11 ± 0.03	Ekoh	K4

(K1) Gouhier et al. (1974)
(K2) Dunlop (1983)
(K3) Kagou et al. (2001)
(K4) new K/Ar data
(A1) new $^{40}Ar/^{39}Ar$ data

Table 3A Magmatic Group # 1

Group 1	Basanite - Alkali Basalt	Hawaiite
Xenocrysts	0.50%	1%
Olivine	84.5 < Fo < 85.2 0.25 < CaO wt% < 0.30	83.2 < Fo < 84.5 0.23 < CaO wt% < 0.28
Clinopyroxene	40.5 < XMg% < 40.8 13.6 < XFet+Mn% < 13.8 45.4 < XCa% < 45.9	40.5 < XMg% < 43.4 12.4 < XFet+Mn% < 14.1 42.4 < XCa% < 46.7
Feldspar	An 51-40	An 62-59
Phenocrysts and Microphenocrysts	10 - 15 %	10 - 15 %
Olivine	77.1 < Fo < 81.7 0.19 < CaO wt% < 0.25	69.0 < Fo < 79.0 0.22 < CaO wt% < 0.29
Magnetite	17.1 < TiO_2 wt% < 18.6 4.2 < Al_2O_3 wt% < 4.8 4.9 < MgO wt% < 6.6 0.48 < X'Usp < 0.51	17.2 < TiO_2 wt% < 20.9 1.8 < Al_2O_3 wt% < 5.2 2.2 < MgO wt% < 4.6 0.50 < X'Usp < 0.64
Ilmenite	no accurate analyses	X'Ilm = 0.95 Fe^{3+}/Fe^{2+} = 0.12
Clinopyroxene	39.9 < XMg% < 44.0 13.5 < XFet+Mn% < 14.8 41.8 < XCa% < 46.5	39.4 < XMg% < 46.0 11.7 < XFet+Mn% < 16.6 41.6 < XCa% < 47.5
Amphibole		
Biotite		
Feldspar	An 66-60	An 60-51
Microcrysts		
Olivine	74.1 < Fo < 78.4 0.16 < CaO wt% < 0.28	57.9 < Fo < 70.5 0.19 < CaO wt% < 0.44
Magnetite	18.3 < TiO_2 wt% < 20.7 1.9 < Al_2O_3 wt% < 2.4 4.0 < MgO wt% < 4.9 0.50 < X'usp < 0.61	18.3 < TiO_2 wt% < 21.1 2.3 < Al_2O_3 wt% < 3.0 1.8 < MgO wt% < 2.0 0.57 < X'usp < 0.64
Ilmenite		X'ilm = 0.93 Fe^{3+}/Fe^{2+} = 0.18
Clinopyroxene	38.9 < XMg% < 45.4 14.5 < XFet+Mn% < 17.8 40.2 < XCa% < 45.8	39.6 < XMg% < 42.8 14.7 < XFet+Mn% < 15.8 41.7 < XCa% < 44.6
Feldspar	An 60-51	An 53-46

Table 3B Magmatic Group # 2

Group 2	Basanite - Alkali Basalt	Hawaiite	Mugearite
Xenocrysts	0.50%	1%	2%
Olivine	87.0 < Fo < 86.5 0.25 < CaO wt% < 0.20	85.0 < Fo < 82.5 0.21 < CaO wt% < 0.19	77.9 < Fo < 77.3 0.20 < CaO wt% < 0.18
Pyroxene	41.1 < XMg% < 47.9 10.5 < XFet+Mn% < 13.6 41.6 < XCa% < 46.0	41.1 < XMg% < 45.2 9.2 < XFet+Mn% < 15.0 43.0 < XCa% < 46.3	38.1 < XMg% < 42.8 12.0 < XFet+Mn% < 15.3 41.7 < XCa% < 48.6
Feldspar	An 43-39		An 28-22
Phenocrysts and Microphenocrysts	10 - 15 %	5 - 10%	5 - 10%
Olivine	83.0 < Fo < 78.1 0.30 < CaO wt% < 0.20	78.7 < Fo < 70.5 0.37 < CaO wt% < 0.21	77.1 < Fo < 64.4 0.32 < CaO wt% < 0.16
Magnetite	13.3 < TiO_2 wt% < 17.9 4.8 < Al_2O_3 wt% < 8.0 5.0 < MgO wt% < 5.5 3.5 < Cr_2O_3 < 12.3 0.60 < X'usp < 0.65	16.8 < TiO_2 wt% < 22.1 2.7 < Al_2O_3 wt% < 5.1 3.5 < MgO wt% < 5.5 0.1 < Cr_2O_3 < 2.7 0.53 < X'usp < 0.69	17.2 < TiO_2 wt% < 21.8 2.7 < Al_2O_3 wt% < 5.7 2.7 < MgO wt% < 4.6 0.54 < X'usp < 0.67
Ilmenite	X'ilm = 0.96 Fe^{3+}/Fe^{2+} = 0.09	X'ilm = 0.96 Fe^{3+}/Fe^{2+} = 0.10	X'ilm = 0.94 Fe^{3+}/Fe^{2+} = 0.13
Pyroxene	33.8 < XMg% < 48.5 11.2 < XFet+Mn% < 17.6 38.6 < XCa% < 50.2	40.0 < XMg% < 44.9 11.9 < XFet+Mn% < 17.1 41.1 < XCa% < 45.1	37.2 < XMg% < 43.6 11.9 < XFet+Mn% < 16.9 42.1 < XCa% < 48.1
Amphibole	0.74 <Mg/Mg+Fe^{2+}< 0.79 3.7 < TiO_2 wt% < 4.7	0.67 <Mg/Mg+Fe^{2+}< 0.72 5.2 < TiO_2 wt% < 5.8	0.67 <Mg/Mg+Fe^{2+}< 0.79 2.6 < TiO_2 wt% < 5.8
Biotite			0.76 <Mg/Mg+Fe^{2+}< 0.80 4.4 < TiO_2 wt% < 5.9
Feldspar	An 66-60	An 60-50	An 55-43
Microcrysts			
Olivine	78.7 < Fo < 72.2 0.40 < CaO wt% < 0.16	71.2 < Fo < 65.8 0.35 < CaO wt% < 0.27	62.9 < Fo < 54.0 0.42 < CaO wt% < 0.26
Magnetite	16.7 < TiO_2 wt% < 20.1 3.3 < Al_2O_3 wt% < 5.4 3.4 < MgO wt% < 5.1 0.51 < X'usp < 0.63	20.5 < TiO_2 wt% < 22.9 0.3 < Al_2O_3 wt% < 1.9 0.3 < MgO wt% < 3.0 0.48 < X'usp < 0.64	21.2 < TiO_2 wt% < 23.2 1.5 < Al_2O_3 wt% < 2.8 1.7 < MgO wt% < 3.2 0.55 < X'usp < 0.70
Ilm		X'ilm = 0.93 Fe^{3+}/Fe^{2+} = 0.15	
Px	37.2 < XMg% < 43.4 10.6 < XFet+Mn% < 17.5 41.3 < XCa% < 46.7	37.3 < XMg% < 42.4 14.5 < XFet+Mn% < 21.8 40.7 < XCa% < 45.2	35.1 < XMg% < 36.8 19.2 < XFet+Mn% < 21.2 43.7 < XCa% < 44.8
F	An 62-52	An 55-45	An 47-32 An 11-6, Or 32-46

Table 4. Selected chemical analyses of minerals. A, Olivine

Manengouba, stage 1

#	MA2b	CT45	CT45	CT45	ML2	ML2
Petrographical facies	Bs	alk-B	alk-B	alk-B	H	H
Mineral type	xenocryst	phenocryst	microcryst	microcryst	xenocryst	phenocryst
SiO_2	40.82	39.09	38.20	38.92	40.39	39.45
TiO_2	0.04	0.00	0.05	0.08	0.03	0.03
Al_2O_3	0.03	0.00	0.00	0.00	0.08	0.04
FeO	14.29	16.87	19.32	21.98	14.86	19.66
MnO	0.19	0.27	0.47	0.52	0.22	0.27
MgO	46.81	42.79	40.21	39.13	46.13	42.00
CaO	0.30	0.19	0.16	0.28	0.23	0.22
NiO		0.08	0.00	0.42		
Total	102.48	99.29	98.41	101.33	101.94	101.67
Si	0.996	0.999	0.998	1.000	0.994	0.995
Ti	0.001	0.000	0.001	0.002	0.001	0.001
Al	0.001	0.000	0.000	0.000	0.002	0.001
Fe^{2+}	0.292	0.360	0.422	0.472	0.306	0.415
Mn	0.004	0.006	0.010	0.011	0.005	0.006
Mg	1.702	1.630	1.566	1.498	1.692	1.580
Ca	0.008	0.005	0.004	0.008	0.006	0.006
Ni	0.000	0.002	0.000	0.009	0.000	0.000
Total	3.003	3.001	3.001	2.999	3.005	3.003
% Fo	85.21	81.65	78.36	75.60	84.50	78.97
% Fa	14.79	18.35	21.64	24.40	15.50	21.03

Table 4. Selected analyses of minerals. B, Magnetite

	Manengouba, stage 1				Manengouba, stage 2		
#	MA2b	MA2b	ML2	ML2	NS2	Eb11	Eb11
Petrographical facies	Bs	Bs	H	H	H	M	M
Mineral type	phenocryst	microcryst	phenocryst	microcryst	phenocryst	phenocryst	microcryst
SiO_2	0.01	0.00	0.05	0.03	0.02	0.05	0.04
TiO_2	17.51	18.59	20.85	19.25	17.23	16.21	17.11
Al_2O_3	4.83	4.15	5.17	2.30	1.83	2.47	2.02
Cr_2O_3	0.03	0.03	0.08	0.06	0.02	0.12	0.01
FeO	69.24	68.05	67.73	73.12	73.75	77.34	75.59
MnO	0.56	0.38	0.50	0.71	0.46	0.67	0.85
MgO	6.25	6.55	4.54	1.78	2.22	1.16	0.47
Total	98.43	97.75	98.92	97.25	95.51	98.02	96.09
Si	0.003	0.000	0.014	0.009	0.004	0.015	0.012
Al	1.578	1.367	1.706	0.797	0.642	0.850	0.715
Ti	3.650	3.906	4.390	4.254	3.862	3.558	3.863
Fe^{3+}	7.111	6.814	5.468	6.664	7.621	7.977	7.532
Fe^{2+}	8.939	9.088	10.391	11.306	10.766	10.902	11.449
Mg	2.582	2.728	1.895	0.780	0.986	0.505	0.210
Mn	0.131	0.090	0.119	0.177	0.115	0.166	0.216
Cr	0.007	0.007	0.018	0.014	0.004	0.028	0.002
Total	24.000	24.000	24.000	24.000	24.000	24.000	24.000

Table 4. Selected analyses of minerals. C, Ilmenite

	Manengouba, stage 2				**Manengouba, stage 3**	
#	NS2	EB30	Eb11	Eb11	EL4	Eb17
Petrographical facies	H	M	M	M	Bn	Bn
Mineral type	microcryst	phenocryst	phenocryst	microcryst	phenocryst	microcryst
SiO_2	0.00	0.00	0.00	0.00	0.00	0.00
TiO_2	49.71	50.17	49.66	48.22	48.92	51.12
Al_2O_3	0.36	0.14	0.20	0.43	0.47	0.04
Cr_2O_3	0.00	0.00	0.03	0.00	0.00	0.00
FeO	41.92	42.46	45.39	48.20	44.44	44.69
MnO	0.63	0.77	0.94	0.81	0.64	1.38
MgO	4.89	4.01	3.42	1.81	5.45	0.86
CaO	0.03	0.03	0.03	0.03	0.05	0.05
Total	97.54	97.58	99.67	99.50	99.97	98.14
Si	0.000	0.000	0.000	0.000	0.000	0.000
Al	0.021	0.008	0.012	0.025	0.027	0.002
Ti	1.854	1.885	1.834	1.804	1.770	1.962
Fe^{3+}	0.263	0.218	0.315	0.359	0.424	0.072
Fe^{2+}	1.476	1.556	1.549	1.647	1.364	1.836
Mg	0.361	0.299	0.250	0.134	0.391	0.065
Mn	0.026	0.033	0.039	0.034	0.026	0.060
Cr	0.000	0.000	0.001	0.000	0.000	0.000
Ca	0.001	0.002	0.002	0.002	0.003	0.003
Total	4.002	4.000	4.001	4.003	4.002	3.998

Table 4. Selected analyses of minerals. D, Pyroxenes

Manengouba, stage 1

#	MA2B	MA2B	MA2B	MA2B	MA2B	ML2
Petrographical facies	Na-Bs	Na-Bs	Na-Bs	Na-Bs	Na-Bs	H
Mineral type	xenocryst	phenocryst	phenocryst	microcryst	microcryst	xenocryst
SiO_2	47.39	48.98	49.27	50.27	52.45	47.45
TiO_2	2.27	2.03	2.02	1.06	0.77	2.12
Al_2O_3	7.13	5.49	4.75	3.37	1.90	5.87
FeO	8.17	8.18	8.10	8.33	10.58	7.84
Cr_2O_3	0.04	0.00	0.18	0.00	0.00	0.04
MnO	0.17	0.16	0.20	0.27	0.56	0.26
MgO	13.86	14.25	14.62	15.16	13.93	13.94
CaO	21.44	21.03	21.25	18.65	20.94	21.59
Na_2O	0.65	0.70	0.33	0.56	0.52	0.57
K_2O	0.01	0.00	0.00	0.00	0.02	0.00
Total	101.13	100.82	100.72	97.66	101.67	99.68
Si	1.733	1.796	1.814	1.899	1.928	1.761
Al^{IV}	0.267	0.204	0.186	0.101	0.072	0.239
T	2.000	2.000	2.000	2.000	2.000	2.000
Al^{VI}	0.040	0.033	0.020	0.049	0.010	0.018
Ti^{VI}	0.062	0.056	0.056	0.030	0.021	0.059
Fe^{3+}	0.147	0.108	0.073	0.032	0.057	0.141
Cr	0.001	0.000	0.005	0.000	0.000	0.001
Fe^{2+}	0.090	0.125	0.152	0.189	0.237	0.091
Mg	0.660	0.678	0.694	0.699	0.675	0.689
M1	1.000	1.000	1.000	1.000	1.000	1.000
Fe2+	0.013	0.019	0.024	0.042	0.031	0.011
Mg	0.096	0.101	0.108	0.154	0.089	0.082
Mn	0.005	0.005	0.006	0.009	0.017	0.008
Ca	0.840	0.826	0.838	0.755	0.825	0.859
Na	0.046	0.050	0.024	0.041	0.037	0.041
K	0.000	0.000	0.000	0.000	0.001	0.000
M2	1.001	1.000	1.000	1.000	1.000	1.001
Mg %	44.34	44.42	44.01	46.19	40.74	44.33

Table 4. Selected analyses of minerals. E, Amphibole

	Manengouba, stage 2				**Manengouba,**
#	EB11	Eb10	Eb10	Eb10	EK1C
Petrographical facies	M	M	M	M	H
Mineral type	nicrophenocrys Edenite	phenocryst Kaersutite	phenocryst Kaersutite	phenocryst Kaersutite	phenocryst Kaersutite
SiO_2	45.40	40.84	40.24	39.59	39.53
TiO_2	2.10	6.03	5.85	6.16	5.20
Al_2O_3	6.71	13.03	12.34	13.65	12.85
Cr_2O_3	0.00	0.02	0.00	0.05	0.00
FeO	10.66	11.24	11.11	10.63	11.55
MnO	0.39	0.21	0.22	0.17	0.12
MgO	16.42	12.25	13.12	12.09	13.10
CaO	10.45	11.65	11.77	11.96	11.77
Na_2O	2.88	2.69	3.14	2.81	2.90
K_2O	1.17	0.88	0.89	0.95	1.02
Total	96.17	98.84	98.68	98.06	98.05
Si	6.661	5.993	5.930	5.888	5.847
Al^{IV}	1.160	2.007	2.070	2.112	2.153
Ti	0.179	0.000	0.000	0.000	0.000
Total	8.000	8.000	8.000	8.000	8.000
Al^{VI}	0.000	0.247	0.073	0.281	0.088
Ti	0.053	0.665	0.648	0.689	0.579
Cr	0.000	0.002	0.000	0.006	0.000
Fe^{3+}	0.721	0.000	0.000	0.000	0.152
Fe^{2+}	0.586	1.379	1.369	1.322	1.277
Mn	0.049	0.026	0.027	0.021	0.015
Mg	3.591	2.680	2.882	2.680	2.889
Total	5.000	5.000	5.000	5.000	5.000
Ca	1.642	1.832	1.858	1.906	1.865
Na	0.358	0.168	0.142	0.094	0.135
Total	2.000	2.000	2.000	2.000	2.000
Na	0.461	0.597	0.756	0.716	0.697
K	0.218	0.165	0.167	0.180	0.193
Total	0.679	0.762	0.923	0.896	0.890

Table 4. Selected analyses of minerals. F, Mica

	Manengouba, stage 2		**Manengouba, stage 4**	
#	Eb11	Eb11	KOS7	KOS7
Petrographical facies	M	M	M	M
Mineral type	phenocryst	phenocryst	microphenocrys	microcryst
SiO_2	40.56	41.02	39.60	39.27
TiO_2	3.92	3.90	4.99	5.74
Al_2O_3	12.33	11.88	11.97	12.36
Cr_2O_3	0.00	0.11	0.00	0.00
FeO	9.56	8.97	9.51	10.02
MgO	20.59	20.61	19.60	18.54
CaO	0.08	0.00	0.01	0.03
MnO	0.11	0.00	0.13	0.11
Na_2O	0.99	0.84	1.40	1.02
K_2O	9.00	9.31	8.49	8.60
Total	97.14	96.64	95.70	95.69
Si	3.152	3.196	3.128	3.107
Al^{IV}	0.848	0.804	0.872	0.893
Total	4.000	4.000	4.000	4.000
Al^{VI}	0.282	0.287	0.241	0.260
Ti	0.229	0.229	0.296	0.342
Fe	0.621	0.584	0.628	0.663
Mg	2.386	2.394	2.308	2.187
Mn	0.007	0.000	0.009	0.008
Total	3.525	3.493	3.482	3.459
K	0.894	0.927	0.857	0.870
Na	0.149	0.127	0.215	0.156
Total	1.044	1.054	1.072	1.026

Table 4. Selected analyses of minerals. G, Feldspars

Manengouba, stage 1

#	CT46	MA2B	MA2B	MA2B	MA2B	MA2B	ML2
Petrographical facies	alk-B	Na-Bs	Na-Bs	Na-Bs	Na-Bs	Na-Bs	H
Mineral type	phenocryst	phenocryst	phenocryst	microcryst	microcryst	xenocryst	phenocryst
SiO_2	50.55	50.02	50.79	52.90	54.49	56.41	52.87
Al_2O_3	31.66	31.97	29.79	30.11	28.51	28.25	30.19
Fe_2O_3	1.05	0.98	0.82	0.93	0.53	0.43	0.33
CaO	13.02	13.02	12.16	11.39	10.48	9.63	12.32
Na_2O	3.71	3.55	3.98	4.52	5.22	5.69	4.33
K_2O	0.01	0.26	0.25	0.31	0.36	0.53	0.23
Total	100.00	99.80	97.78	100.16	99.59	100.94	100.27
Si	2.300	2.284	2.359	2.393	2.470	2.515	2.389
Al	1.698	1.720	1.631	1.605	1.523	1.485	1.608
Fe^{3+}	0.036	0.034	0.029	0.032	0.018	0.014	0.011
Ca	0.635	0.637	0.605	0.552	0.509	0.460	0.597
Na	0.327	0.314	0.359	0.396	0.459	0.492	0.379
K	0.001	0.015	0.015	0.018	0.021	0.030	0.014
Total	4.997	5.004	4.998	4.996	4.999	4.996	4.998
% Ab	34.00	32.52	36.64	41.02	46.41	50.08	38.34
% An	65.94	65.91	61.86	57.12	51.48	46.84	60.29
% Or	0.06	1.57	1.49	1.86	2.11	3.08	1.37

Table 5. Chemical analyses of the rocks

Manengouba, stage 1

Location	Ekon-Nkam fall	Mantem	N Manjo Mahongué river	E Manjo Moo river	Enyandong Mbe river
#	KO1	CT46	MA2B	ML2	DN1
Setting type	flow	flow	flow	flow	flow
Petrographical facies	Ank	alk B	Na-Bs	H	Na-H
SiO_2	43.38	46.58	45.83	47.47	46.62
TiO_2	2.61	2.47	2.71	2.67	2.75
Al_2O_3	13.10	15.14	15.03	16.17	17.13
Fe_2O_3t	12.79	12.72	11.89	11.38	10.98
MnO	0.17	0.17	0.17	0.18	0.18
MgO	11.04	8.51	6.94	5.55	3.85
CaO	10.67	8.19	9.94	9.15	9.30
Na_2O	2.66	2.67	3.24	3.83	4.47
K_2O	1.29	1.43	1.61	1.54	1.61
P_2O_5	0.61	0.62	0.65	0.77	0.88
LOI	1.40	1.47	1.64	0.91	1.87
TOTAL	99.72	99.97	99.65	99.62	99.64
DI	24.37	31.88	33.80	39.33	42.20
V	251	192.2	213	183	192
Cr	399	318.7	236	128	39.0
Co	49.3	45.02	36.3	29.4	24.0
Ni	241.0	222.5	113.0	73.0	19.0
Cu	68.93	61.06	46.95	40.89	23.37
Ga	20.32	23.84	23.4	24.33	23.1
Rb	35.00	32.91	52.00	36.00	35.00
Sr	661.0	564.5	790.0	1027.0	808.0
Y	23.30	48.29	26.70	30.10	31.80
Zr	201.0	314.6	243.0	282.0	244.0
Nb	57.82	58.37	68.43	75.02	58.9
Ba	492.0	539.6	533.0	637.0	504.0
Hf	4.00	6.84	6.03	6.23	5.53
Ta	4.04	4.32	4.95	5.22	4.35
Pb	2.17	2.79	3.89	3.02	2.75
Th	4.60	4.84	6.77	6.87	4.40
U	1.30	1.28	2.27	1.70	1.18
La	40.05	58.87	61.17	68.12	49.28
Ce	77.90	92.85	118.00	135.00	103.00

Table 6 Isotopic data

Location	Sample	Rock type	Age (Ma)	Rb	Sr	$^{87}Sr/^{86}Sr$ ± 2 σ	Sm	Nd	$^{143}Nd/^{144}Nd$ ± 2 σ	εNd	U	Th	Pb	$^{206}Pb/^{204}Pb$	$^{207}Pb/^{204}Pb$	$^{208}Pb/^{204}Pb$
Pre-Manengouba																
NW borders																
Essom	CT-107	T	13.56	96.0	116	0.706216 ± 5	14.18	81.18	0.512558 ± 11	-1.35	3.22	13.2	13.6	18.45	15.59	38.85
Bakossi	CT-103	Ph	7.55	254	33.8	0.707574 ± 6	10.81	61.67	0.512756 ± 5	2.49						
E-volc. substratum																
NE-Nlonako	KBT 5	H	9.27	37	900	0.703326 ± 7	11.1	56.9	0.512910 ± 12	5.44						
Manengouba																
Ekom	CT-155	Rh	1.02	200	6.2	0.708554 ± 5	4.04	17.0	0.512764 ± 19	2.47	1.8	31.4	3.77	18.79	15.60	39.04
Caldera																
Eboga SE-floor	KEB 19	H	0.28	50.9	616	0.703114 ± 7	9.28	46.3	0.512924 ± 12	5.58						
Eboga NW-floor	KEB 33	H	0.14	36.0	524	0.703045 ± 7	7.42	35.0	0.512923 ± 16	5.56						
Flank activity																
Mboassoum	CT-108	H	0.45	30.9	513	0.703055 ± 7	8.06	37.0	0.512948 ± 10	6.05	1.3	4.86	2.15	19.75	15.63	39.45
W-Bangen	CT-105	T-P	0.21	144	417	0.703042 ± 9	10.8	61.7	0.512869 ± 22	4.62	6.38	23.0	8.12	19.78	15.63	39.48
Ekoh	CT-55	Bs	0.11	43.9	957	0.703041 ± 6	10.4	55.4	0.512933 ± 9	5.76						
S-Mbouroukou	KME 2a	H	0.10	32.5	746	0.703083 ± 6	9.33	45.89	0.512917 ± 16	5.44						

Fig. 1

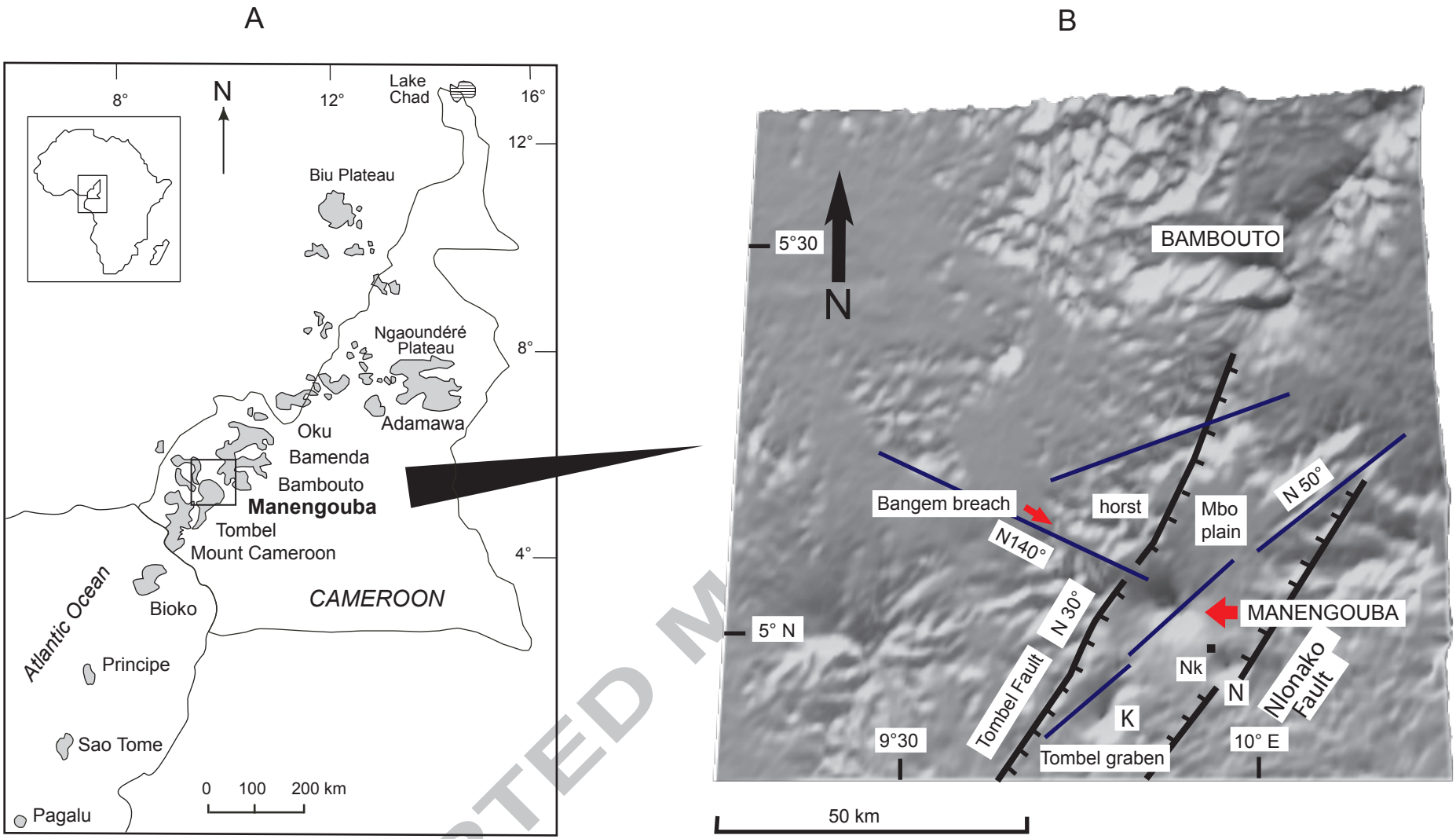

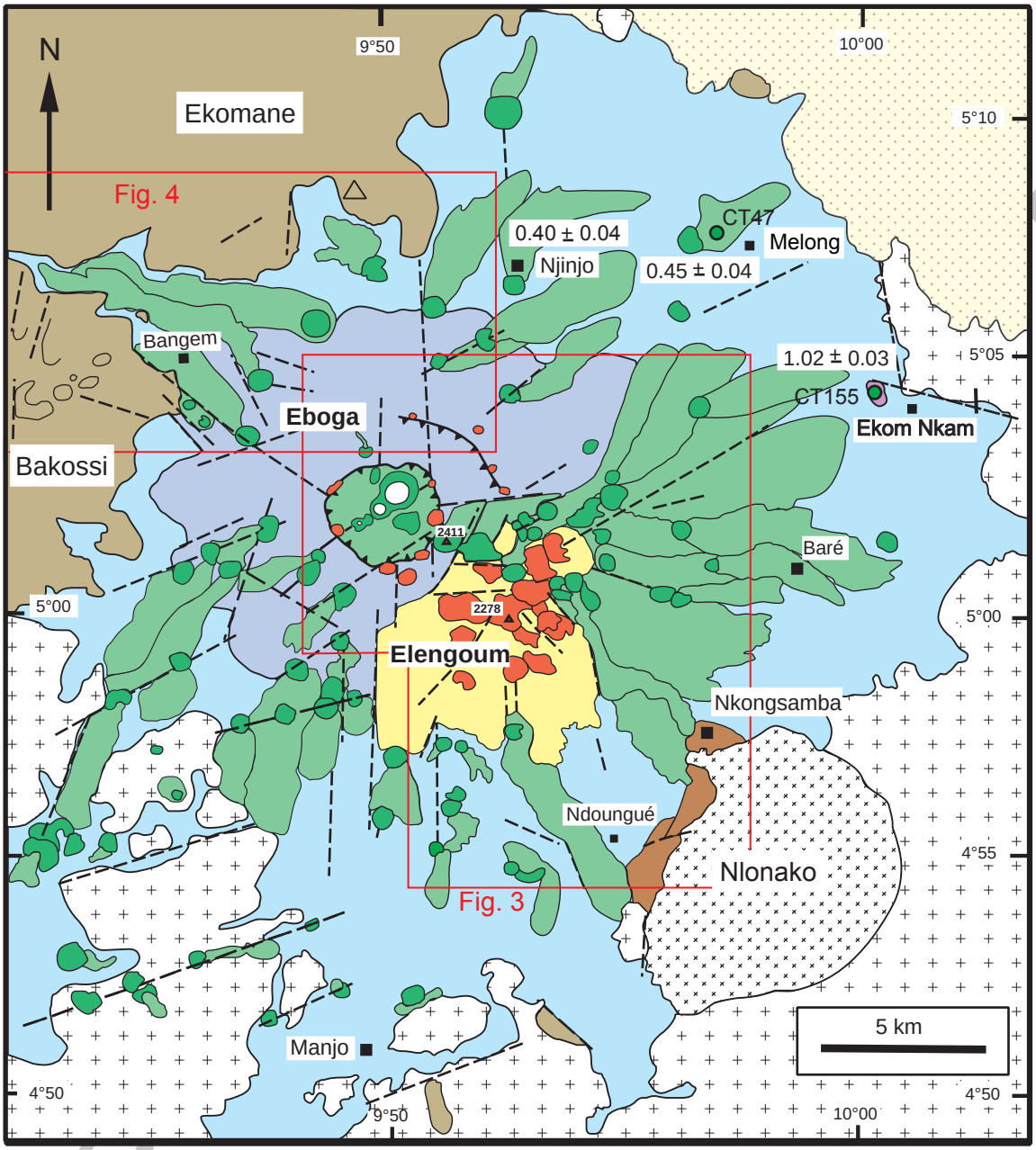

MANENGOUBA Volcanic System

1 - Early Manengouba shield volcano (1.55 - 0.94 Ma)

2 - Eboga stratovolcano
hawaiite - mugearite - benmoreite flows

3 - Elengoum Extrusive Complex
benmoreite and trachyte extrusions (0.9 - 0.7 Ma)

trachyte pyroclastic flows

4 - Flank volcanoes, cones and flows (0.5 - 0.1 Ma)

Unrelated lavas

rhyolite of Ekom (1.02 Ma)

Pre-Manengouba lava flows (9 Ma)

North-western trachyte and phonolite of the Bakossi - Ekomane shield (13.6 -7.4 Ma) and of limited southern sites

Eocene syenite intrusion

Neoproterozoic granite basement

Quaternary sediments

Fault and fracture

Caldera

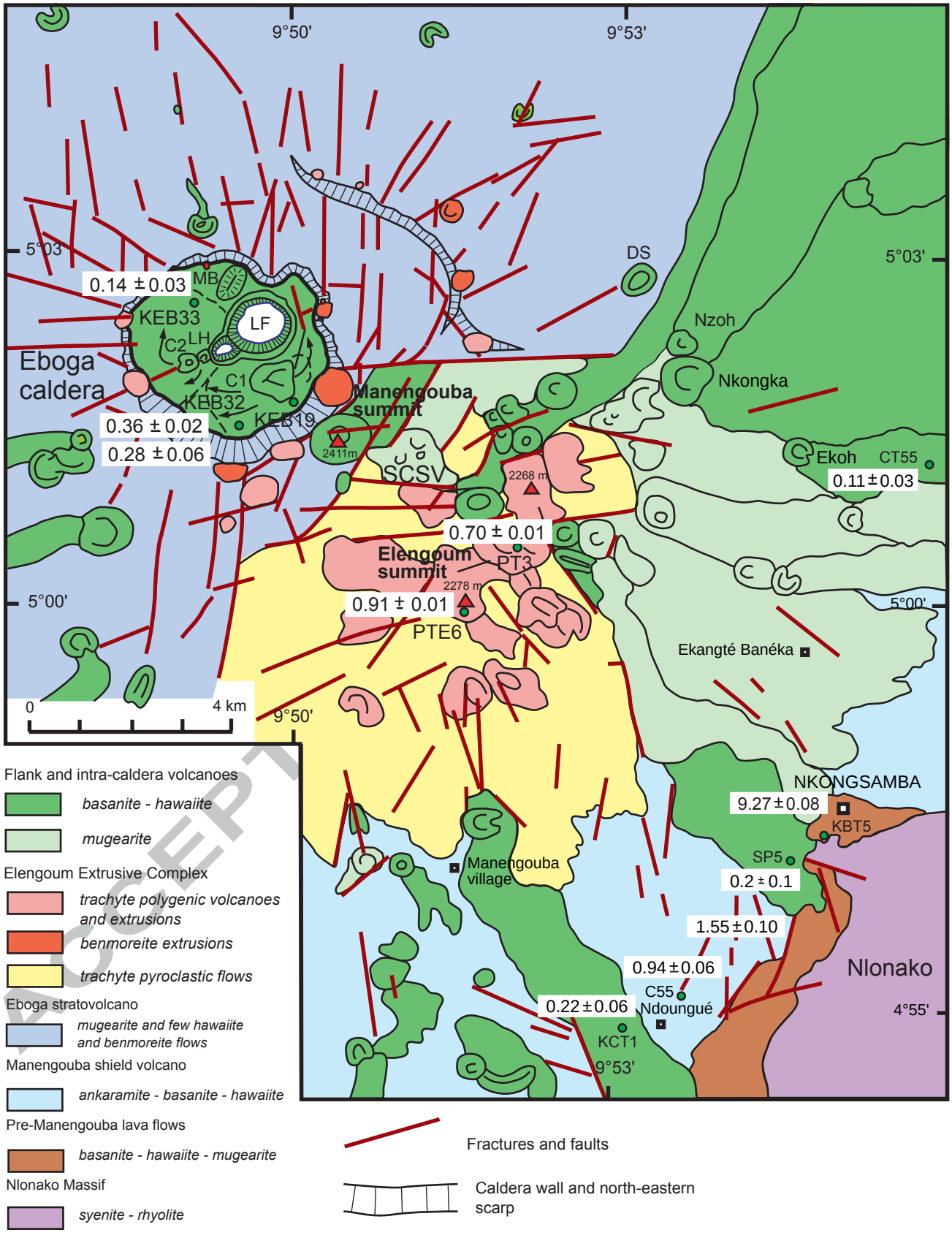

Fig. 4

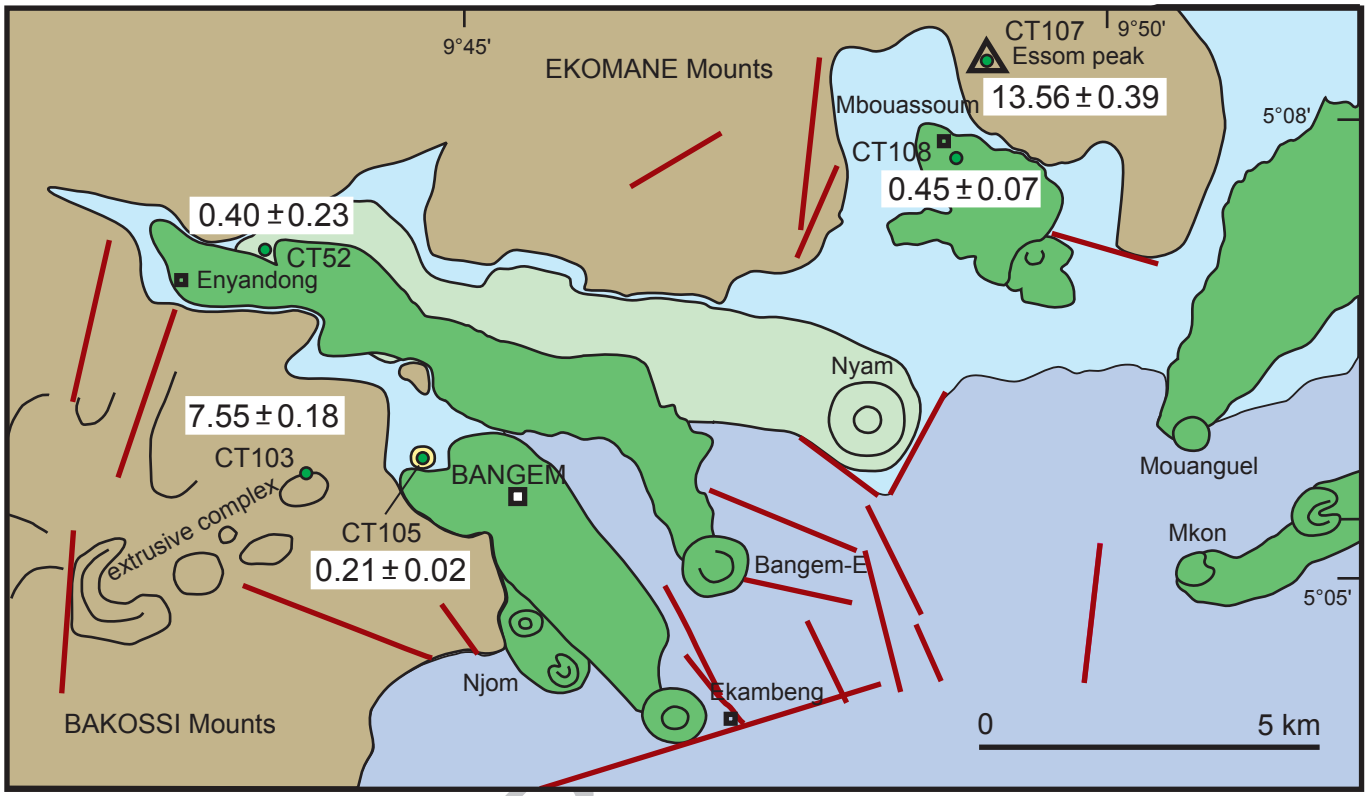

Flank volcanoes

basanite - hawaiite

mugearite

trachy-phonolite

Eboga stratovolcano

hawaiite - mugearite - benmoreite

Manengouba shield lava flows

basanite

Pre-Manengouba volcanic rocks

trachyte - phonolite

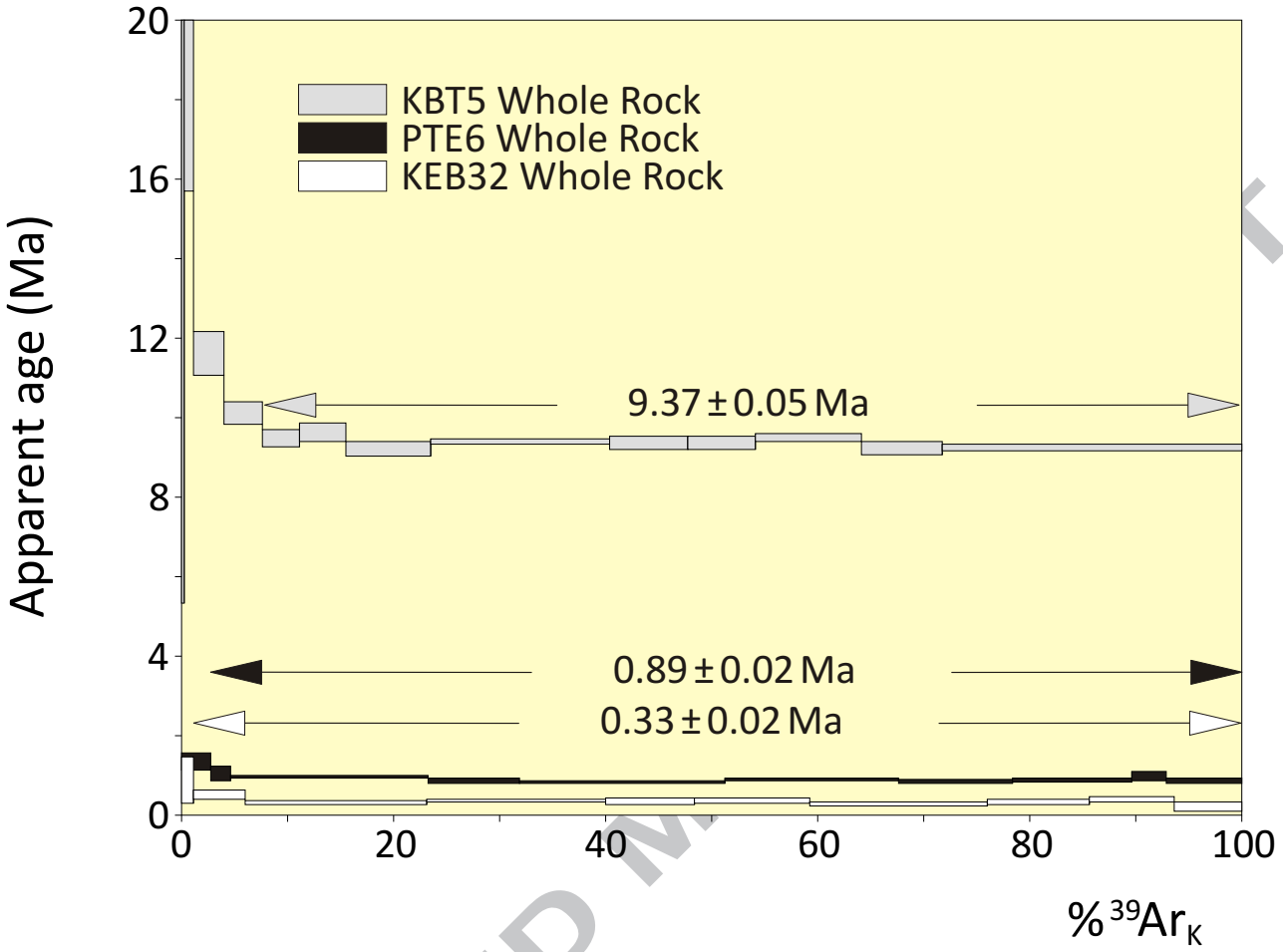

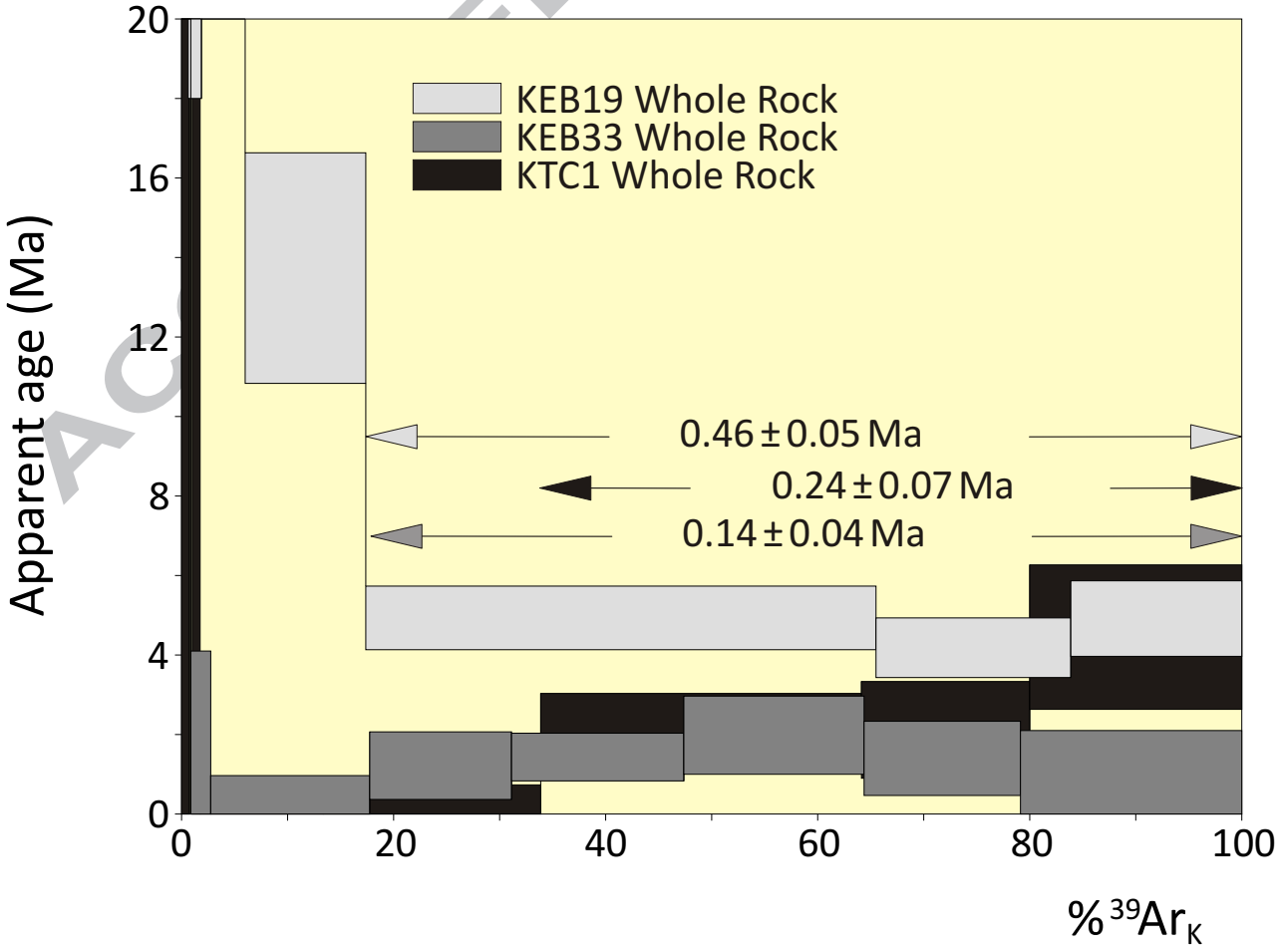

Fig. 6

St 1 - Manengouba shield
St 2 - Eboga stratovolcano
St 3a - Elengoum acidic extrusions and
Eboga caldera collapse
St 3b - Acidic extrusions and caldera infilling
End of the first magmatic activity

St 4 - Renewal of the activity inside the caldera
and on the flanks

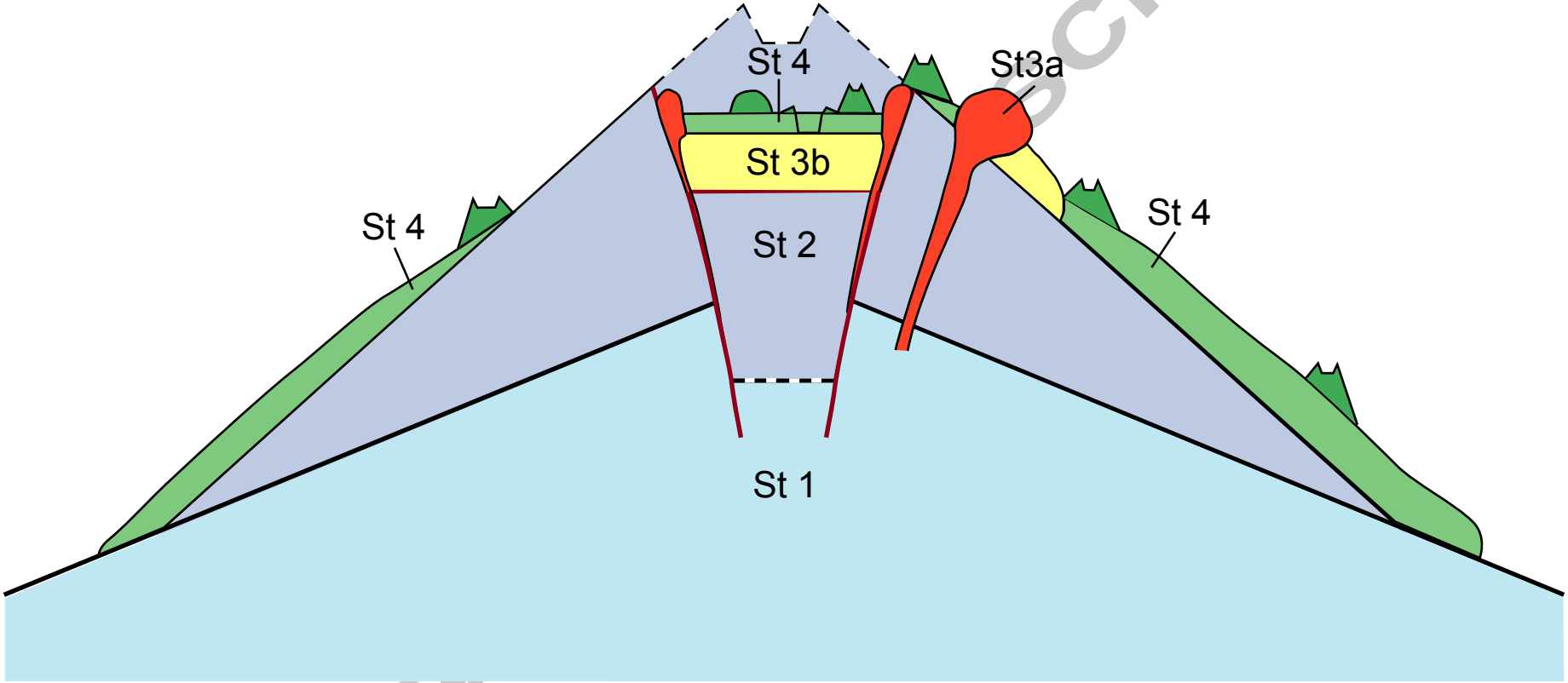

Fig. 7

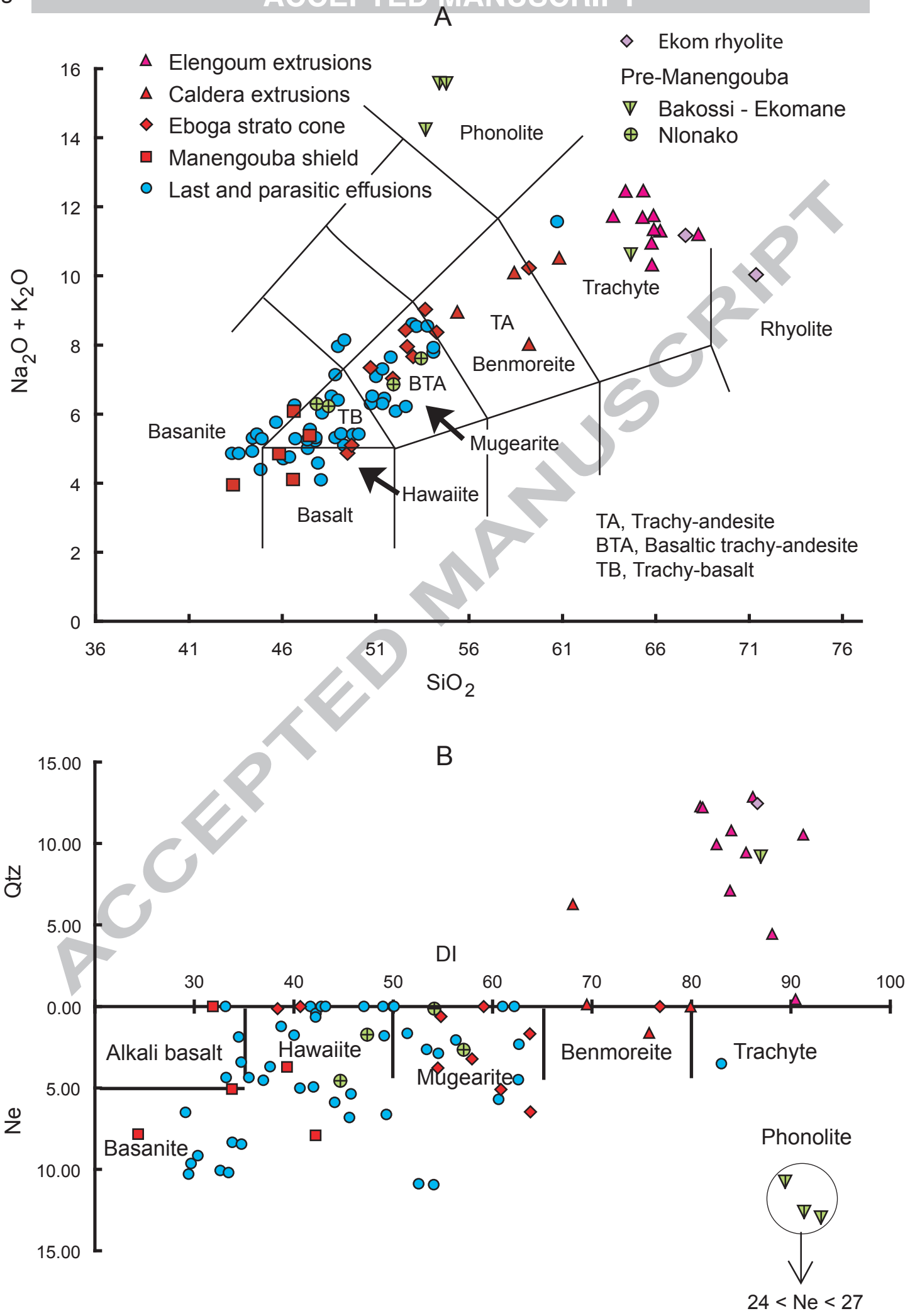

Fig. 8

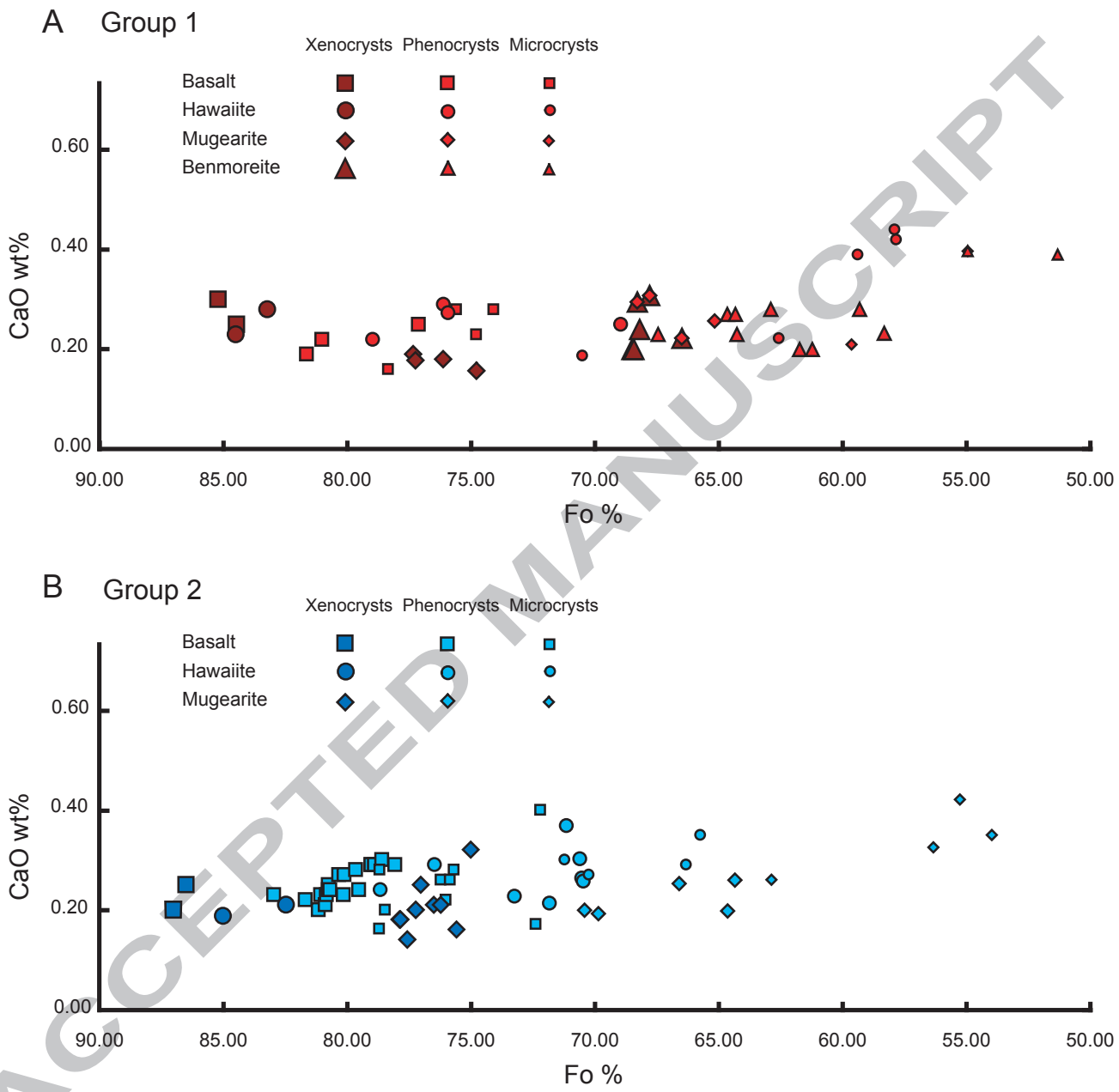

Fig. 9

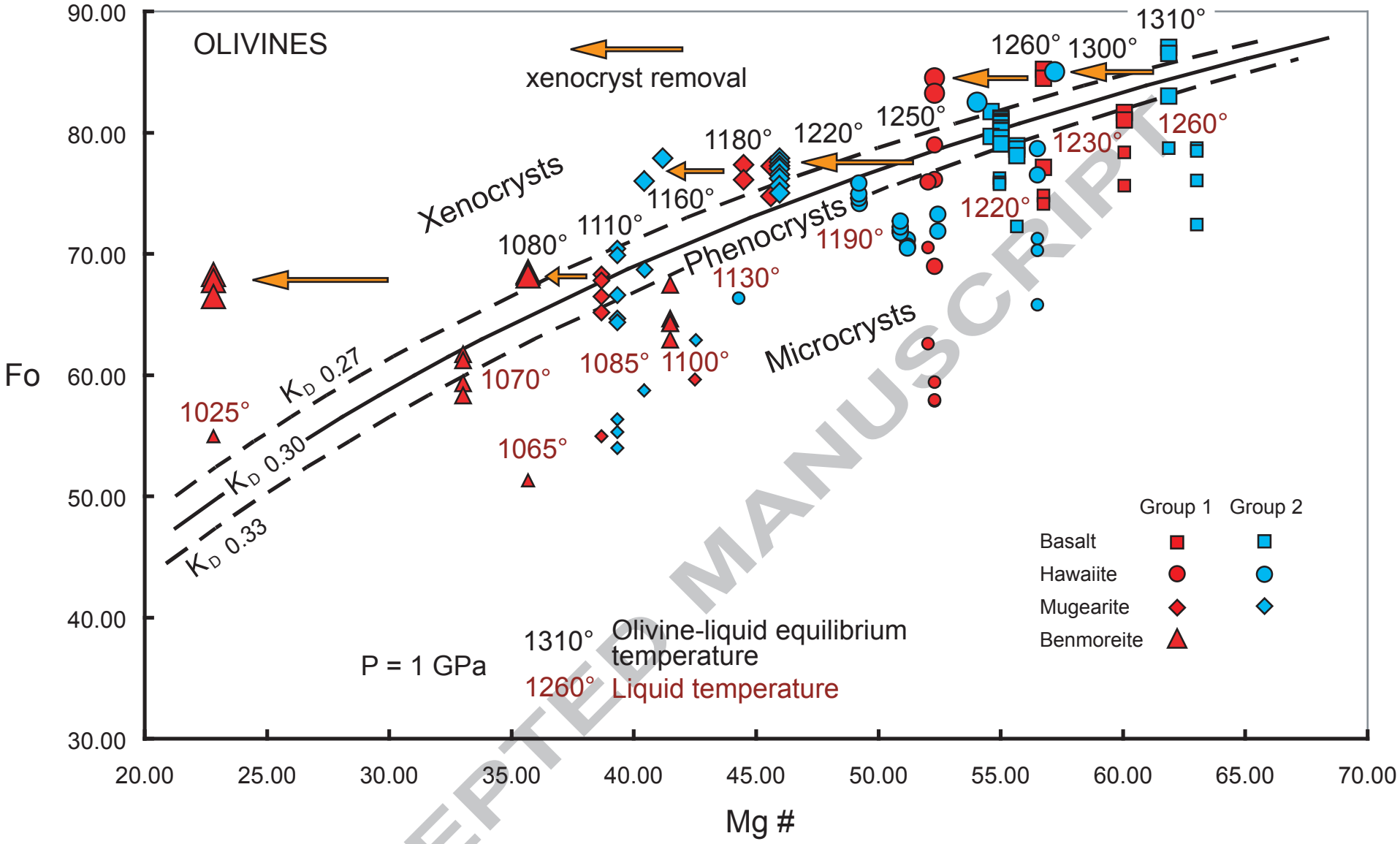

Fig. 10

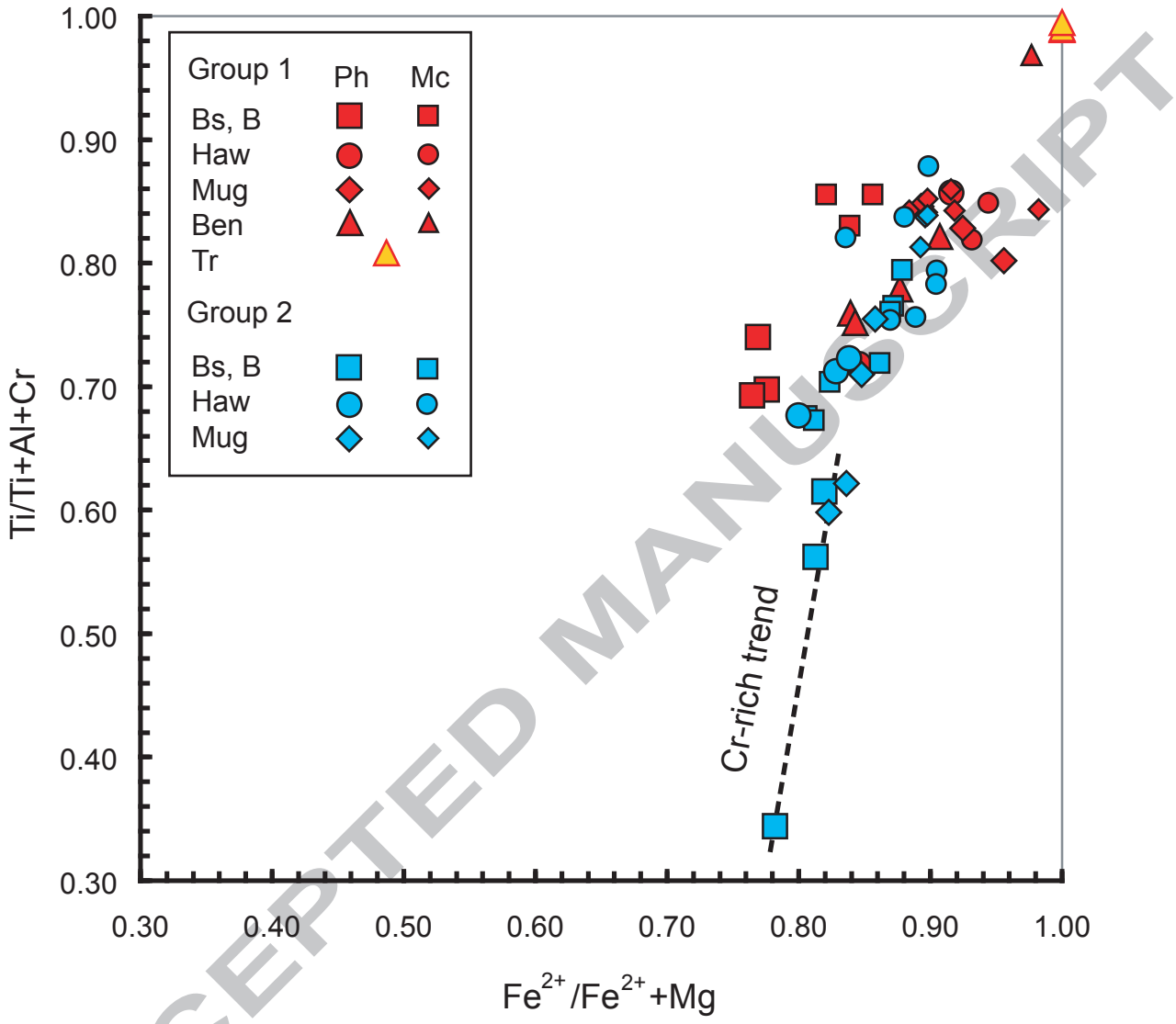

Fig. 11

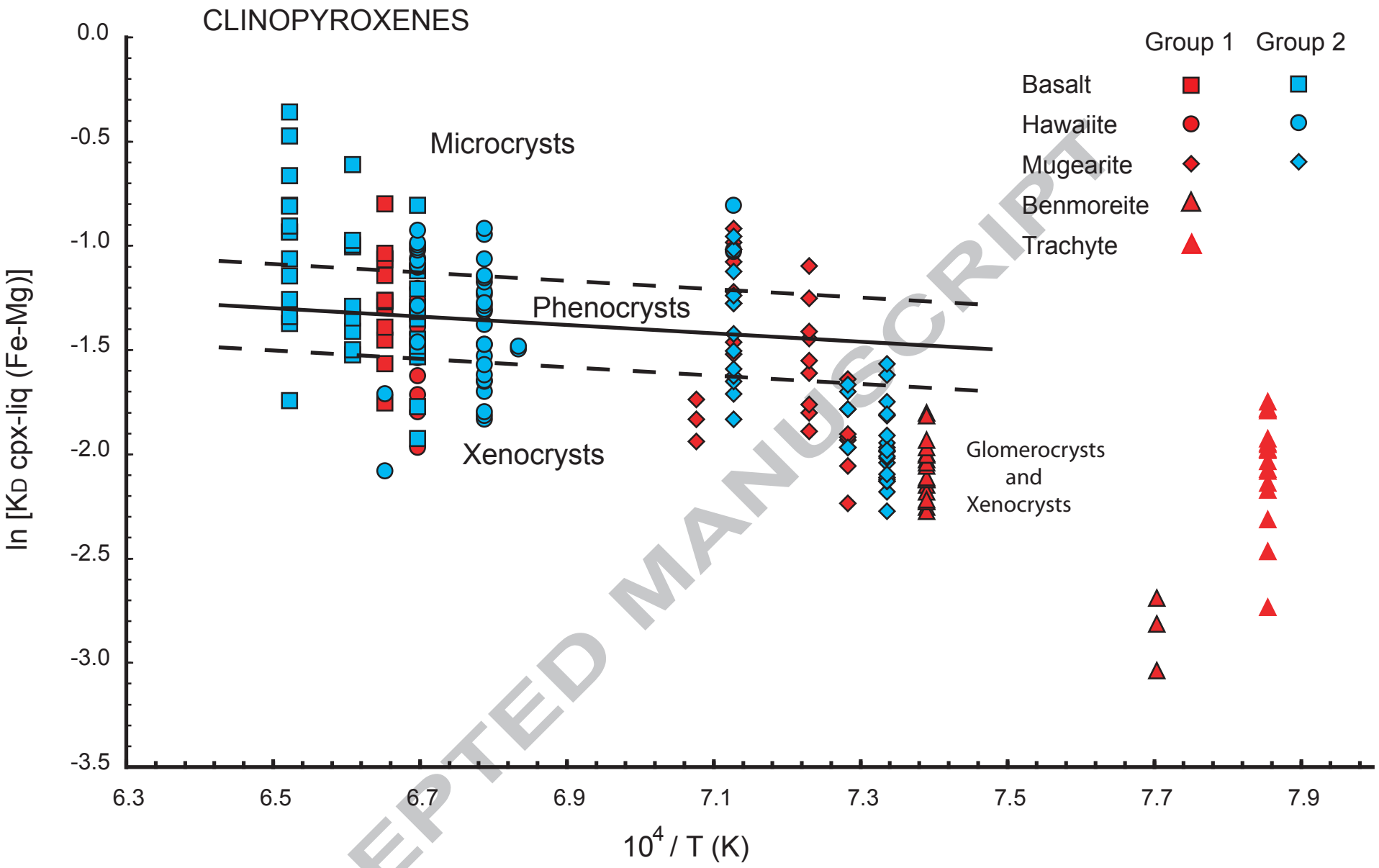

Fig. 12

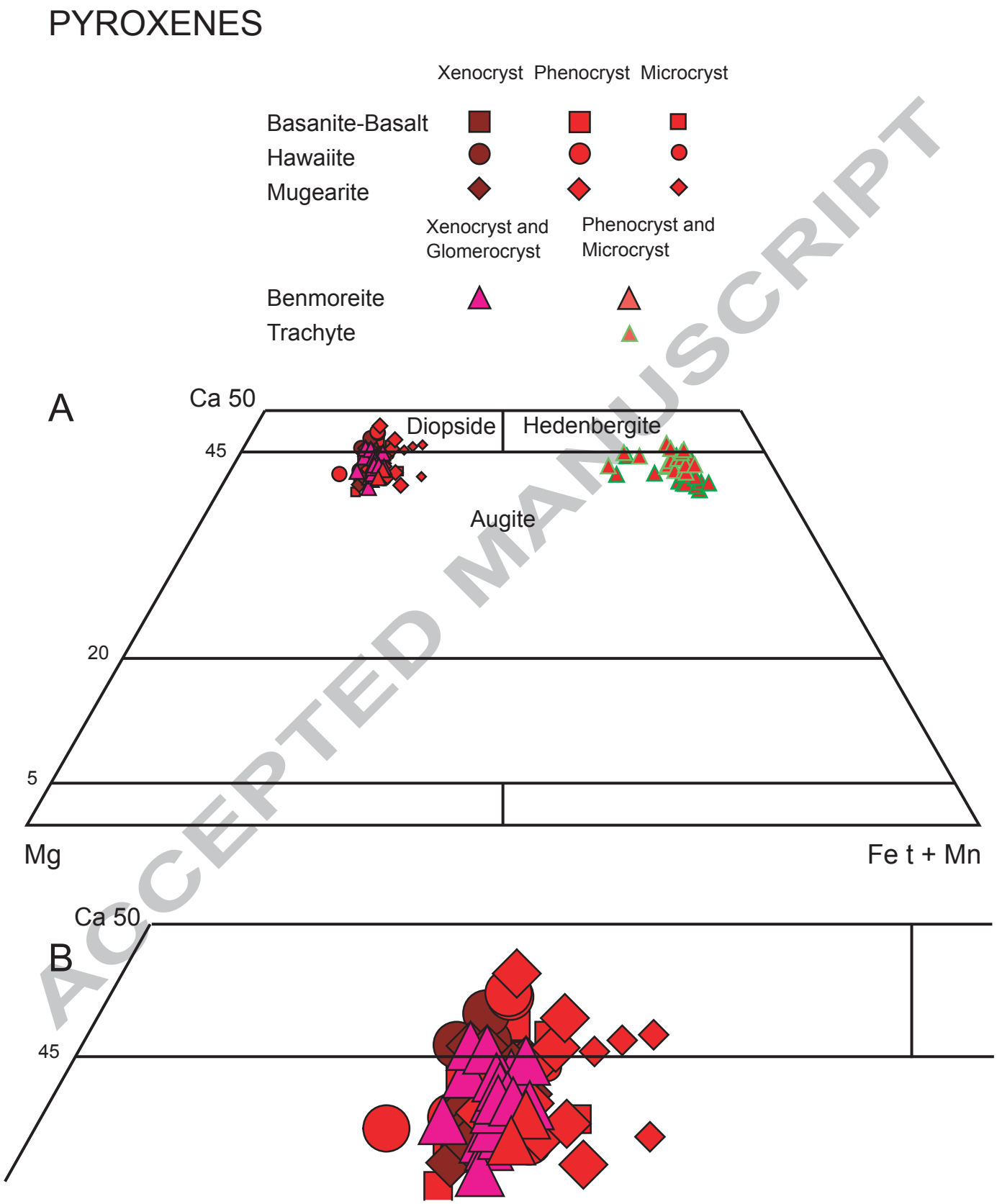

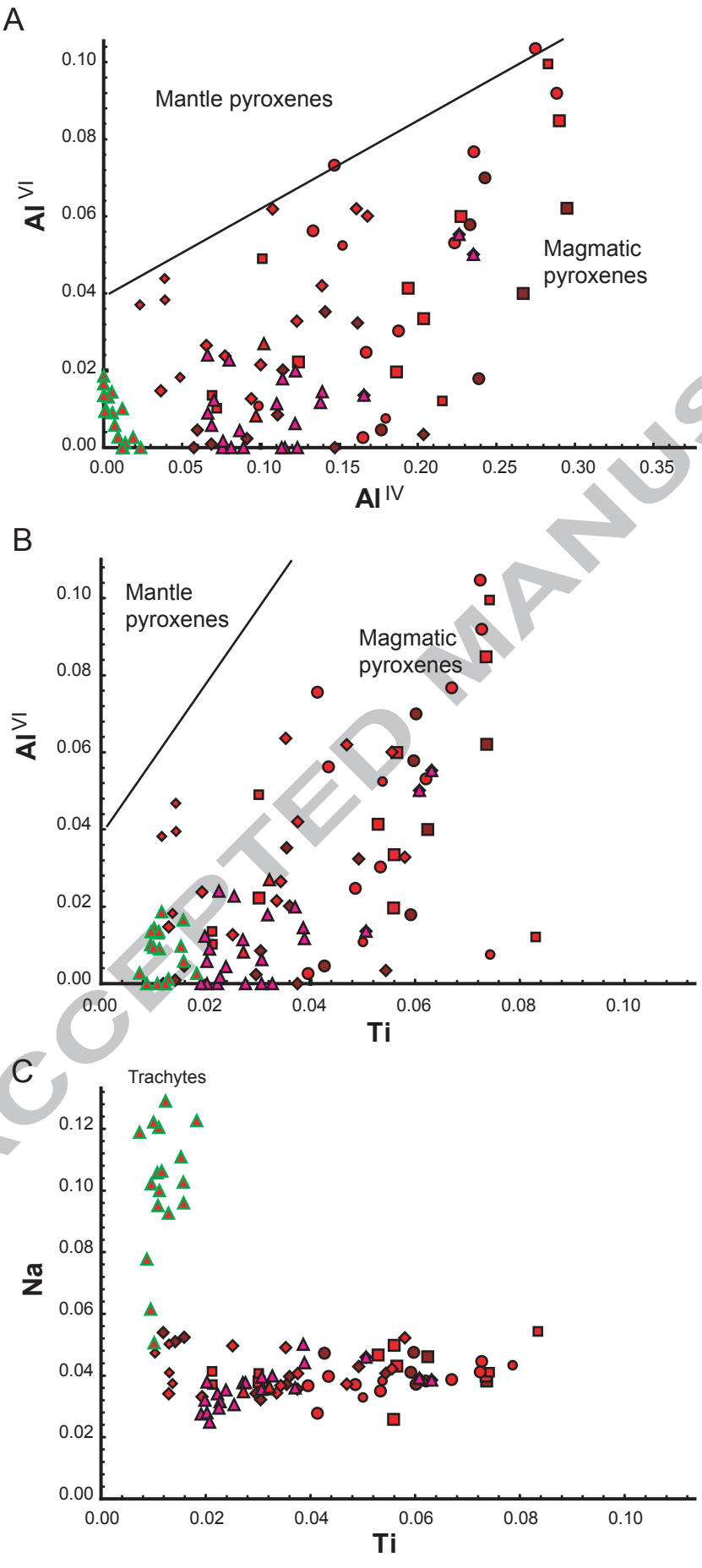

Fig. 14

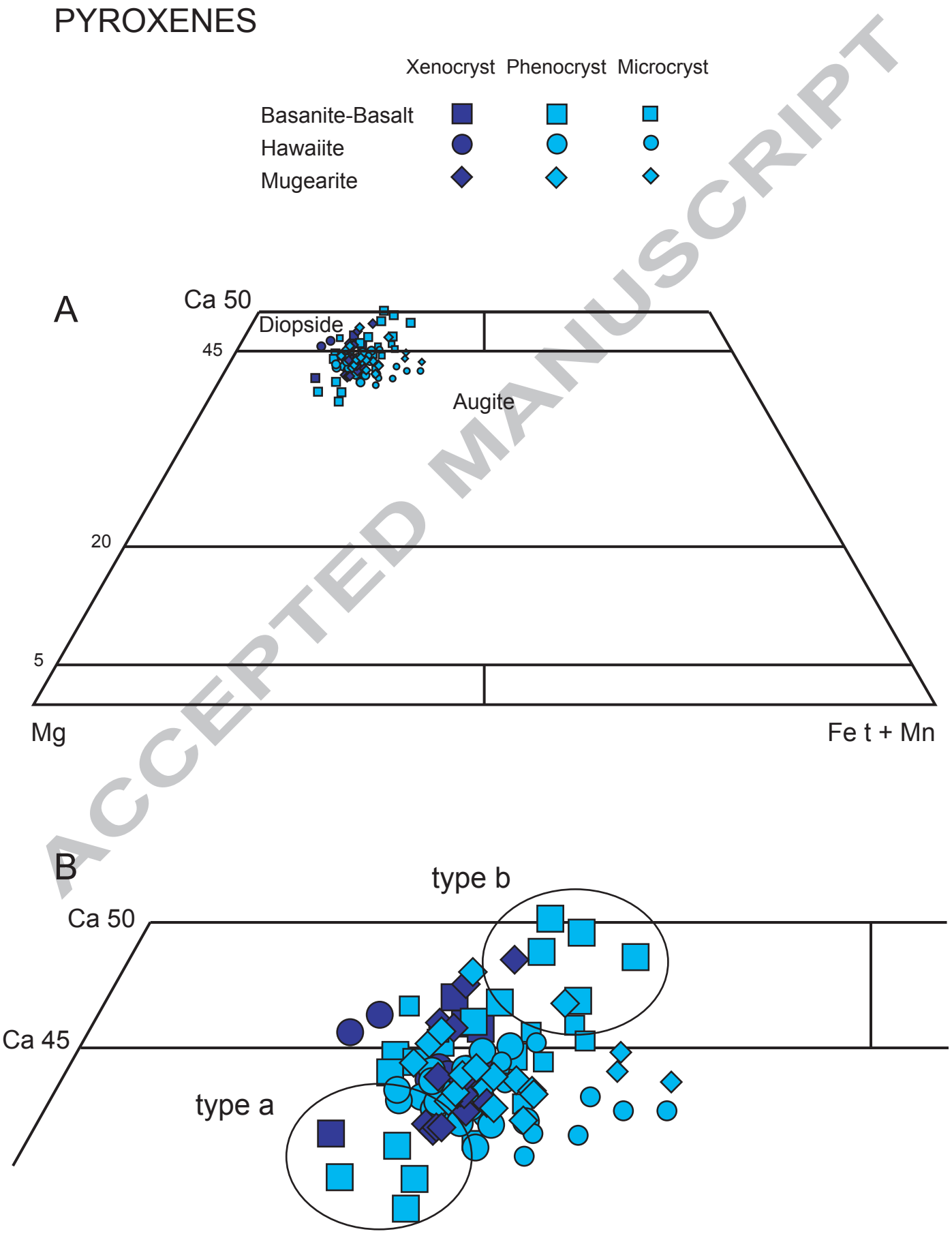

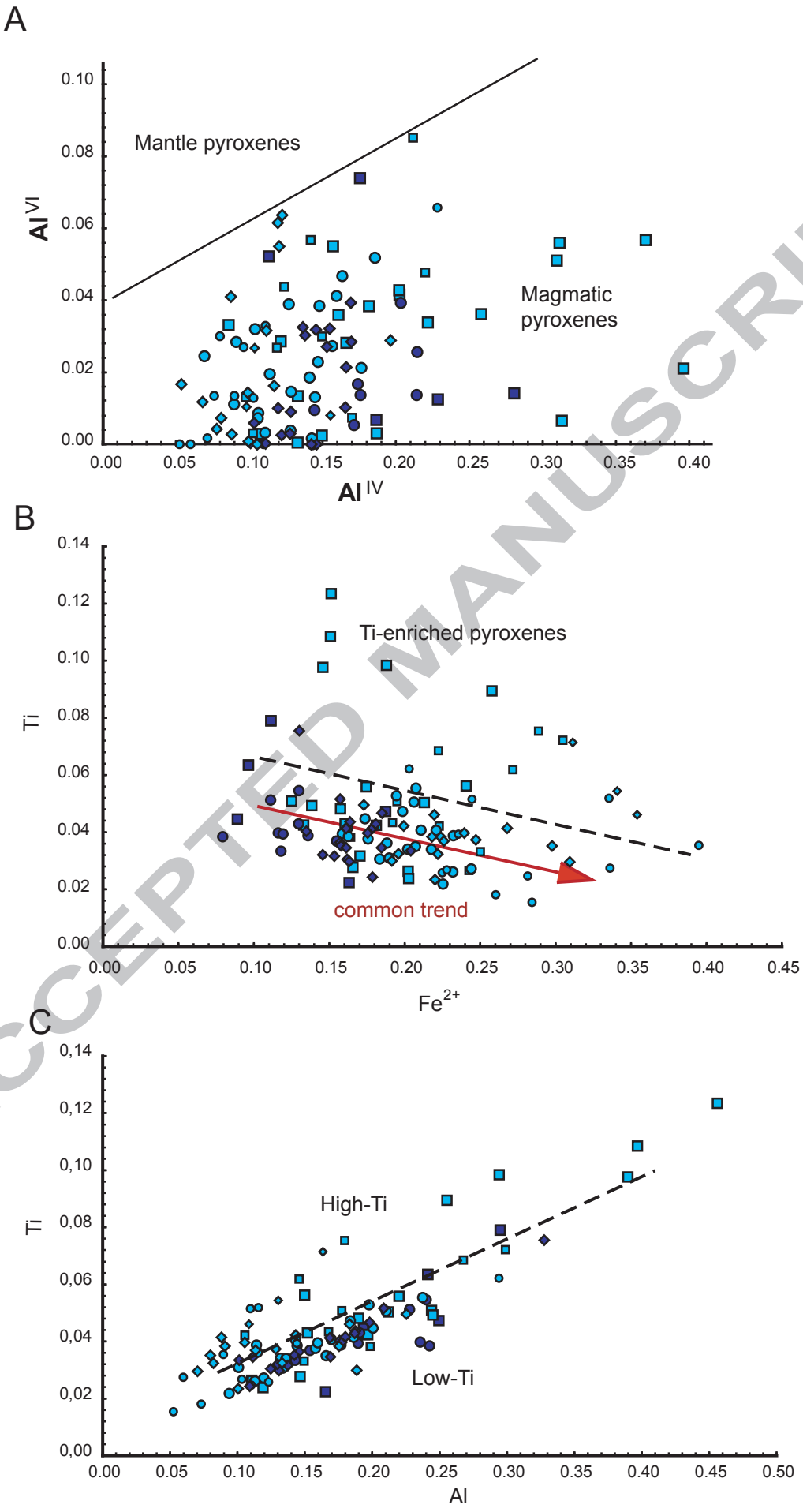

Fig. 16A

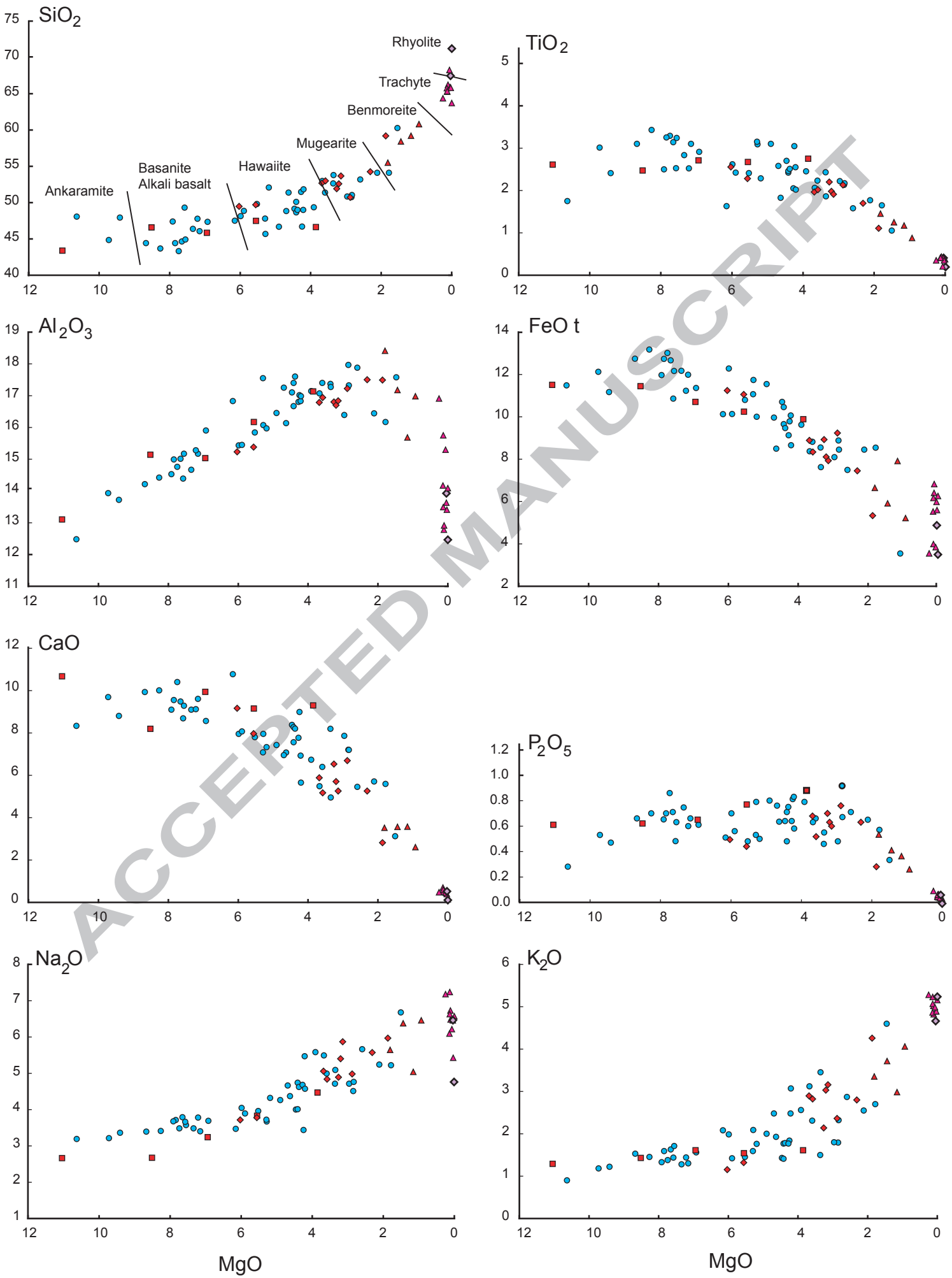

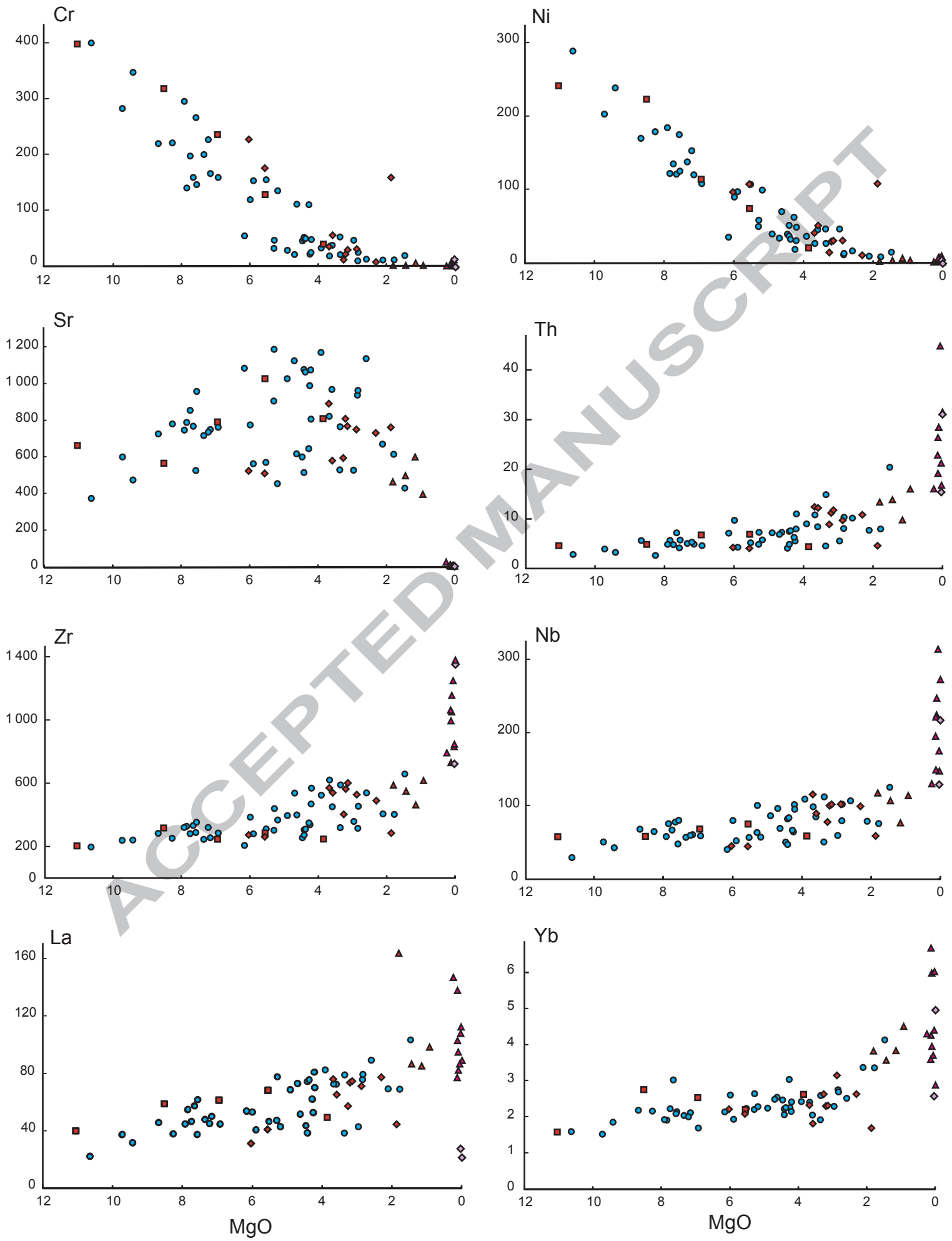

Fig. 17

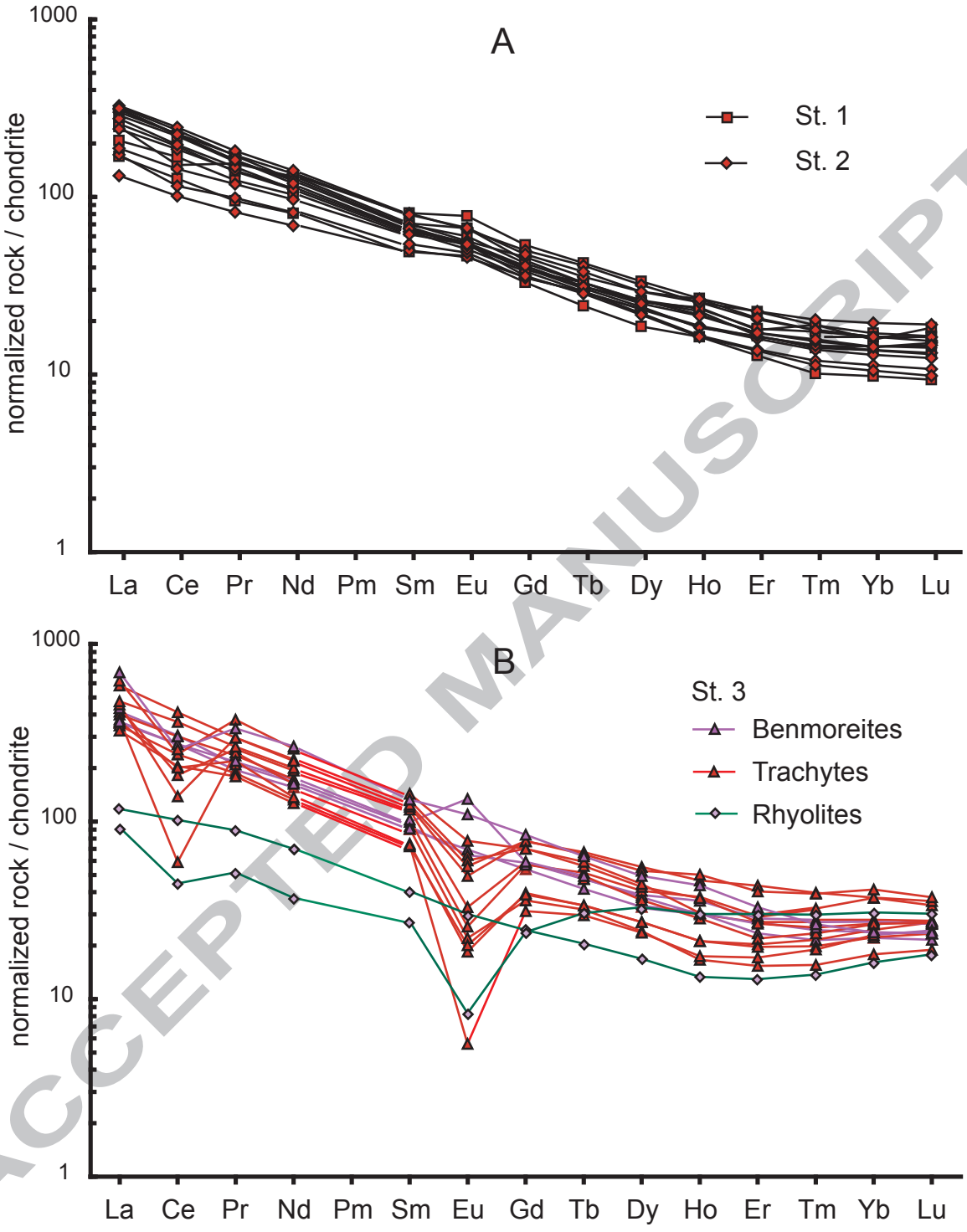

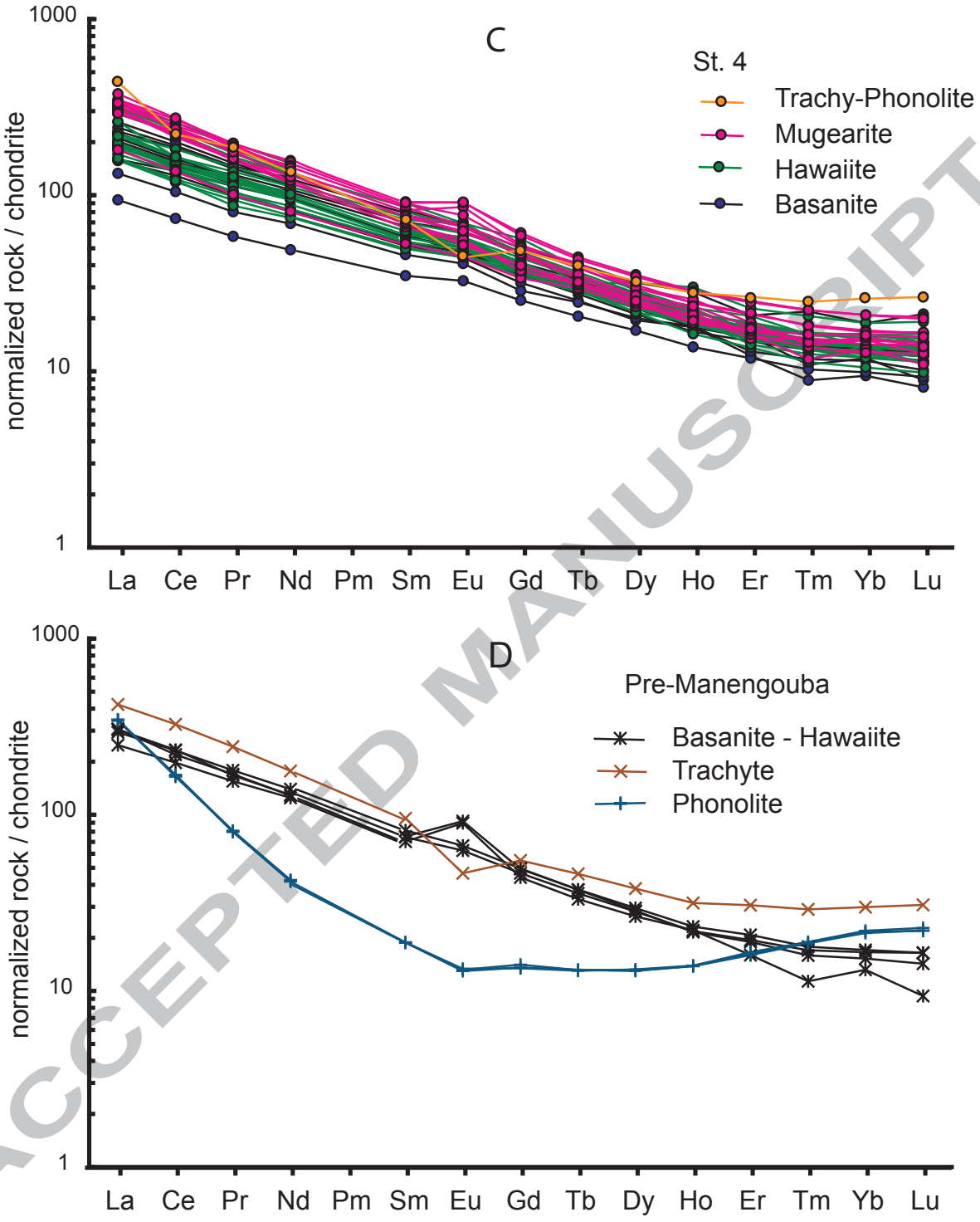

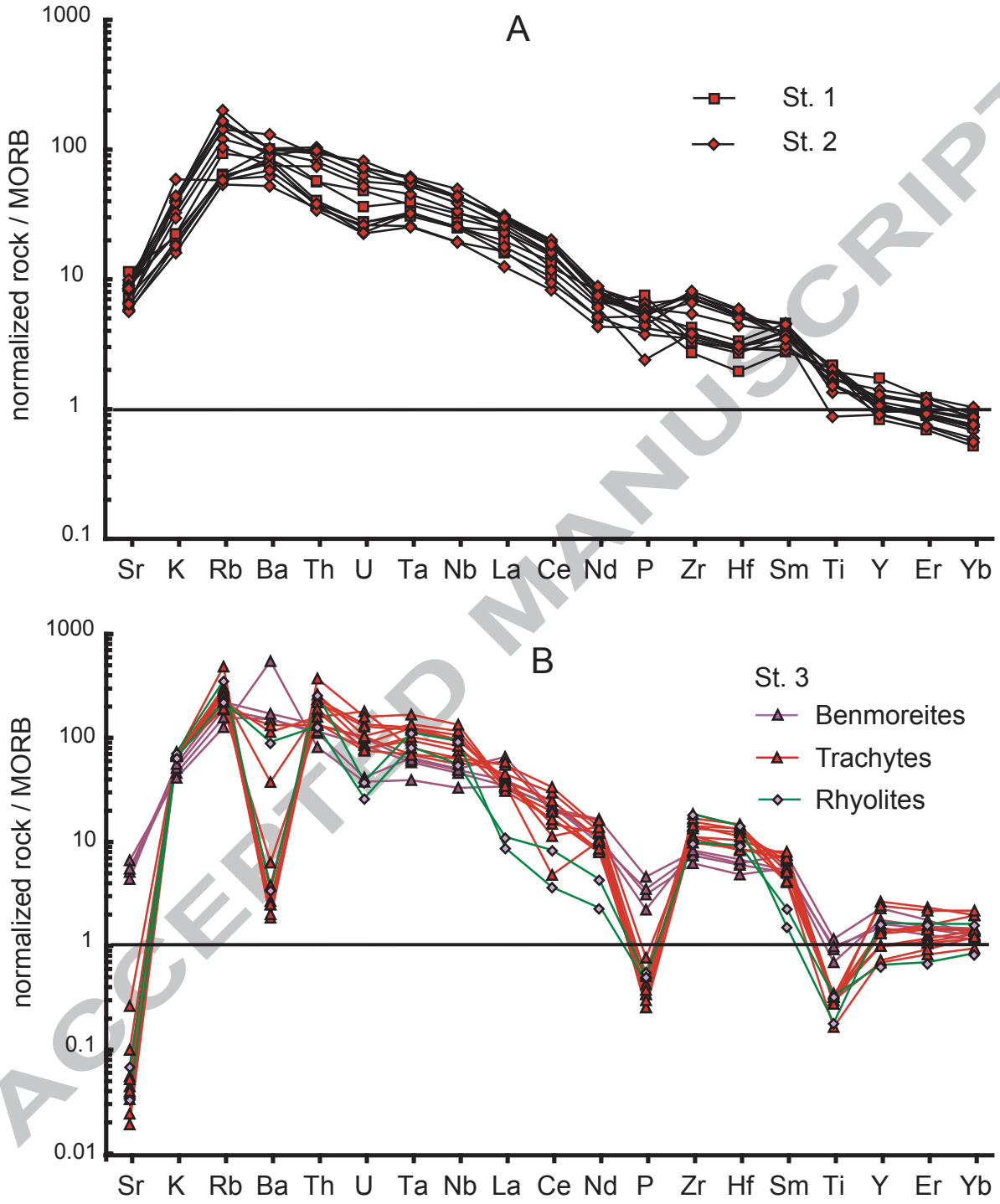

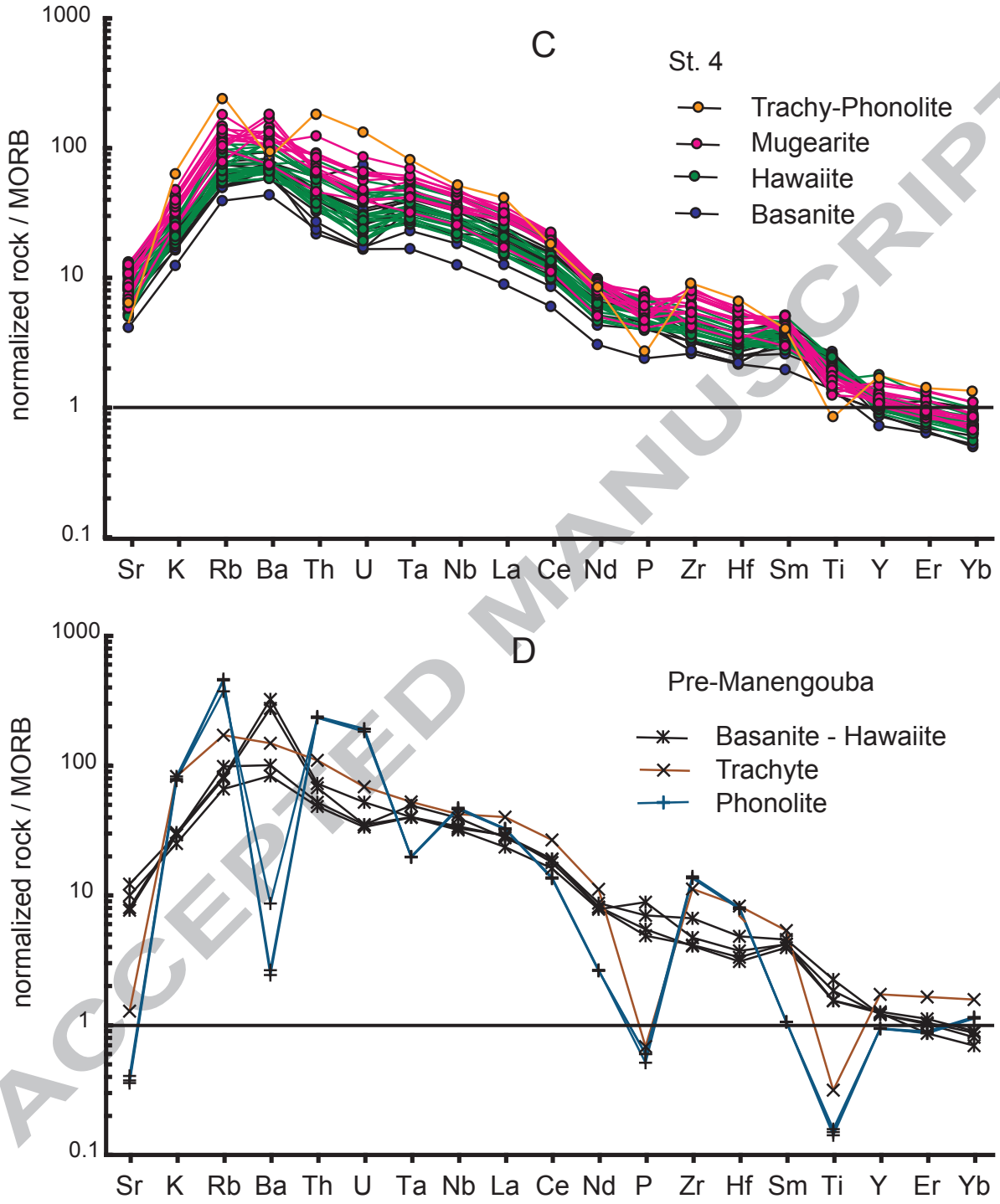

Fig. 19

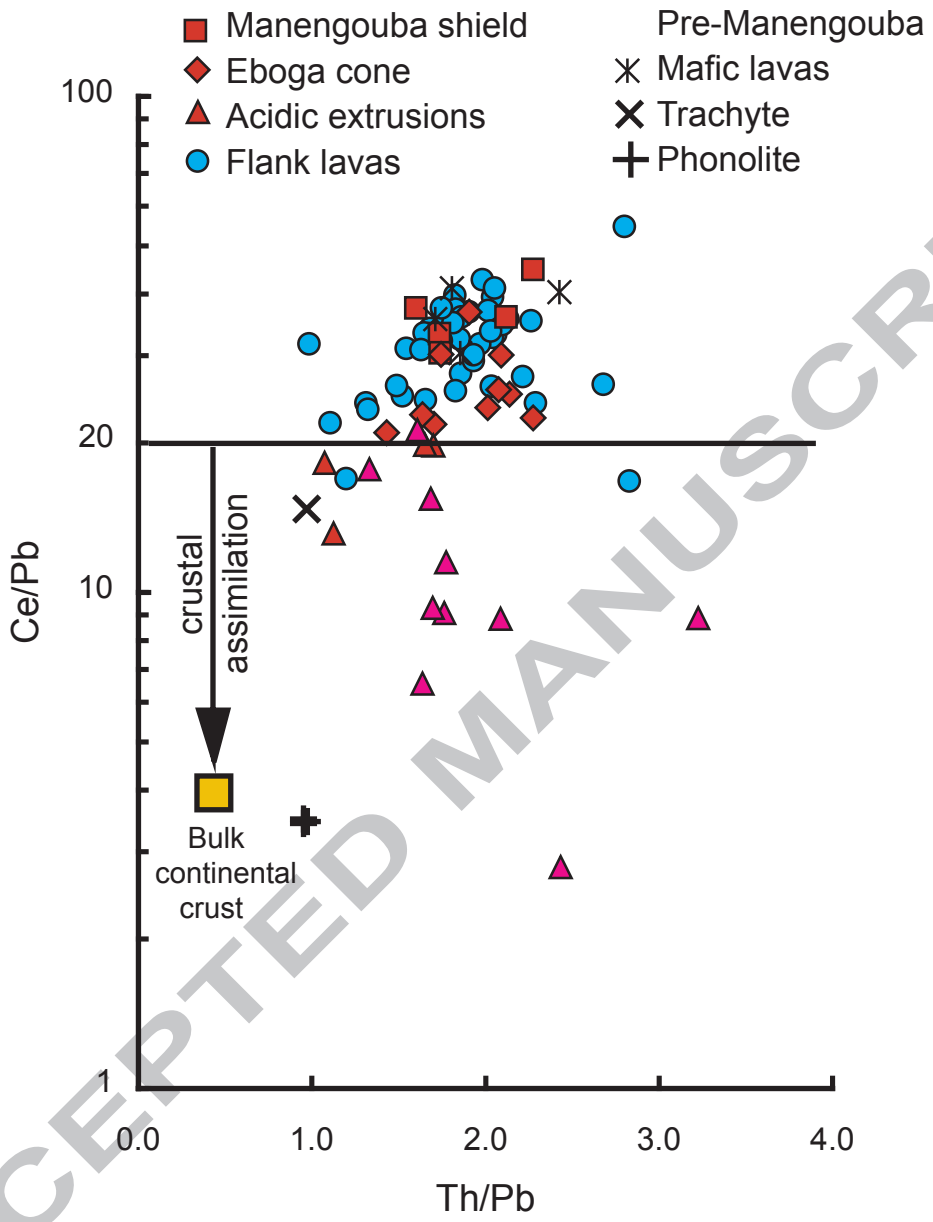

Fig. 20

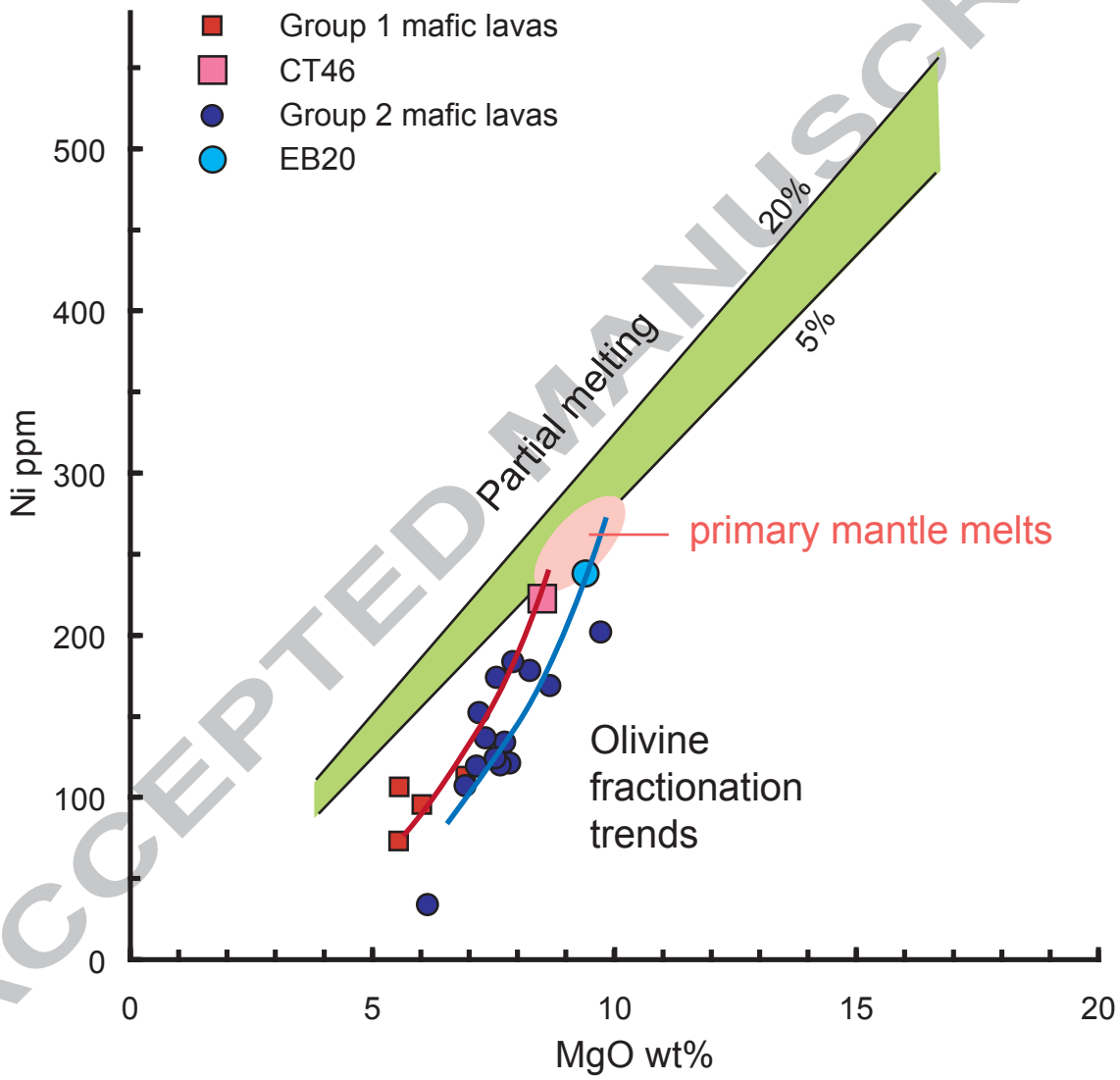

Fig. 21

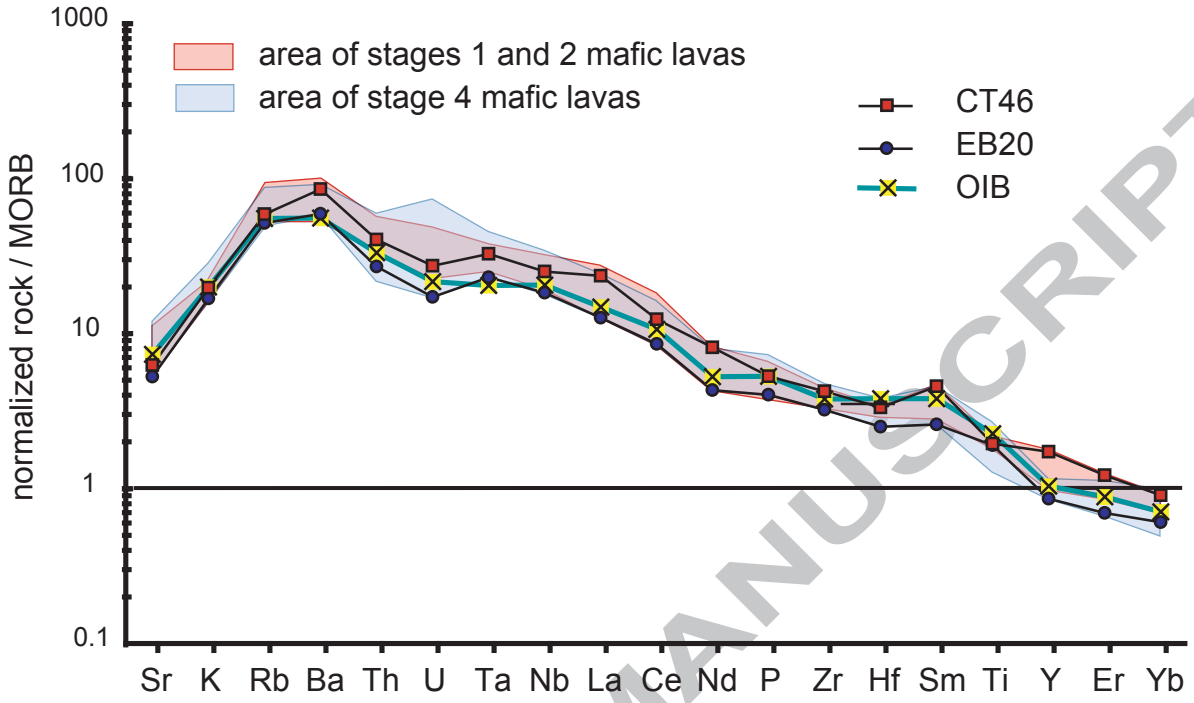

Fig. 22

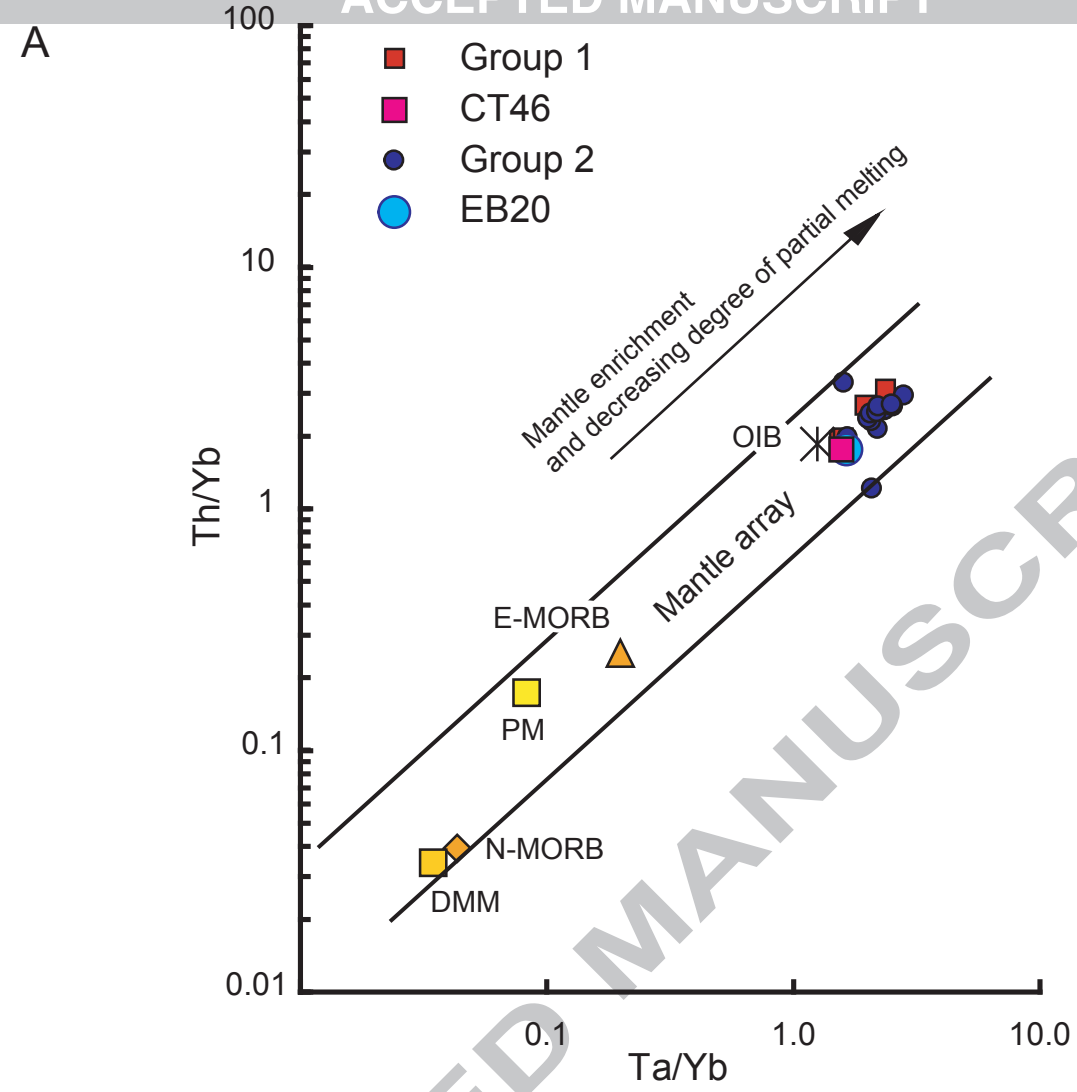

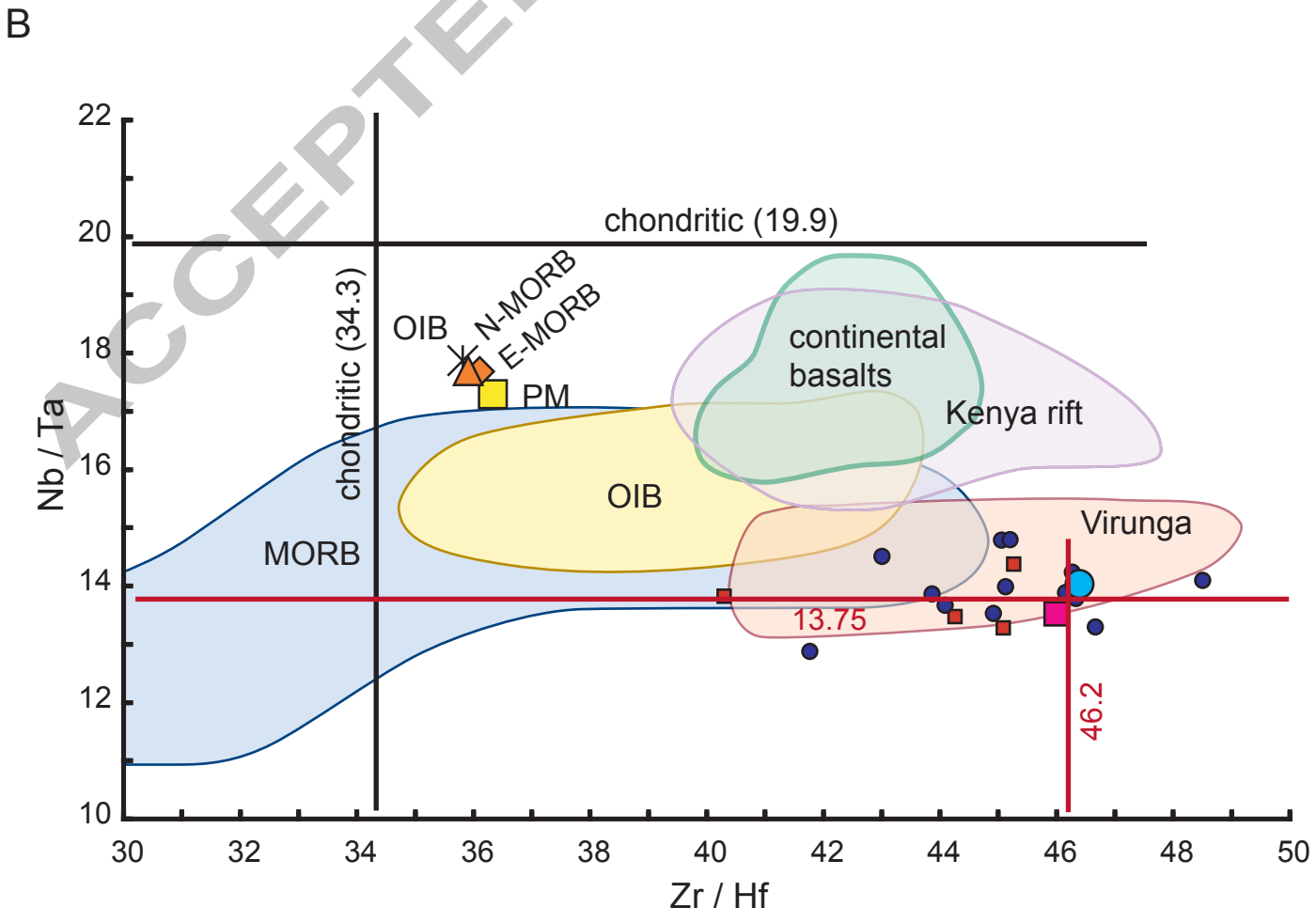

Fig. 23

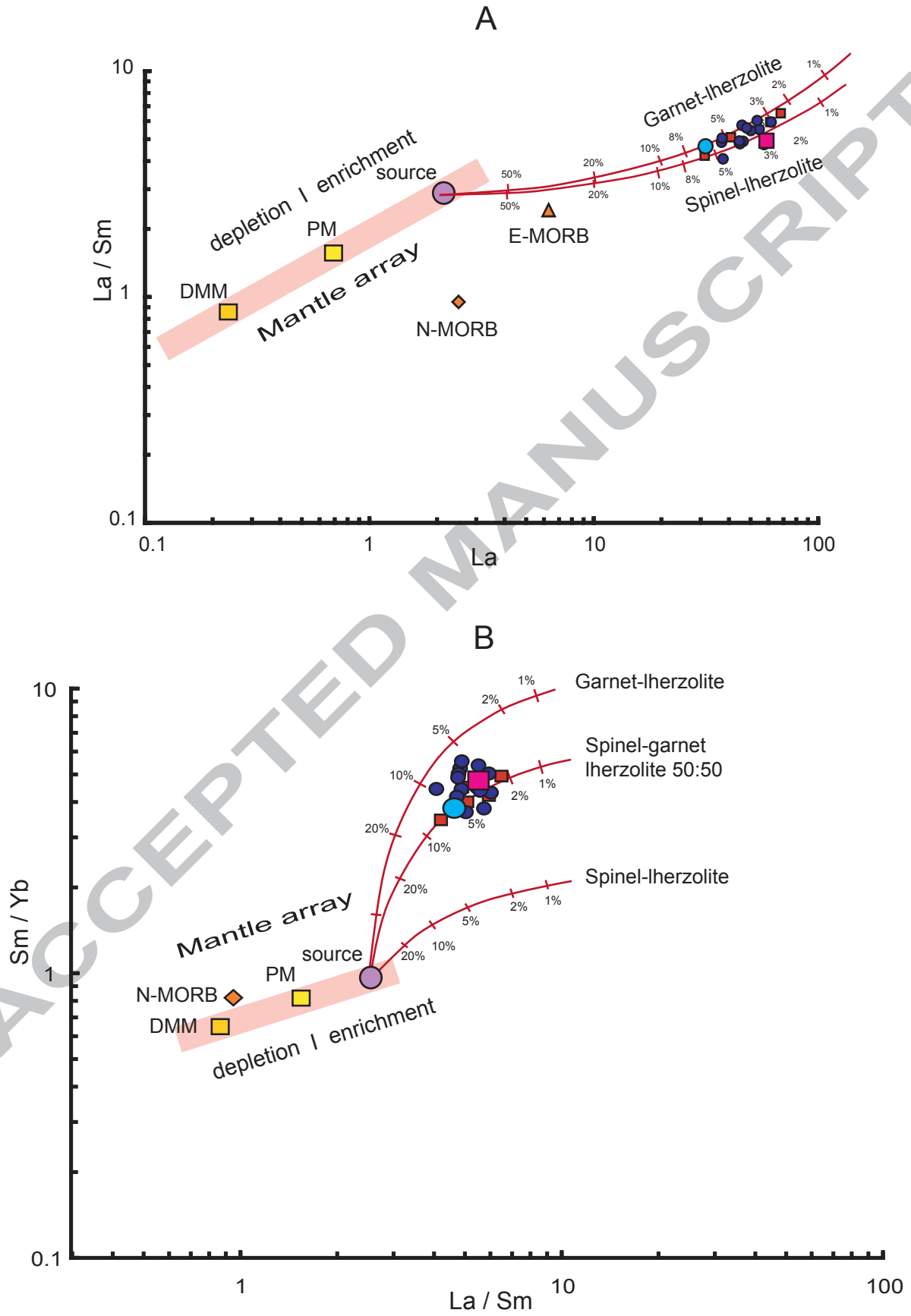

Fig. 24

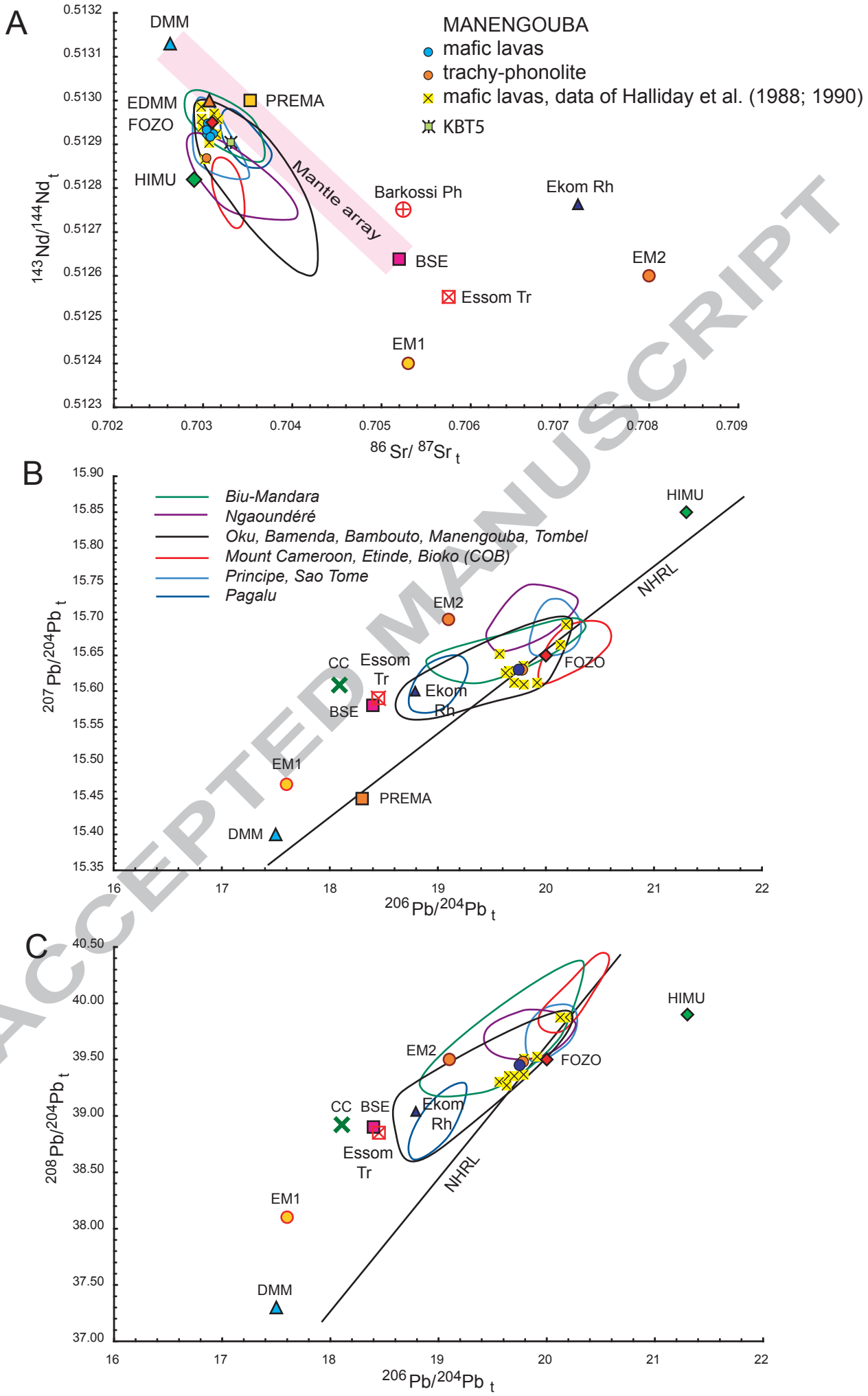

Fig. 24

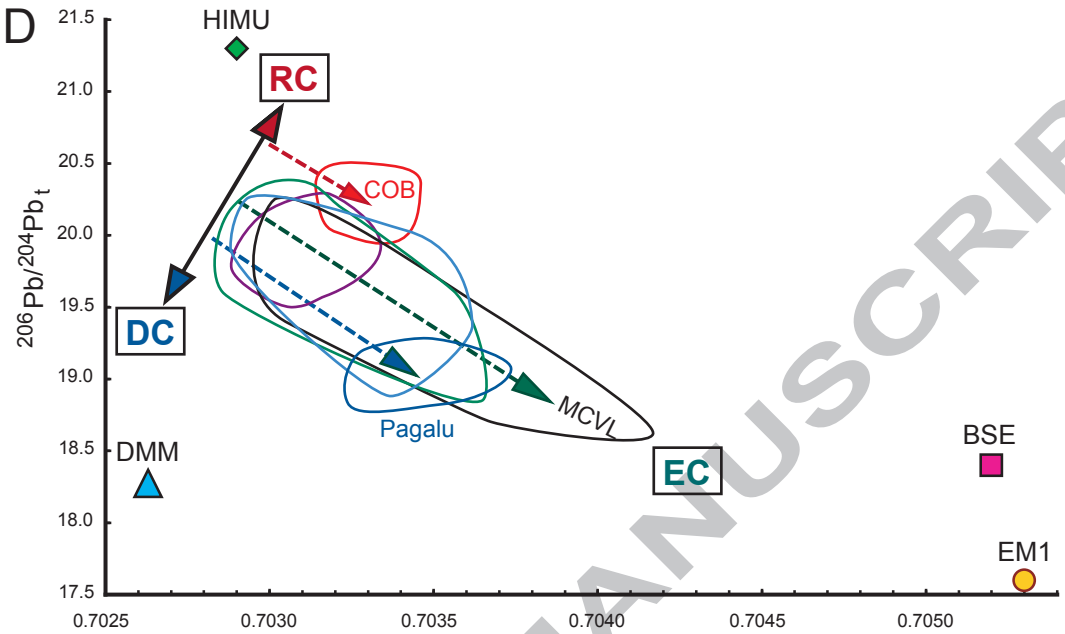

The Mount Manengouba, a complex volcano of the Cameroon Line: Volcanic history, petrological and geochemical features by André Pouclet et al.

Highlights

The volcanic history of the Manengouba fit with four stages between 1.55 and 0.11 Ma.
The volume of the volcano is calculated at 320 km^3 ± 5%.
The magma was generated with 3 to 6% of partial melting of a fairly enriched source.
Melting of the source occurred in the lithospheric spinel to garnet transition zone.
Three source components are distinguished: depleted, radiogenic, and enriched.

Table 4. Selected chemical analyses of minerals. A, Olivine

	Manengouba, stage 1								**Manengouba, stage 2**						**Manengouba, stage 4**											**Pre-Manengouba lavas**	
#	MA2b	CT45	CT45	CT45	ML2	ML2	ML2	ML2	Eb10	EB30	EB30	EL4	Eb17	EL4	GO1	NZ7	EM2	CT55	SA1b	CT55	KME2A	CT47	KEB19C	CT47	EE4	KOS7	Eb14	KOS7	PL5	PL5
Petrographical facies	Bs	alk-B	alk-B	alk-B	H	H	H	H	M	M	M	Bn	Bn	Bn	Bs	Bs	Bs	Na-Bs	B	Na-Bs	H	H	H	H	M	M	M	M	M	M
Mineral type	xenocryst	phenocryst	microcryst	microcryst	xenocryst	phenocryst	phenocryst	microcryst	xenocryst	phenocryst	microcryst total	xenocryst	phenocryst	microcryst	xenocryst	xenocryst	phenocryst	phenocryst	phenocryst	microcryst	xenocryst	phenocryst	phenocryst	microcryst	xenocryst	phenocryst	phenocryst	microcryst	xenocryst	phenocryst
SiO_2	40.82	39.09	38.20	38.92	40.39	39.45	39.20	36.40	39.17	37.57	36.05	38.23	37.39	35.50	40.44	39.99	39.46	38.46	38.93	37.72	39.20	38.28	37.07	37.22	38.37	38.03	36.54	35.55	40.29	39.28
TiO_2	0.04	0.00	0.05	0.08	0.03	0.03	0.02	0.21	0.00	0.03	0.05	0.00	0.02	0.07	0.00	0.00	0.08	0.14	0.05	0.01	0.00	0.04	0.10	0.05	0.00	0.01	0.05	0.06	0.00	0.06
Al_2O_3	0.03	0.00	0.00	0.00	0.08	0.04	0.06	0.17	0.00	0.00	0.00	0.00	0.03	0.13	0.07	0.18	0.03	0.00	0.01	0.00	0.02	0.00	0.03	0.00	0.03	0.03	0.00	0.03	0.00	0.06
FeO	14.29	16.87	19.32	21.98	14.86	19.66	21.87	35.59	20.68	28.40	37.32	28.05	33.61	40.07	12.14	17.36	17.61	19.09	21.65	24.07	14.01	18.92	25.14	25.68	19.75	26.56	31.90	37.96	13.67	21.62
MnO	0.19	0.27	0.47	0.52	0.22	0.27	0.30	0.98	0.26	0.44	1.21	0.58	1.07	1.40	0.17	0.18	0.20	0.21	0.38	0.80	0.11	0.50	0.37	0.67	0.35	0.64	0.34	1.10	0.13	0.32
MgO	46.81	42.79	40.21	39.13	46.13	42.00	39.64	28.16	40.13	34.08	26.38	34.83	30.74	24.54	46.34	43.98	42.19	40.51	39.67	36.30	44.99	40.23	35.32	34.94	39.71	35.39	30.66	25.73	46.31	40.07
CaO	0.30	0.19	0.16	0.28	0.23	0.22	0.29	0.42	0.19	0.31	0.40	0.20	0.20	0.39	0.20	0.22	0.23	0.29	0.26	0.40	0.19	0.24	0.37	0.27	0.18	0.19	0.26	0.35	0.25	0.25
NiO		0.08	0.00	0.42														0.27		0.00		0.27		0.16						
Total	102.48	99.29	98.41	101.33	101.94	101.67	101.38	101.93	100.43	100.83	101.41	101.89	103.06	102.10	99.36	101.91	99.80	98.97	100.95	99.30	98.52	98.48	98.40	98.99	98.39	100.85	99.75	100.78	100.65	101.66
Si	0.996	0.999	0.998	1.000	0.994	0.995	1.002	0.994	1.005	0.999	1.000	1.002	0.998	0.993	1.007	0.995	1.005	0.998	1.000	1.001	0.996	0.999	0.997	0.999	1.003	1.002	1.000	0.997	0.998	1.000
Ti	0.001	0.000	0.001	0.002	0.001	0.001	0.000	0.004	0.000	0.001	0.001	0.000	0.000	0.001	0.000	0.000	0.002	0.003	0.001	0.000	0.000	0.001	0.002	0.001	0.000	0.000	0.001	0.001	0.000	0.001
Al	0.001	0.000	0.000	0.000	0.002	0.001	0.002	0.005	0.000	0.000	0.000	0.000	0.001	0.004	0.002	0.005	0.001	0.000	0.000	0.000	0.001	0.000	0.001	0.000	0.001	0.001	0.000	0.001	0.000	0.002
Fe^{2+}	0.292	0.360	0.422	0.472	0.306	0.415	0.468	0.813	0.444	0.632	0.866	0.615	0.750	0.937	0.253	0.361	0.375	0.414	0.465	0.534	0.298	0.413	0.566	0.576	0.432	0.585	0.730	0.890	0.283	0.460
Mn	0.004	0.006	0.010	0.011	0.005	0.006	0.006	0.023	0.006	0.010	0.029	0.013	0.024	0.033	0.004	0.004	0.004	0.005	0.008	0.018	0.002	0.011	0.008	0.015	0.008	0.014	0.008	0.026	0.003	0.007
Mg	1.702	1.630	1.566	1.498	1.692	1.580	1.510	1.147	1.535	1.351	1.091	1.361	1.223	1.023	1.721	1.631	1.601	1.567	1.518	1.435	1.703	1.565	1.416	1.398	1.548	1.390	1.251	1.075	1.711	1.521
Ca	0.008	0.005	0.004	0.008	0.006	0.006	0.008	0.012	0.005	0.009	0.012	0.006	0.006	0.012	0.005	0.006	0.006	0.008	0.007	0.011	0.005	0.007	0.011	0.008	0.005	0.005	0.008	0.011	0.007	0.007
Ni	0.000	0.002	0.000	0.009	0.000	0.000	0.000	0.000	0.000	0.000	0.000	0.000	0.000	0.000	0.000	0.000	0.000	0.006	0.000	0.000	0.000	0.006	0.000	0.003	0.000	0.000	0.000	0.000	0.000	0.000
Total	3.003	3.001	3.001	2.999	3.005	3.003	2.997	2.999	2.995	3.001	2.999	2.998	3.002	3.004	2.992	3.002	2.993	3.000	2.999	2.999	3.004	3.000	3.001	3.000	2.996	2.997	2.999	3.001	3.002	2.998
% Fo	85.21	81.65	78.36	75.60	84.50	78.97	76.11	57.84	77.35	67.80	54.95	68.43	61.23	51.32	87.03	81.71	80.85	78.91	76.24	72.23	85.03	78.68	71.16	70.26	77.88	69.87	62.89	54.00	85.68	76.50
% Fa	14.79	18.35	21.64	24.40	15.50	21.03	23.89	42.16	22.65	32.20	45.05	31.57	38.77	48.68	12.97	18.29	19.15	21.09	23.76	27.77	14.97	21.32	28.84	29.74	22.12	30.13	37.11	46.00	14.32	23.50

Table 4. Selected analyses of minerals. B, Magnetite

	Manengouba, stage 1				Manengouba, stage 2			Manengouba, stage 3				Manengouba, stage 4										Pre-Manengouba	
#	MA2b	MA2b	ML2	ML2	NS2	Eb11	Eb11	EL4	Eb17	Eb17	KEB26	EM2	EM2	EM2	CT55	SA1b	CT47	SP5	SP5	KOS7	KOS7	KBT5	PL5
Petrographical facies	Bs	Bs	H	H	H	M	M	Bn	Bn	Bn	Tr	Na-Bs	Na-Bs	Na-Bs	Na-Bs	alk-B	H	H	H	M	M	H	M
Mineral type	phenocryst	microcryst	phenocryst	microcryst	phenocryst	phenocryst	microcryst	phenocryst	phenocryst	microcryst	microcryst	phenocryst	phenocryst	phenocryst	microcryst	phenocryst	phenocryst	phenocryst	microcryst	phenocryst	microcryst	phenocryst	microcryst
SiO_2	0.01	0.00	0.05	0.03	0.02	0.05	0.04	0.04	0.00	0.01	0.06	0.00	0.00	0.00	0.00	0.03	0.00	0.05	0.07	0.03	0.02	0.00	0.06
TiO_2	17.51	18.59	20.85	19.25	17.23	16.21	17.11	18.32	19.85	19.29	16.68	17.08	13.33	17.87	16.69	20.06	21.17	18.05	16.77	21.82	23.19	18.04	19.59
Al_2O_3	4.83	4.15	5.17	2.30	1.83	2.47	2.02	3.68	2.72	3.49	0.06	4.86	8.00	4.76	5.09	3.26	2.52	4.61	5.11	3.20	2.83	4.49	4.22
Cr_2O_3	0.03	0.03	0.08	0.06	0.02	0.12	0.01	0.03	0.04	0.00	0.00	5.43	12.26	3.54	0.14	0.08	2.73	0.07	0.00	0.00	0.02	0.20	1.06
FeO	69.24	68.05	67.73	73.12	73.75	77.34	75.59	71.28	71.67	70.80	75.01	62.34	56.32	64.67	68.29	69.38	64.64	70.04	70.37	66.94	66.09	68.42	66.24
MnO	0.56	0.38	0.50	0.71	0.46	0.67	0.85	0.63	1.02	0.69	1.47	0.66	0.49	0.58	0.33	0.41	0.79	0.47	0.57	0.98	0.82	0.59	0.61
MgO	6.25	6.55	4.54	1.78	2.22	1.16	0.47	4.49	2.60	3.46	0.00	5.01	5.54	4.95	5.08	3.44	3.14	4.79	5.49	3.09	3.01	4.08	4.68
Total	98.43	97.75	98.92	97.25	95.51	98.02	96.09	98.47	97.90	97.74	93.27	95.38	95.94	96.37	95.62	96.66	94.99	98.06	98.38	96.06	95.98	95.81	96.46
Si	0.003	0.000	0.014	0.009	0.004	0.015	0.012	0.011	0.000	0.003	0.018	0.000	0.000	0.000	0.000	0.009	0.000	0.013	0.019	0.009	0.006	0.000	0.018
Al	1.578	1.367	1.706	0.797	0.642	0.850	0.715	1.224	0.929	1.181	0.021	1.656	2.665	1.607	1.722	1.117	0.886	1.529	1.677	1.109	0.986	1.533	1.430
Ti	3.650	3.906	4.390	4.254	3.862	3.558	3.863	3.889	4.325	4.166	3.929	3.713	2.833	3.849	3.602	4.387	4.749	3.823	3.510	4.825	5.151	3.931	4.234
Fe^{3+}	7.111	6.814	5.468	6.664	7.621	7.977	7.532	6.968	6.411	6.482	8.086	5.678	4.930	5.894	7.042	6.072	4.972	6.785	7.265	5.222	4.697	6.560	5.824
Fe^{2+}	8.939	9.088	10.391	11.306	10.766	10.902	11.449	9.861	10.954	10.520	11.557	9.393	8.382	9.595	9.349	10.804	11.153	9.715	9.117	11.237	11.628	10.024	10.099
Mg	2.582	2.728	1.895	0.780	0.986	0.505	0.210	1.889	1.121	1.481	0.000	2.159	2.334	2.113	2.173	1.491	1.396	2.009	2.277	1.354	1.323	1.763	2.006
Mn	0.131	0.090	0.119	0.177	0.115	0.166	0.216	0.151	0.250	0.168	0.389	0.162	0.117	0.141	0.080	0.101	0.200	0.111	0.135	0.244	0.205	0.144	0.148
Cr	0.007	0.007	0.018	0.014	0.004	0.028	0.002	0.007	0.010	0.000	0.000	1.241	2.740	0.802	0.032	0.018	0.644	0.015	0.000	0.000	0.004	0.045	0.240
Total	24.000	24.000	24.000	24.000	24.000	24.000	24.000	24.000	24.000	24.000	24.000	24.000	24.000	24.000	24.000	24.000	24.000	24.000	24.000	24.000	24.000	24.000	24.000

Table 4. Selected analyses of minerals. C, Ilmenite

	Manengouba, stage 2				Manengouba, stage 3			Manengouba, stage 4			Pre-Man
#	NS2	EB30	Eb11	Eb11	EL4	Eb17	KNS1	Eb20	Eb14	Eb14	PL5
Petrographical facies	H	M	M	M	Bn	Bn	Tr	Alk-B	M	M	M
Mineral type	microcryst	phenocryst	phenocryst	microcryst	phenocryst	microcryst	icrophenocryst	phenocryst corr	phenocryst	phenocryst	microphenocryst
SiO_2	0.00	0.00	0.00	0.00	0.00	0.00	0.00	0.05	0.00	0.00	0.03
TiO_2	49.71	50.17	49.66	48.22	48.92	51.12	47.68	47.92	49.88	49.15	48.85
Al_2O_3	0.36	0.14	0.20	0.43	0.47	0.04	0.03	0.08	0.00	0.03	0.40
Cr_2O_3	0.00	0.00	0.03	0.00	0.00	0.00	0.00	0.00	0.00	0.15	0.10
FeO	41.92	42.46	45.39	48.20	44.44	44.69	45.68	44.30	46.89	46.64	42.88
MnO	0.63	0.77	0.94	0.81	0.64	1.38	2.09	1.32	0.80	0.89	0.44
MgO	4.89	4.01	3.42	1.81	5.45	0.86	0.00	1.94	1.10	1.14	5.02
CaO	0.03	0.03	0.03	0.03	0.05	0.05	0.00	0.06	0.00	0.00	0.08
Total	97.54	97.58	99.67	99.50	99.97	98.14	95.48	95.67	98.67	98.00	97.80
Si	0.000	0.000	0.000	0.000	0.000	0.000	0.000	0.003	0.000	0.000	0.001
Al	0.021	0.008	0.012	0.025	0.027	0.002	0.002	0.005	0.000	0.002	0.023
Ti	1.854	1.885	1.834	1.804	1.770	1.962	1.891	1.867	1.898	1.882	1.815
Fe^{3+}	0.263	0.218	0.315	0.359	0.424	0.072	0.217	0.258	0.204	0.225	0.334
Fe^{2+}	1.476	1.556	1.549	1.647	1.364	1.836	1.798	1.661	1.781	1.761	1.437
Mg	0.361	0.299	0.250	0.134	0.391	0.065	0.000	0.150	0.083	0.087	0.370
Mn	0.026	0.033	0.039	0.034	0.026	0.060	0.093	0.058	0.034	0.038	0.018
Cr	0.000	0.000	0.001	0.000	0.000	0.000	0.000	0.000	0.000	0.006	0.004
Ca	0.001	0.002	0.002	0.002	0.003	0.003	0.000	0.003	0.000	0.000	0.004
Total	4.002	4.000	4.001	4.003	4.002	3.998	4.000	4.001	4.000	4.001	4.002

Table 4. Selected analyses of minerals. D, Pyroxenes

	Manangoubia, stage 1										Manangoubia, stage 2										Manangoubia, stage 3							Manangoubia, stage 4														Pre-Manangoubia	
#	MA2B	MA2B	MA2B	MA2B	MA2B	ML2	ML2	ML2	ML2	ML2	KNS2	KNS2	KNS2	KEB30	KEB30	KEB30	EB11	EB10	EB11	EB10	EL4	EL4	KPT7	PT3	PT3	KPT7	GO-1	NZ-7	GO-1	NZ-7	CT-55	EB-20	SA1b	KME-2A	SP-5	CT-47	CT-47	CT-53	CT-47	KEB-19	KOS-7	KOS-7	KOS-7	EB-14	EB-14	EB-14	PL5	PL5
Petrographic cal facies	Na-Bs	Na-Bs	Na-Bs	Na-Bs	Na-Bs	H	H	H	H	H	H	H	H	M	M	M	M	M	M	M	Bs	Bs	Tr	Tr	Tr	Tr	Ank	Na-Bs	Ank	Na-Bs	Na-Bs	Alk-B	Alk-B	H	H	H	H	H	H	H	M	M	M	M	M	M	M	M
Mineral type	xenocryst	phenocryst	phenocryst	microcryst	xenocryst	xenocryst	phenocryst	phenocryst	microcryst	microcryst	phenocryst	phenocryst	microcryst	xenocryst	xenocryst	xenocryst	phenocryst	phenocryst	microcryst	microcryst	xenocryst	xenocryst	phenocryst	phenocryst	microcryst	microcryst	xenocryst	xenocryst	phenocryst	phenocryst	phenocryst	microcryst	microcryst	xenocryst	xenocryst	phenocryst	phenocryst	phenocryst	microcryst	microcryst	xenocryst	xenocryst	phenocryst	phenocryst	phenocryst	microcryst	microcryst	phenocryst	phenocryst
SiO_2	47.39	48.98	49.27	50.27	52.45	47.45	47.61	46.18	49.35	48.93	47.15	48.80	48.62	46.77	48.11	49.88	51.32	52.54	52.58	52.54	51.47	51.47	48.24	49.68	49.50	48.66	48.77	47.24	49.06	44.01	50.83	50.21	47.48	47.36	48.22	49.40	50.42	50.03	46.79	50.83	49.09	49.86	49.93	51.26	48.58	50.00	48.69	48.45
TiO_2	2.27	2.03	2.02	1.06	0.77	2.12	2.14	2.61	1.53	2.81	2.19	1.45	1.88	2.14	1.30	1.17	0.90	0.46	0.49	0.46	0.98	0.98	0.42	0.36	0.52	0.32	1.68	2.25	1.78	3.43	0.94	1.85	2.54	1.35	1.84	1.33	1.20	1.24	2.18	0.63	1.43	1.12	0.82	1.24	2.50	1.61	1.63	1.50
Al_2O_3	7.13	5.49	4.75	3.37	1.90	5.87	6.66	8.71	4.25	4.27	8.23	4.97	4.57	6.42	3.24	2.71	2.44	1.16	1.53	1.71	2.81	2.81	0.31	0.34	0.27	0.21	5.66	5.46	4.79	8.74	2.52	4.13	6.72	5.43	5.22	3.57	3.07	3.76	6.59	1.64	3.99	3.11	2.24	1.80	3.65	2.42	4.86	4.27
FeO	8.17	8.18	8.10	8.33	10.58	7.84	7.37	7.50	7.81	9.25	8.17	6.78	8.86	7.51	9.01	8.94	11.01	9.20	12.07	10.61	8.00	8.00	24.66	24.28	25.91	25.92	7.41	7.12	7.69	8.51	8.68	9.47	9.85	5.70	8.42	8.32	8.03	8.00	8.95	10.32	8.19	8.03	9.73	9.86	11.10	12.38	8.78	8.73
Cr_2O_3	0.04	0.00	0.18	0.00	0.00	0.04	0.00	0.20	0.00	0.00	0.15	0.58	0.00	0.00	0.00	0.11	0.00	0.00	0.04	0.00	0.00	0.00	0.01	0.00	0.00	0.00	0.05	0.00	0.12	0.13	0.00	0.08	0.06	0.57	0.00	0.02	0.00	0.18	0.01	0.04	0.00	0.00	0.00	0.00	0.00	0.12	0.00	0.00
MnO	0.17	0.16	0.20	0.27	0.56	0.26	0.20	0.14	0.19	0.25	0.19	0.00	0.18	0.01	0.32	0.17	0.52	0.50	0.62	0.59	0.30	0.30	1.57	1.40	1.57	1.60	0.22	0.14	0.14	0.14	0.47	0.24	0.12	0.11	0.24	0.17	0.12	0.20	0.20	0.49	0.31	0.25	0.55	0.26	0.26	0.25	0.33	0.27
MgO	13.86	14.25	14.62	15.16	13.93	13.94	13.45	12.74	14.38	13.34	13.86	14.92	14.01	13.71	13.69	13.46	13.90	13.52	13.07	11.98	14.86	14.86	3.32	2.97	2.75	2.34	13.54	13.81	13.53	11.23	16.50	15.14	11.92	14.52	14.03	14.38	14.70	14.86	12.63	14.32	14.69	15.21	14.00	13.76	12.24	11.71	13.93	13.82
CaO	21.44	21.03	21.25	18.85	20.94	21.59	21.54	21.24	19.63	20.95	19.82	19.11	19.01	20.83	20.44	20.85	19.71	21.98	20.43	21.60	21.75	21.75	17.81	19.47	18.31	17.44	21.08	22.07	21.29	22.00	18.91	20.13	20.14	21.35	21.16	21.06	20.43	20.05	20.38	19.46	20.44	20.03	20.02	20.65	20.40	20.27	19.74	19.69
Na_2O	0.65	0.70	0.33	0.56	0.52	0.57	0.66	0.62	0.54	0.60	0.52	0.38	0.52	0.54	0.48	0.47	0.69	0.47	0.52	0.69	0.53	0.53	1.16	1.22	1.23	1.53	0.52	0.52	0.42	0.59	0.22	0.49	0.48	0.43	0.73	0.39	0.42	0.42	0.58	0.47	0.64	0.59	0.51	0.37	0.50	0.65	0.64	0.51
K_2O	0.01	0.00	0.00	0.00	0.02	0.00	0.00	0.02	0.03	0.00	0.01	0.00	0.01	0.00	0.00	0.04	0.01	0.03	0.00	0.00	0.00	0.00	0.00	0.01	0.03	0.02	0.02	0.01	0.00	0.02	0.00	0.01	0.00	0.00	0.01	0.03	0.00	0.00	0.00	0.00	0.02	0.01	0.01	0.00	0.00	0.00	0.01	0.00
Total	101.13	100.82	100.72	97.66	101.67	99.68	99.63	99.96	97.69	100.40	98.29	96.99	97.66	97.93	96.60	97.79	100.50	99.86	101.35	100.18	100.70	100.70	97.49	99.73	100.09	98.06	98.95	98.62	98.82	98.80	99.07	101.76	99.31	96.82	99.87	98.67	98.39	98.74	98.31	98.20	98.80	98.20	97.80	99.20	99.23	99.41	98.59	97.22
Si	1.733	1.796	1.814	1.899	1.928	1.761	1.767	1.711	1.867	1.820	1.777	1.853	1.848	1.765	1.851	1.900	1.906	1.964	1.951	1.971	1.890	1.890	1.986	1.997	1.993	1.999	1.824	1.771	1.843	1.665	1.892	1.830	1.792	1.797	1.786	1.855	1.896	1.873	1.772	1.929	1.835	1.872	1.900	1.932	1.845	1.902	1.830	1.849
Al^{iv}	0.267	0.204	0.186	0.101	0.072	0.239	0.233	0.289	0.133	0.180	0.223	0.147	0.152	0.235	0.147	0.100	0.094	0.036	0.049	0.029	0.110	0.110	0.014	0.003	0.007	0.001	0.176	0.229	0.157	0.335	0.108	0.170	0.208	0.203	0.214	0.145	0.104	0.127	0.228	0.071	0.165	0.128	0.100	0.068	0.155	0.098	0.170	0.151
T	2.000	2.000	2.000	2.000	2.000	2.000	2.000	2.000	2.000	2.000	2.000	2.000	2.000	2.000	1.999	2.000	2.000	2.000	2.000	2.000	2.000	2.000	2.000	2.000	2.000	2.000	2.000	2.000	2.000	2.000	2.000	2.000	2.000	2.000	2.000	2.000	2.000	2.000	2.000	2.000	2.000	2.000	2.000	2.000	2.000	2.000	2.000	2.000
Al^{vi}	0.040	0.033	0.020	0.049	0.010	0.018	0.058	0.092	0.056	0.008	0.053	0.076	0.052	0.050	0.000	0.022	0.013	0.015	0.018	0.047	0.011	0.011	0.001	0.013	0.006	0.009	0.074	0.012	0.055	0.055	0.003	0.007	0.001	0.039	0.014	0.013	0.032	0.039	0.066	0.002	0.008	0.006	0.001	0.012	0.008	0.010	0.046	0.041
Ti^{vi}	0.062	0.056	0.056	0.030	0.021	0.059	0.060	0.073	0.043	0.079	0.062	0.041	0.054	0.061	0.036	0.034	0.025	0.013	0.014	0.013	0.027	0.027	0.013	0.011	0.016	0.010	0.047	0.063	0.050	0.098	0.026	0.051	0.072	0.038	0.051	0.038	0.034	0.035	0.062	0.018	0.040	0.032	0.023	0.035	0.071	0.046	0.046	0.043
Fe^{3+}	0.147	0.108	0.073	0.032	0.057	0.141	0.103	0.090	0.032	0.058	0.080	0.000	0.031	0.102	0.110	0.044	0.081	0.031	0.039	0.006	0.082	0.082	0.079	0.063	0.067	0.094	0.044	0.127	0.029	0.124	0.068	0.094	0.006	0.102	0.150	0.085	0.035	0.043	0.080	0.067	0.121	0.099	0.090	0.013	0.041	0.040	0.079	0.061
Cr	0.001	0.000	0.005	0.000	0.000	0.001	0.000	0.006	0.000	0.000	0.004	0.017	0.000	0.000	0.000	0.003	0.000	0.000	0.001	0.000	0.000	0.000	0.000	0.000	0.000	0.000	0.001	0.000	0.004	0.004	0.000	0.002	0.002	0.017	0.000	0.001	0.000	0.005	0.000	0.001	0.000	0.005	0.000	0.000	0.000	0.004	0.000	0.000
Fe^{2+}	0.090	0.125	0.152	0.189	0.237	0.091	0.113	0.124	0.182	0.203	0.149	0.176	0.207	0.117	0.159	0.215	0.223	0.239	0.294	0.306	0.147	0.147	0.717	0.738	0.756	0.751	0.166	0.089	0.189	0.135	0.163	0.162	0.259	0.071	0.099	0.155	0.188	0.175	0.175	0.222	0.117	0.131	0.192	0.261	0.273	0.313	0.167	0.186
Mg	0.660	0.678	0.694	0.699	0.675	0.689	0.667	0.615	0.686	0.653	0.652	0.690	0.656	0.670	0.695	0.682	0.658	0.702	0.634	0.628	0.732	0.732	0.190	0.174	0.155	0.155	0.667	0.709	0.673	0.585	0.740	0.684	0.570	0.733	0.687	0.709	0.711	0.702	0.616	0.690	0.711	0.729	0.694	0.679	0.607	0.587	0.662	0.669
M1	1.000	1.000	1.000	1.000	1.000	1.000	1.000	1.000	1.000	1.000	1.000	1.000	1.000	1.000	1.000	1.000	1.000	1.000	1.000	1.000	1.000	1.000	1.000	1.000	1.000	1.000	1.000	1.000	1.000	1.000	1.000	1.000	1.000	1.000	1.000	1.000	1.000	1.000	1.000	1.000	1.000	1.000	1.000	1.000	1.000	1.000	1.000	1.000
Fe2+	0.013	0.019	0.024	0.042	0.031	0.011	0.013	0.018	0.033	0.027	0.029	0.039	0.044	0.018	0.021	0.026	0.038	0.017	0.041	0.021	0.016	0.016	0.053	0.015	0.049	0.045	0.022	0.008	0.024	0.011	0.039	0.033	0.046	0.009	0.013	0.021	0.030	0.032	0.028	0.039	0.018	0.022	0.028	0.036	0.039	0.041	0.030	0.032
Mg	0.096	0.101	0.108	0.154	0.089	0.082	0.077	0.089	0.124	0.087	0.127	0.155	0.138	0.101	0.091	0.082	0.112	0.051	0.089	0.042	0.081	0.081	0.014	0.003	0.010	0.008	0.088	0.063	0.084	0.048	0.176	0.139	0.101	0.088	0.088	0.097	0.113	0.127	0.097	0.120	0.107	0.122	0.100	0.094	0.086	0.077	0.118	0.117
Mn	0.005	0.005	0.006	0.009	0.017	0.008	0.006	0.004	0.006	0.008	0.006	0.000	0.006	0.000	0.011	0.006	0.016	0.016	0.019	0.019	0.009	0.009	0.055	0.048	0.054	0.056	0.007	0.004	0.004	0.004	0.015	0.007	0.004	0.004	0.007	0.005	0.004	0.006	0.006	0.016	0.010	0.008	0.018	0.008	0.008	0.008	0.010	0.009
Ca	0.840	0.826	0.838	0.755	0.825	0.859	0.856	0.843	0.795	0.835	0.800	0.778	0.774	0.842	0.843	0.851	0.784	0.880	0.812	0.868	0.856	0.856	0.785	0.839	0.790	0.768	0.845	0.887	0.857	0.892	0.754	0.786	0.814	0.868	0.840	0.847	0.823	0.804	0.827	0.789	0.818	0.805	0.816	0.834	0.830	0.826	0.795	0.805
Na	0.046	0.050	0.024	0.041	0.037	0.041	0.047	0.045	0.040	0.043	0.038	0.028	0.038	0.039	0.036	0.034	0.050	0.034	0.037	0.050	0.038	0.038	0.093	0.095	0.096	0.122	0.038	0.038	0.051	0.043	0.016	0.035	0.035	0.032	0.053	0.028	0.031	0.030	0.043	0.035	0.046	0.043	0.037	0.027	0.037	0.048	0.046	0.037
K	0.000	0.000	0.000	0.000	0.001	0.000	0.000	0.001	0.002	0.000	0.000	0.000	0.000	0.000	0.000	0.002	0.000	0.001	0.000	0.000	0.000	0.000	0.000	0.001	0.002	0.001	0.001	0.000	0.000	0.001	0.000	0.000	0.000	0.000	0.000	0.001	0.000	0.000	0.000	0.000	0.000	0.001	0.000	0.000	0.000	0.000	0.001	0.000
M2	1.001	1.000	1.000	1.000	1.000	1.001	1.000	1.000	1.000	1.000	1.000	1.000	1.000	1.000	1.000	1.000	1.000	1.000	1.000	1.000	1.000	1.000	1.000	1.000	1.000	1.000	1.000	1.000	1.000	1.000	1.000	1.000	1.000	1.000	1.000	1.000	1.000	1.000	1.000	1.000	1.000	1.000	1.000	1.001	1.000	1.000	1.000	1.000
Mg %	44.34	44.42	44.01	46.19	40.74	44.33	42.95	41.55	44.37	40.82	44.16	45.96	43.51	44.10	43.18	41.05	42.02	39.53	38.25	35.57	44.16	44.16	11.24	9.80	9.10	8.13	42.08	43.87	41.36	37.80	48.52	45.41	37.39	46.34	44.70	43.90	44.10	44.90	40.76	43.15	45.94	46.82	42.98	40.41	37.60	35.85	43.78	43.24
Fe^{3+} + Mn %	6.37	8.45	10.01	12.95	15.24	6.33	7.61	8.66	12.11	13.12	10.43	11.72	14.06	7.73	10.48	13.22	15.15	14.28	18.77	18.34	9.39	9.39	45.46	44.05	47.36	48.32	10.84	5.74	11.87	8.97	11.51	11.18	17.21	4.69	6.85	9.88	11.86	11.56	11.97	14.71	8.11	8.87	12.86	16.00	17.35	19.55	11.63	12.46
Ca %	49.30	47.12	45.98	40.86	44.02	49.34	49.44	49.79	43.52	46.07	45.41	42.32	42.43	48.16	46.34	45.73	42.83	46.19	42.98	46.09	46.45	46.45	43.30	46.15	43.54	43.55	47.08	50.39	46.77	53.23	39.97	43.41	45.40	48.97	48.45	46.21	44.95	43.54	47.27	42.14	45.95	44.30	44.16	43.59	45.04	44.60	44.59	44.29

Table 4. Selected analyses of minerals. E, Amphibole Adv

	Manengouba, stage 2				Manengouba, stage 4						
#	EB11	Eb10	Eb10	Eb10	EK1C	EK1C	KOS7	EE4	EE4	KK3A	KK3A
Petrographical facies	M	M	M	M	H	H	M	M	M	M	M
Mineral type	nicrophenocrys Edenite	phenocryst Kaersutite	phenocryst Kaersutite	phenocryst Kaersutite	phenocryst Kaersutite	phenocryst Kaersutite	microcryst Edenite	phenocryst Kaersutite	microcryst Kaersutite	phenocryst Kaersutite	phenocryst Edenite
SiO_2	45.40	40.84	40.24	39.59	39.53	39.57	44.73	40.79	40.20	39.81	41.99
TiO_2	2.10	6.03	5.85	6.16	5.20	5.26	3.41	4.87	5.14	5.19	4.42
Al_2O_3	6.71	13.03	12.34	13.65	12.85	12.76	7.27	12.39	14.40	13.22	10.62
Cr_2O_3	0.00	0.02	0.00	0.05	0.00	0.00	0.00	0.00	0.00	0.00	0.08
FeO	10.66	11.24	11.11	10.63	11.55	11.14	10.56	11.00	10.35	10.73	13.93
MnO	0.39	0.21	0.22	0.17	0.12	0.33	0.24	0.10	0.19	0.22	0.31
MgO	16.42	12.25	13.12	12.09	13.10	13.16	15.84	13.36	13.08	13.69	12.64
CaO	10.45	11.65	11.77	11.96	11.77	11.84	10.64	11.84	11.17	10.79	10.43
Na_2O	2.88	2.69	3.14	2.81	2.90	2.78	3.58	2.77	2.67	3.00	2.93
K_2O	1.17	0.88	0.89	0.95	1.02	1.01	1.23	0.83	0.94	0.98	1.01
Total	96.17	98.84	98.68	98.06	98.05	97.84	97.52	97.95	98.14	97.62	98.34
Si	6.661	5.993	5.930	5.888	5.847	5.862	6.569	6.009	5.849	5.825	6.159
Al^{IV}	1.160	2.007	2.070	2.112	2.153	2.138	1.259	1.991	2.151	2.175	1.835
Ti	0.179	0.000	0.000	0.000	0.000	0.000	0.172	0.000	0.000	0.000	0.006
Total	8.000	8.000	8.000	8.000	8.000	8.000	8.000	8.000	8.000	8.000	8.000
Al^{VI}	0.000	0.247	0.073	0.281	0.088	0.088	0.000	0.160	0.318	0.105	0.000
Ti	0.053	0.665	0.648	0.689	0.579	0.586	0.205	0.539	0.562	0.571	0.481
Cr	0.000	0.002	0.000	0.006	0.000	0.000	0.000	0.000	0.000	0.000	0.010
Fe^{3+}	0.721	0.000	0.000	0.000	0.152	0.131	0.248	0.068	0.296	0.508	0.559
Fe^{2+}	0.586	1.379	1.369	1.322	1.277	1.248	1.048	1.287	0.963	0.805	1.150
Mn	0.049	0.026	0.027	0.021	0.015	0.042	0.030	0.012	0.023	0.027	0.038
Mg	3.591	2.680	2.882	2.680	2.889	2.905	3.468	2.933	2.837	2.985	2.763
Total	5.000	5.000	5.000	5.000	5.000	5.000	5.000	5.000	5.000	5.000	5.000
Ca	1.642	1.832	1.858	1.906	1.865	1.879	1.675	1.869	1.741	1.691	1.639
Na	0.358	0.168	0.142	0.094	0.135	0.121	0.325	0.131	0.259	0.309	0.361
Total	2.000	2.000	2.000	2.000	2.000	2.000	2.000	2.000	2.000	2.000	2.000
Na	0.461	0.597	0.756	0.716	0.697	0.677	0.694	0.660	0.494	0.541	0.471
K	0.218	0.165	0.167	0.180	0.193	0.191	0.230	0.156	0.174	0.183	0.188
Total	0.679	0.762	0.923	0.896	0.890	0.868	0.924	0.816	0.669	0.723	0.659

Table 4. Selected analyses of minerals. F, Mica

	Manengouba, stage 2		Manengouba, stage 4	
#	Eb11	Eb11	KOS7	KOS7
Petrographical facies	M	M	M	M
Mineral type	phenocryst	phenocryst	microphenocrys	microcryst
SiO_2	40.56	41.02	39.60	39.27
TiO_2	3.92	3.90	4.99	5.74
Al_2O_3	12.33	11.88	11.97	12.36
Cr_2O_3	0.00	0.11	0.00	0.00
FeO	9.56	8.97	9.51	10.02
MgO	20.59	20.61	19.60	18.54
CaO	0.08	0.00	0.01	0.03
MnO	0.11	0.00	0.13	0.11
Na_2O	0.99	0.84	1.40	1.02
K_2O	9.00	9.31	8.49	8.60
Total	97.14	96.64	95.70	95.69
Si	3.152	3.196	3.128	3.107
Al^{IV}	0.848	0.804	0.872	0.893
Total	4.000	4.000	4.000	4.000
Al^{VI}	0.282	0.287	0.241	0.260
Ti	0.229	0.229	0.296	0.342
Fe	0.621	0.584	0.628	0.663
Mg	2.386	2.394	2.308	2.187
Mn	0.007	0.000	0.009	0.008
Total	3.525	3.493	3.482	3.459
K	0.894	0.927	0.857	0.870
Na	0.149	0.127	0.215	0.156
Total	1.044	1.054	1.072	1.026

Table 4. Selected analyses of minerals. G, Feldspars

	Manengouba, stage 1									**Manengouba, stage 2**					**Manengouba, stage 3**							**Manengouba, stage 4**											
#	CT46	MA2B	MA2B	MA2B	MA2B	MA2B	ML2	ML2	NS2	KEB30	EB10	KEB30	ELG4	EB11	EB17	EL4	KEB3	EL4	KNS1	KPT7	KEB26	GO1	EM2	EM2	EM2	EB20	CT41	CT53	SP5	SA1b	SP5	KOS7	KOS7	EB14	KK3A
Petrographical facies	alk-B	Na-Bs	Na-Bs	Na-Bs	Na-Bs	Na-Bs	H	H	H	M	M	M	M	M	Bn	Bn	Bn	Bn	Tr	Tr	Tr	Ank	Na-Bs	Na-Bs	Na-Bs	Bs	H	H	H	H	H	M	M	M	M
Mineral type	phenocryst	phenocryst	phenocryst	microcryst	microcryst	xenocryst	phenocryst	phenocryst	microcryst	phenocryst	microcryst	microcryst	icrophenocry	xenocryst	phenocryst	phenocryst	microcryst	microcryst	phenocryst	phenocryst	phenocryst	phenocryst	phenocryst	phenocryst	microcryst	xenocryst	phenocryst	phenocryst	phenocryst	microcryst	microcryst	phenocryst	phenocryst	phenocryst	xenocryst
SiO_2	50.55	50.02	50.79	52.90	54.49	56.41	52.87	55.03	54.91	53.07	58.16	56.95	62.23	52.44	56.93	58.41	56.95	58.34	65.39	65.78	64.56	50.65	51.35	51.74	54.02	58.12	51.20	54.16	53.68	54.55	55.25	52.61	54.67	57.28	61.34
Al_2O_3	31.66	31.97	29.79	30.11	28.51	28.25	30.19	29.05	28.05	27.94	27.11	25.07	21.68	30.06	27.75	26.55	25.07	24.69	18.69	18.67	18.64	30.28	29.91	29.70	26.97	26.33	30.32	28.87	28.09	28.23	28.04	27.86	27.49	25.43	23.32
Fe_2O_3	1.05	0.98	0.82	0.93	0.53	0.43	0.33	0.56	0.95	0.48	0.50	0.50	0.16	0.56	0.46	0.71	0.50	0.46	0.18	0.00	0.25	0.64	0.90	1.13	1.75	0.20	0.59	0.70	0.57	0.52	0.34	0.48	0.30	0.64	0.34
CaO	13.02	13.02	12.16	11.39	10.48	9.63	12.32	10.66	9.88	10.24	8.31	7.53	3.16	12.29	8.88	7.88	7.53	6.37	0.12	0.01	0.19	13.54	12.67	12.43	10.45	8.77	11.75	11.25	10.18	9.88	9.54	10.87	9.78	9.20	5.06
Na_2O	3.71	3.55	3.98	4.52	5.22	5.69	4.33	5.30	5.49	5.11	6.46	6.66	8.35	4.20	6.02	6.54	6.66	6.92	7.11	7.43	7.42	3.62	3.86	3.94	4.86	6.29	4.18	4.89	5.31	5.45	5.64	4.91	5.56	6.11	8.00
K_2O	0.01	0.26	0.25	0.31	0.36	0.53	0.23	0.31	0.40	0.43	0.66	0.64	1.74	0.34	0.57	0.57	0.64	0.99	6.23	5.91	5.48	0.25	0.37	0.38	0.79	0.70	0.25	0.32	0.35	0.35	0.39	0.34	0.33	0.63	1.10
Total	100.00	99.80	97.78	100.16	99.59	100.94	100.27	100.91	99.68	97.27	101.20	97.35	97.32	99.89	100.61	100.66	97.35	97.77	97.72	97.81	96.54	98.98	99.06	99.32	98.84	100.41	98.29	100.19	98.18	98.98	99.19	97.07	98.13	99.29	99.16
Si	2.300	2.284	2.359	2.393	2.470	2.515	2.389	2.462	2.487	2.464	2.579	2.623	2.836	2.382	2.542	2.600	2.623	2.667	2.989	2.997	2.981	2.332	2.359	2.370	2.482	2.598	2.361	2.446	2.469	2.484	2.506	2.452	2.508	2.597	2.754
Al	1.698	1.720	1.631	1.605	1.523	1.485	1.608	1.532	1.497	1.529	1.417	1.361	1.164	1.609	1.461	1.393	1.361	1.330	1.007	1.003	1.014	1.643	1.619	1.604	1.461	1.387	1.648	1.537	1.523	1.515	1.499	1.531	1.487	1.359	1.234
Fe^{2+}	0.036	0.034	0.029	0.032	0.018	0.014	0.011	0.019	0.032	0.017	0.017	0.017	0.006	0.019	0.015	0.024	0.017	0.016	0.006	0.000	0.009	0.022	0.031	0.039	0.061	0.007	0.020	0.024	0.020	0.018	0.012	0.017	0.010	0.022	0.011
Ca	0.635	0.637	0.605	0.552	0.509	0.460	0.597	0.511	0.479	0.510	0.395	0.372	0.154	0.598	0.425	0.376	0.372	0.312	0.006	0.001	0.009	0.668	0.624	0.610	0.514	0.420	0.581	0.544	0.502	0.482	0.464	0.543	0.481	0.447	0.243
Na	0.327	0.314	0.359	0.396	0.459	0.492	0.379	0.460	0.482	0.460	0.555	0.595	0.737	0.370	0.521	0.565	0.595	0.614	0.630	0.657	0.664	0.323	0.344	0.350	0.433	0.545	0.374	0.428	0.474	0.481	0.496	0.444	0.495	0.537	0.696
K	0.001	0.015	0.015	0.018	0.021	0.030	0.014	0.018	0.023	0.025	0.037	0.037	0.101	0.020	0.033	0.032	0.037	0.058	0.364	0.344	0.324	0.015	0.022	0.022	0.046	0.040	0.015	0.018	0.020	0.020	0.023	0.020	0.019	0.037	0.063
Total	4.997	5.004	4.998	4.996	4.999	4.996	4.998	5.001	5.001	5.005	5.001	5.005	4.999	4.998	4.997	4.990	5.005	4.996	5.002	5.002	5.001	5.004	4.999	4.995	4.997	4.997	4.999	4.997	5.007	5.000	4.998	5.006	5.000	4.999	5.003
% Ab	34.00	32.52	36.64	41.02	46.41	50.08	38.34	46.52	48.96	46.24	56.24	59.26	74.25	37.45	53.26	58.03	59.26	62.41	63.00	65.57	66.62	32.13	34.76	35.63	43.57	54.23	38.57	43.21	47.58	48.92	50.48	44.08	49.74	52.63	69.44
% An	65.94	65.91	61.86	57.12	51.48	46.84	60.29	51.70	48.69	51.21	39.98	37.02	15.55	60.55	43.41	38.64	37.02	31.74	0.57	0.06	0.92	66.41	63.05	62.11	51.77	41.79	59.91	54.93	50.37	49.01	47.20	53.93	48.33	43.79	24.27
% Or	0.06	1.57	1.49	1.86	2.11	3.08	1.37	1.78	2.35	2.55	3.79	3.72	10.20	2.00	3.33	3.33	3.72	5.85	36.43	34.36	32.46	1.46	2.20	2.27	4.67	3.98	1.52	1.86	2.05	2.07	2.32	1.99	1.92	3.58	6.30

Table 5. Chemical analyses of the rocks

	Manengouba, stage 1					Manengouba, stage 2										Manengouba, stage 3							
Location	Ekon-Nkam fall	Mantem	N Manjo Mahongué river	E Manjo Moo river	Enyandong Mbe river	Eboga Nsoung	Eboga Ekambeng	Eboga aldera-SSW wal	Eboga SW slope	Eboga Elong-N slope	Eboga ouanguel-NE sl	Eboga caldera-SW wall	Eboga E slope	Eboga aldera-WNW wa	Eboga Ekambeng	Eboga caldera	Eboga E slope	Eboga caldera	Eboga caldera	Elengoum summit	Elengoum summit	Elengoum summit	Elengoum Nkongsamba
#	KO1	CT46	MA2B	ML2	DN1	KNS2	CT49	KEB30	EB11	ELG4	MLG1	EB15	EL1	EB10	CT50	KEB3	EL4	EB17	EB2	PT3	KPT7	GE6	CT214
Setting type	flow	flow	flow	flow	flow	flow	flow	flow	flow	flow	flow	flow	flow	flow	flow	extrusion	extrusion	extrusion	extrusion	extrusion	flow	extrusion	flow
Petrographical facies	Ank	alk B	Na-Bs	H	Na-H	H	H	M	M	M	M	M	M	M	Bn	Bn	Bn	Bn	Bn	Tr	Tr	Tr	Tr
SiO_2	43.38	46.58	45.83	47.47	46.62	49.48	49.71	50.73	51.91	52.68	53.00	52.60	54.25	53.66	59.20	59.20	55.36	58.42	60.82	65.87	66.23	65.28	63.72
TiO_2	2.61	2.47	2.71	2.67	2.75	2.56	2.28	2.13	2.20	1.96	2.02	1.98	1.70	1.91	1.11	1.17	1.47	1.25	0.88	0.41	0.44	0.41	0.38
Al_2O_3	13.10	15.14	15.03	16.17	17.13	15.23	15.38	17.22	16.80	16.78	16.94	16.70	17.50	16.84	17.49	15.69	18.39	17.18	16.98	12.78	12.92	13.49	14.09
Fe_2O_3t	12.79	12.72	11.89	11.38	10.98	12.50	12.29	10.26	9.92	9.87	9.27	9.01	8.28	8.81	5.93	8.79	7.34	6.57	5.80	7.12	7.59	6.86	6.96
MnO	0.17	0.17	0.17	0.18	0.18	0.17	0.18	0.18	0.16	0.17	0.15	0.15	0.16	0.15	0.12	0.30	0.14	0.14	0.12	0.22	0.24	0.16	0.19
MgO	11.04	8.51	6.94	5.55	3.85	6.03	5.56	2.88	3.26	3.68	3.58	3.20	2.31	3.14	1.87	1.16	1.81	1.44	0.93	0.11	0.11	0.13	0.00
CaO	10.67	8.19	9.94	9.15	9.30	9.17	7.97	6.70	6.53	5.89	5.17	5.71	5.26	5.26	2.82	3.58	3.49	3.57	2.61	0.59	0.57	0.52	0.15
Na_2O	2.66	2.67	3.24	3.83	4.47	3.71	3.78	4.98	4.89	5.06	4.84	5.40	5.57	5.87	5.97	5.04	5.62	6.38	6.46	6.73	6.48	6.63	6.57
K_2O	1.29	1.43	1.61	1.54	1.61	1.15	1.32	2.36	2.14	2.90	2.82	3.03	2.80	3.16	4.26	2.98	3.34	3.72	4.06	5.02	4.82	5.07	5.16
P_2O_5	0.61	0.62	0.65	0.77	0.88	0.49	0.44	0.76	0.70	0.68	0.52	0.63	0.63	0.60	0.28	0.36	0.54	0.41	0.26	0.04	0.06	0.05	0.03
LOI	1.40	1.47	1.64	0.91	1.87	-0.42	1.00	0.78	1.18	-0.02	1.77	1.19	1.14	0.19	0.86	1.65	2.11	-0.16	0.63	0.80	0.22	1.10	2.42
TOTAL	99.72	99.97	99.65	99.62	99.64	100.07	99.91	98.99	99.69	99.65	100.08	99.60	99.60	99.59	99.91	99.92	99.61	98.92	99.55	99.69	99.68	99.70	99.67
DI	24.37	31.88	33.80	39.33	42.20	38.37	40.67	54.49	54.80	57.92	59.10	60.84	63.73	63.82	76.82	68.09	69.48	75.75	79.93	80.89	81.11	82.51	83.90
V	251	192.2	213	183	192	207.1	175.3	108.8	122	112.6	103	114	71	108	204.6		43	33	13	0.0		0.0	
Cr	399	318.7	236	128	39.0	227.4	175.8	30.2	11.0	34.6	55.02	21.0	7.0	29.0	158.8	5.33	1.0	1.0	1.0	3.0	7.55	1.0	
Co	49.3	45.02	36.3	29.4	24.0	42.21	39.94	20.66	18.9	22.48	25.16	20.1	13.6	19.3	44.14	1.00	7.2	4.7	3.4	0.2	0.50	0.4	
Ni	241.0	222.5	113.0	73.0	19.0	95.52	106.3	29.23	13.0	39.69	49.64	28.0	9.0	29.0	107.0	4.99	1.0	2.0	2.0	1.0	6.49	1.0	
Cu	68.93	61.06	46.95	40.89	23.37	71.97	48.3	47.76	20.21	35.09	25.27	20.15	12.02	20.0	37.85	8.40	7.57	4.91	5.11	3.43	12.01	3.1	
Ga	20.32	23.84	23.4	24.33	23.1	25.04	23.09	27.91	26.76	24.73	26.54	25.19	26.9	25.69	23.62	27.86	29.42	28.04	29.62	40.11	38.38	41.32	41.00
Rb	35.00	32.91	52.00	36.00	35.00	30.15	32.99	67.55	58.00	88.87	80.11	112.00	80.00	93.00	32.45	71.18	88.00	105.00	124.00	168.00	171.6	151.00	161.00
Sr	661.0	564.5	790.0	1027.0	808.0	522.6	509.2	749.1	593.0	890.7	579.1	808.0	730.0	768.0	761.0	598.5	463.0	496.0	395.0	3.0	1.73	5.0	2.18
Y	23.30	48.29	26.70	30.10	31.80	28.44	30.75	39.39	34.70	29.60	25.62	29.70	36.10	29.70	25.32	45.69	64.00	41.80	49.70	37.80	28.23	28.00	19.31
Zr	201.0	314.6	243.0	282.0	244.0	271.0	258.4	526.0	401.0	568.8	537.3	562.0	488.0	600.0	282.3	461.3	586.0	548.0	615.0	1051.0	1155.0	994.0	1380.0
Nb	57.82	58.37	68.43	75.02	58.9	45.16	44.88	102.3	78.00	115.6	89.69	100.2	99.22	102.00	59.15	77.01	117.7	107.00	114.00	224.00	246.9	221.0	272.2
Ba	492.0	539.6	533.0	637.0	504.0	330.0	390.7	609.9	473.0	641.8	562.0	629.0	824.0	643.0	435.1	3460.0	955.0	952.0	1080.0	17.0	11.76	24.0	15.76
Hf	4.00	6.84	6.03	6.23	5.53	6.01	5.84	10.57	9.04	10.98	10.74	11.76	10.28	12.1	6.26	9.97	12.75	12.31	13.93	27.55	27.07	25.45	29.42
Ta	4.04	4.32	4.95	5.22	4.35	3.40	3.33	7.00	5.97	8.16	6.87	7.72	7.23	7.93	4.23	5.19	8.52	7.67	8.09	16.63	16.51	15.78	17.86
Pb	2.17	2.79	3.89	3.02	2.75	2.95	2.34	4.63	5.22	5.81	5.38	5.39	6.61	5.85	2.40	9.13	7.88	8.41	14.23	16.06	16.11	12.64	12.96
Th	4.60	4.84	6.77	6.87	4.40	4.23	4.07	9.69	8.89	12.42	12.22	11.18	10.83	11.77	4.58	9.78	13.38	13.88	15.99	28.45	28.4	26.38	31.54
U	1.30	1.28	2.27	1.70	1.18	1.23	1.06	2.667	2.44	3.39	3.31	3.84	2.97	3.41	1.07	1.79	1.96	4.01	4.67	6.38	4.12	6.06	4.92
La	40.05	58.87	61.17	68.12	49.28	31.24	40.93	71.21	57.30	76.13	65.33	73.61	77.39	74.74	44.56	85.26	164.00	86.68	98.38	95.00	82.29	103.00	89.08
Ce	77.90	92.85	118.00	135.00	103.00	62.06	70.58	139.3	114.00	145.6	120.8	138.00	151.00	138.00	88.16	166.8	156.00	167.00	187.00	185.00	146.50	112.00	36.26
Pr	8.83	14.31	12.90	14.67	11.54	7.623	9.16	15.97	13.10	15.83	13.67	14.95	16.90	14.99	10.96	20.13	31.03	18.08	19.41	21.88	17.39	23.73	22.72
Nd	37.00	59.54	50.4	57.68	46.99	31.54	37.33	61.7	51.26	56.95	50.55	56.47	64.31	54.57	44.26	78.79	121.00	71.13	76.00	79.02	60.67	88.37	74.67
Sm	7.26	12.00	10.29	10.49	9.54	7.41	8.05	11.98	10.47	10.04	9.41	9.81	11.78	9.80	9.10	14.74	19.69	13.37	13.91	15.15	11.11	17.28	13.52
Eu	2.62	4.404	3.38	3.76	3.04	2.57	2.73	3.69	3.17	3.03	2.86	3.11	3.77	2.99	3.05	7.54	6.18	3.91	3.65	1.44	1.04	1.85	1.24
Gd	6.58	10.67	8.41	8.75	7.75	7.04	6.98	9.93	9.09	7.88	7.59	8.11	9.45	8.15	7.16	11.77	16.78	10.72	11.64	11.37	7.86	11.82	7.14
Tb	0.88	1.53	1.19	1.19	1.19	1.05	1.06	1.49	1.28	1.10	1.06	1.13	1.37	1.13	1.03	1.72	2.30	1.51	1.71	1.86	1.21	1.78	1.16
Dy	4.59	8.24	6.28	6.40	6.42	5.76	5.72	7.86	7.21	5.92	5.44	6.44	7.19	6.16	5.34	9.21	12.14	8.12	9.48	10.02	6.68	8.87	5.94
Ho	0.89	1.47	1.30	1.24	1.28	1.03	1.02	1.39	1.39	1.00	0.91	1.19	1.45	1.17	0.89	1.64	2.39	1.66	1.95	2.05	1.16	1.55	0.91
Er	2.05	3.62	2.85	2.64	2.9	2.61	2.55	3.63	3.27	2.63	2.21	2.74	3.32	2.74	2.18	4.33	5.26	3.76	4.54	4.71	3.26	3.51	2.46
Tm	0.25	0.47	0.47	0.35	0.43	0.36	0.34	0.50	0.44	0.36	0.30	0.38	0.44	0.39	0.28	0.60	0.65	0.53	0.69	0.80	0.53	0.58	0.38
Yb	1.58	2.75	2.53	2.20	2.62	2.21	2.08	3.15	2.63	2.33	1.82	2.30	2.63	2.31	1.69	3.83	3.82	3.56	4.50	5.97	3.95	4.25	2.88
Lu	0.23	0.40	0.45	0.32	0.40	0.33	0.31	0.47	0.38	0.35	0.26	0.37	0.40	0.36	0.24	0.58	0.58	0.53	0.68	0.83	0.67	0.68	0.47

Undetermined relationships **Manengouba, stage 4**

Eboga	Elengoum	Elengoum	Eboga	Elengoum	Eboga	Ekom	Ekom	Ngol	Nzoh cone	Mkon	Njom	Manjo	Caldera	Djeu Seh	Etam Manjo	Passim - Ekoh	Caldera	SE Ndoungué	Manengouba vill	Melong	Melong	Ekambeng	Caldera
E slope	Nkongsamba	summit	E slope	Elengoum pike	SW caldera			NW Manjo		S Mouanguel	S Bangem		W floor	E Mbouroukou			W floor					E Bangem	NW Floor
LG3B	CT216	KNS1	LG3E	CT124	KEB26	K03	CT155	GO1	NZ7	MK3	NJ"	DB5	CT110	CT18	EM2	CT55	EB20	CT44	KCT1	KME2A	CT47	CT50i	KEB33
extrusion	flow	extrusion	extrusion	extrusion	extrusion	dome	dome	flow	flow	flow	flow	flow	flow	flow	flow	flow	flow	flow	flow	flow	flow	flow	flow
Tr	Tr	Tr	Tr	Tr	Tr	Rh	Rh	Ank	Na-Bs	Na-Bs	Na-Bs	Na-Bs	alk-B	Na-Bs	Na-Bs	Na-Bs	Bs	Bs	alk-B	H	H	H	H
65.89	65.77	65.80	65.33	64.37	68.27	67.58	71.36	44.84	43.32	43.67	44.41	44.42	48.07	46.06	44.64	44.91	47.92	47.50	46.38	47.38	47.77	47.35	49.30
0.41	0.41	0.35	0.41	0.35	0.21	0.42	0.23	3.01	3.29	3.43	3.10	3.25	1.75	3.10	3.14	3.24	2.41	1.63	2.84	2.50	2.52	2.91	2.53
13.63	14.17	13.41	15.75	16.91	15.30	13.96	12.48	13.93	14.76	14.42	14.21	14.99	12.48	15.17	15.01	15.17	13.72	16.83	14.67	14.53	15.28	15.90	14.39
6.65	6.14	6.22	4.44	3.95	4.27	5.47	3.94	13.47	14.46	14.64	14.16	14.15	12.76	13.32	14.07	13.52	12.41	11.25	13.53	13.30	12.48	12.62	12.06
0.18	0.18	0.33	0.12	0.07	0.115	0.16	0.05	0.17	0.20	0.20	0.19	0.18	0.18	0.20	0.20	0.17	0.16	0.17	0.20	0.19	0.17	0.16	0.17
0.04	0.14	0.03	0.13	0.25	0.07	0.04	0.00	9.72	7.74	8.26	8.67	7.84	10.63	7.15	7.65	7.55	9.41	6.15	7.34	7.91	7.21	6.92	7.57
0.44	0.71	0.39	0.60	0.48	0.46	0.54	0.13	9.69	10.4	10.01	9.93	9.55	8.33	9.61	9.48	9.28	8.80	10.77	9.10	9.09	9.12	8.56	8.68
6.46	6.10	5.43	7.24	7.18	6.22	6.49	4.78	3.21	3.48	3.41	3.39	3.71	3.19	3.40	3.79	3.57	3.36	3.47	3.48	3.68	3.78	3.69	3.66
4.89	4.86	4.89	5.23	5.28	4.99	4.68	5.26	1.18	1.38	1.45	1.53	1.59	0.90	1.30	1.63	1.71	1.22	2.08	1.28	1.33	1.44	1.56	1.44
0.04	0.04	0.03	0.06	0.09	0.04	0.06	0.00	0.53	0.86	0.7	0.66	0.70	0.28	0.66	0.71	0.63	0.47	0.51	0.75	0.65	0.60	0.61	0.48
1.09	0.77	2.34	0.36	1.00	0.13	0.29	1.59	-0.06	-0.23	-0.61	-0.51	-0.72	1.16	-0.04	-0.66	0.22	-0.16	-0.37	-0.28	-0.66	-0.41	-0.06	-0.08
99.72	99.29	99.22	99.67	99.93	100.08	99.69	99.82	99.69	99.66	99.58	99.74	99.66	99.73	99.93	99.66	99.97	99.72	99.99	99.29	99.90	99.96	100.22	100.20
83.99	85.50	86.17	88.13	90.48	91.25	86.65	91.20	29.12	29.42	29.67	30.35	32.63	33.16	33.20	33.46	33.83	34.48	34.76	34.72	35.50	36.96	37.65	38.74
0.0			0.0			4.0		256	244	251	260	265	159.9	228.2	260	253	198	306.8	202.6	205.1	199	204.6	200.5
1.0		11.12	2.0			10.37		283	197.3	221	219.88	140	400.7	165.8	159	146	348	54.04	200	295.8	227	158.8	266.7
0.2	0.31	0.41	0.3	0.44	0.30	0.3	0.25	49.0	44.3	47.1	47.06	46.6	57.8	45.29	45.1	49.2	45.1	39.85	43.59	47.1	43.6	44.14	42.21
1.0		8.11	5.0			4.0		202.0	134.0	178.0	169.0	121.0	288.2	119.0	120.0	124.0	238.00	33.89	136.7	183.6	152.00	107.00	173.9
2.68		11.97	4.22			5.19		52.5	66.79	111.0	74.01	53.68	45.23	49.79	53.96	52.5	66.7	128.2	53.75	78.54	45.4	37.85	72.5
37.44	36.23	35.3	32.09	34.44	37.58	35.63	38.60	21.53	21.43	22.4	21.24	23.79	18.31	23.00	24.91	24.2	21.00	22.10	21.69	24.70	25.50	23.62	22.86
143.00	143.2	109.4	128.00	107.9	273.0	125.46	200.4	28.00	34.00	27.82	42.00	41.00	22.00	28.1	42.00	43.9	29.00	48.92	27.95	32.46	34.40	32.45	35.97
4.0	4.7	3.41	9.0	23.69	3.61	3.0	6.20	599.0	854.0	779.0	725.0	788.0	372.4	748.3	767.0	957.0	473.0	1084.0	716.3	745.5	735.0	761.0	524.2
40.10	27.93	74.80	67.80	36.69	20.32	18.46	46.58	24.7	32.7	31.2	29.00	30.6	20.26	28.15	30.4	31.8	24.00	26.5	26.99	27.38	27.50	25.32	28.41
831.0	1062.0	846.1	729.0	791.7	1248.0	727.0	1361.0	236.0	278.0	249.0	280.0	325.0	193.2	252.0	330.0	351.0	238.0	204.1	241.8	317.9	318.0	282.3	285.8
175.00	195.00	147.4	149.0	130.1	313.5	129.78	217.6	50.66	66.97	64.99	68.18	75.54	29.36	60.55	77.78	80.00	42.65	50.44	57	58.09	59.8	59.15	47.88
237.0	15.76	39.96	716.0	832.0	12.68	577.12	21.63	367.0	482.8	431.0	425.92	476.0	274.7	443.2	488.0	524.0	374.0	586.8	443.1	399.8	406.0	435.1	448.4
21.16	23.11	17.49	17.56	16.97	30.37	19.00	29.45	5.1	6.00	5.79	6.00	6.7	4.44	5.75	7.9	7.79	5.13	4.52	5.48	6.87	7.08	6.26	6.19
12.50	13.49	9.20	10.57	9.06	22.16	10.94	14.96	3.56	4.86	4.48	5.13	5.36	2.21	4.37	6.04	5.41	3.04	3.41	4.17	4.18	4.42	4.23	3.45
12.99	13.49	12.60	11.92	9.51	13.90	3.93	3.77	2.32	2.74	2.66	2.72	3.18	1.38	3.17	4.7	2.88	2.93	5.94	3.04	2.82	2.87	2.40	2.78
21.24	22.86	16.76	19.18	16.04	44.83	15.61	31.37	3.90	4.78	2.62	5.61	5.65	2.83	4.90	7.16	5.71	3.24	7.12	5.051	4.85	5.31	4.58	4.15
3.69	3.64	3.55	8.48	4.85	7.49	1.24	1.80	1.11	1.19	0.78	1.53	1.60	0.78	1.20	3.49	1.34	0.81	2.03	1.24	1.32	1.42	1.07	1.06
108.00	77.09	112.5	138.00	147.1	86.70	27.90	21.96	37.19	46.40	37.78	45.82	54.73	22.29	50.12	57.44	61.80	31.54	53.53	48.05	44.63	44.90	44.56	37.37
85.00	125.6	223.2	253.00	146.8	123.30	62.59	27.5	79.00	93.00	84.14	90.00	114.00	45.13	98.25	117.00	123.00	64.25	100.60	95.28	91.72	93.10	88.16	72.71
27.51	16.69	24.43	27.48	34.74	20.36	8.29	4.786	9.32	12.13	10.42	10.79	13.15	5.41	11.77	13.54	14.10	7.48	11.85	11.14	11.30	11.60	10.96	8.70
102.5	58.03	91.29	100.4	117.5	62.54	32.00	16.96	37.63	49.00	43.31	48.18	51.96	22.35	45.67	57.51	55.40	31.46	45.97	43.67	45.89	47.20	44.26	34.97
19.54	10.72	17.94	18.43	21.24	10.93	6.00	4.04	7.70	9.50	9.27	7.98	9.92	5.16	9.21	12.18	10.40	6.81	8.88	8.60	9.33	9.42	9.10	7.42
3.39	1.13	2.78	3.15	4.39	0.32	1.70	0.47	2.48	3.13	2.97	2.67	3.04	1.83	2.94	3.80	3.53	2.30	2.64	2.85	3.07	3.24	3.05	2.53
14.02	7.71	15.38	15.51	13.95	6.24	4.86	4.76	6.33	8.22	7.70	7.46	7.95	5.03	7.98	9.96	9.15	5.70	7.04	7.42	7.88	8.11	7.16	6.86
2.03	1.22	2.43	2.36	2.14	1.07	0.74	1.10	0.91	1.21	1.11	1.05	1.13	0.74	1.12	1.47	1.18	0.89	0.99	1.05	1.12	1.16	1.03	1.02
10.52	6.69	13.63	12.98	10.93	5.83	4.14	8.11	4.81	6.91	6.15	5.89	6.05	4.19	5.95	7.87	6.55	4.95	5.21	5.60	5.85	5.72	5.34	5.62
2.02	1.16	2.55	2.74	1.66	0.95	0.73	1.65	0.97	1.21	1.06	1.07	1.13	0.75	1.03	1.54	1.14	0.98	0.92	0.97	1.00	1.07	0.89	1.01
4.35	3.14	6.97	6.47	4.26	2.75	2.07	4.83	1.96	2.74	2.72	2.39	2.51	1.90	2.59	3.32	2.71	2.07	2.37	2.48	2.45	2.38	2.18	2.57
0.67	0.49	0.98	0.97	0.63	0.47	0.34	0.74	0.22	0.34	0.36	0.34	0.27	0.25	0.34	0.54	0.38	0.29	0.33	0.33	0.33	0.34	0.28	0.34
4.39	3.59	6.01	6.66	4.29	3.70	2.59	4.96	1.52	2.22	2.16	2.18	1.91	1.59	2.11	3.02	2.14	1.85	2.13	2.03	1.92	2.00	1.69	2.09
0.65	0.58	0.88	0.92	0.66	0.60	0.44	0.75	0.20	0.35	0.35	0.31	0.22	0.23	0.30	0.52	0.30	0.25	0.32	0.30	0.28	0.284	0.24	0.31

NW-Bangem	Ekoh Nyabang	Ngol	Caldera Cone SE	SE Nkongsamba	Bayon Ndom	Ndipsi I E Bangem	Mboassoum	Ndom Nyabang	Manengolé NE Manjo	Manengolé	Caldera SE floor	Caldera Mboriko	Caldera SE floor	Caldera SE floor	Nkongsamba	N Nkongsamba Ossoua river	Caldera Mboriko	NW Nkongsamba	NE Enyandong	Moumekeng	Badjoungué S Eboga	Elom	Ndipsi II	Baré
CT104	EK1C	CT41	KCE2	SP5	CT28	CT53	CT108	ND1	CT37	CT38	KEB19c	EB6	EB16	KEB19	CT35	KOS7	EB14	EE4	CT52	KG3	MA3A	CT118	CT51	CT60
flow	flow	flow	flow	flow	flow	flow	flow	flow	flow	flow	flow	plug dome	flow	flow	flow	flow	plug dome	flow	flow	flow	flow	flow	flow	flow
H	H	H	H	H	H	H	H	H	H	H	H	H	H	H	H	M	M	M	M	M	M	M	M	M
46.70	45.68	47.80	48.14	48.85	49.14	49.79	50.10	46.66	48.64	48.98	52.07	52.63	51.47	51.37	48.84	50.74	50.83	48.99	51.03	49.34	51.38	51.82	52.97	54.10
3.05	3.09	3.15	2.62	2.42	2.70	2.41	2.42	3.10	2.46	2.51	2.29	2.43	2.05	1.83	2.58	2.13	2.22	2.55	2.17	2.45	2.23	2.02	2.06	1.77
17.01	16.07	17.55	15.43	15.45	17.10	15.84	16.67	16.45	17.40	17.60	15.97	17.37	16.8	16.13	17.25	17.97	16.39	16.83	17.32	17.14	17.40	16.98	17.07	16.44
10.87	13.04	12.30	13.65	11.26	11.89	12.00	11.62	12.83	10.73	10.52	11.12	9.50	10.14	9.44	11.07	9.87	8.99	11.18	9.39	10.69	9.80	9.62	9.30	9.39
0.16	0.19	0.15	0.21	0.16	0.18	0.17	0.15	0.16	0.22	0.19	0.17	0.12	0.14	0.17	0.16	0.20	0.11	0.16	0.22	0.17	0.13	0.16	0.17	0.22
4.24	5.28	5.29	5.99	5.89	4.46	5.52	4.41	4.90	4.41	4.37	5.18	3.36	4.27	4.63	4.69	2.84	2.96	4.21	2.83	3.91	3.59	4.20	3.67	2.11
8.99	7.95	7.08	7.95	8.07	8.38	7.80	7.56	7.43	8.27	8.20	7.33	8.19	7.77	7.07	6.95	7.21	7.86	6.93	7.20	6.73	6.39	5.65	5.48	5.71
3.44	3.67	3.72	4.04	3.89	4.00	3.96	4.01	4.26	4.74	4.62	4.32	4.71	4.68	4.37	4.66	4.51	4.71	5.47	4.76	5.58	4.99	4.57	5.49	5.24
1.84	2.09	1.59	1.99	1.42	1.43	1.45	1.41	2.00	1.77	1.78	1.76	1.50	1.77	1.93	2.48	1.79	1.80	2.48	2.32	2.56	2.31	3.07	3.12	2.55
0.81	0.79	0.53	0.70	0.56	0.64	0.48	0.48	0.80	0.71	0.75	0.50	0.46	0.64	0.63	0.76	0.92	0.48	0.83	0.67	0.79	0.66	0.58	0.63	0.65
2.88	1.98	0.77	-0.25	1.72	-0.01	0.49	1.06	1.02	0.63	0.46	0.13	-0.36	-0.09	1.76	0.57	1.96	3.32	-0.06	2.09	0.20	0.70	1.34	0.44	1.79
99.99	99.83	99.93	100.47	99.69	99.91	99.91	99.89	99.61	99.98	99.98	100.84	99.91	99.64	99.33	100.01	100.14	99.67	99.57	100.00	99.56	99.58	100.01	100.40	99.97
40.05	40.63	41.68	42.00	42.23	42.22	42.78	43.21	44.13	45.62	45.78	47.08	49.00	49.12	49.99	49.32	50.10	51.44	52.56	53.37	54.08	54.57	56.33	60.62	61.03
174.6	205	184.2	159	183	162.7	203	159.3	179	144.9	142.1	158.8	168	142	112	140	97.5	160	159	111	133	131	122.8	110.3	57.17
20.9	46	31.46	119	153	45.05	155	48.08	28	51.31	49.33	135.1	51.83	110	110.7	20.52	8.99	46	24	24.3	32	37	47.15	17.89	10.56
25.97	33.8	37.38	35.9	32.8	30.55	39.8	31.78	32.8	28.03	24.87	32.61	22.77	24.4	23.96	28.01	19.4	20.4	25.9	19.9	23.6	23.9	25.68	21.77	10.88
17.12	57.00	48.36	88.8	96.00	37.9	106.00	49.83	38.00	35.32	30.92	98.14	45.00	61.00	68.79	32.43	9.65	45.00	29.00	11.5	35.00	44.00	47.48	25.13	7.70
23.09	49.52	27.93	62.3	51.4	38.53	40.3	38.15	43.14	27.95	27.09	41.34	66.21	31.39	38.35	29.29	16.84	57.11	25.44	19.7	24.41	23.81	25	18.55	10.81
21.99	25.24	23.03	21.4	24.36	24.70	26.30	24.05	24.52	24.22	24.59	24.07	25.31	26.32	25.08	25.02	26.7	26.00	25.26	26.70	25.60	27.41	24.59	24.22	27.21
56.27	54.00	30.13	64.7	34.00	30.59	38.10	30.87	52.00	41.32	38.46	33.48	37.42	42.00	50.89	59.72	44.00	55.00	65.00	65.40	71.00	62.00	73.65	82.42	55.45
989.1	1188.0	904.5	774.0	562.0	598.9	569.0	513.4	1027.0	1077.0	1063.0	453.2	528.0	644.0	616.3	1125.0	937.4	526.0	1075.0	963.0	1170.0	968.0	806.1	821.3	668.9
28.94	35.80	28.37	30.60	26.8	32.63	32.5	27.25	33.7	30.93	30.82	27.99	27.33	50.1	31.61	33.7	37.08	28.5	32.7	35.4	35.3	31.2	28.91	29.85	43.52
335.5	437.0	300.3	383.0	277.0	252.0	308.0	269.8	393.0	303.1	306.9	365.3	317.0	346.0	396.7	535.8	312.2	356.0	466.0	452.0	522.0	449.0	567.0	618.5	403.7
64.39	100.48	63.64	79.9	52.31	50.38	56.9	47.37	86.33	82.14	83.61	57.19	50.71	66.76	69.29	96.4	79.6	59.42	101.56	102	109.04	85.13	95.24	98.71	78.96
472.2	655.0	472.4	469.0	414.0	412.7	454.0	367.7	591.0	710.6	710.1	450.9	419.46	477.0	464.5	663.9	913.1	473.0	680.0	853.0	740.0	793.0	629.4	624.1	1061.0
7.17	9.00	6.58	8.19	6.24	5.65	7.10	6.26	8.16	6.57	6.63	7.67	7.00	7.86	8.18	10.47	6.87	7.59	9.46	9.92	10.71	9.55	11.36	11.47	8.80
4.73	7.06	4.62	6.39	3.76	3.81	3.94	3.63	6.23	5.74	5.85	4.18	3.78	4.76	4.99	6.82	5.52	4.22	7.32	7.4	7.85	6.19	7.41	7.516	5.54
3.35	3.98	2.98	4.24	1.52	2.23	2.42	2.15	3.51	4.01	4.18	3.09	2.15	3.19	3.98	3.92	4.61	2.86	3.87	6.22	4.46	4.35	4.97	5.31	5.85
5.53	7.27	4.85	9.71	4.26	4.07	5.16	4.86	7.17	7.47	7.58	5.74	4.51	6.28	7.28	6.85	8.04	5.52	7.95	10.30	9.00	8.40	11.00	10.80	7.69
1.45	1.88	1.42	2.63	1.3	0.95	1.41	1.30	2.12	2.15	1.84	1.12	0.91	0.91	2.12	1.80	1.84	1.86	2.16	2.92	2.64	2.25	2.93	3.01	1.84
52.65	77.67	47.11	53.00	40.48	43.65	46.6	38.37	68.55	74.48	75.38	42.78	38.36	61.92	51.44	72.83	75.74	42.87	80.96	79.40	82.55	72.54	70.00	72.66	69.20
111.70	158.00	91.80	102.00	83.00	82.89	86.00	75.56	138.00	144.00	146.10	85.38	74.39	101.00	101.4	146.4	147.9	83.71	159.00	152.00	165.00	131.00	135.10	138.10	141.00
13.38	18.25	11.22	11.70	9.59	10.55	10.50	9.13	15.33	16.12	16.30	9.77	8.08	12.65	11.83	16.81	16.87	9.34	17.38	18.00	18.26	14.83	14.69	15.03	16.87
53.13	69.00	44.40	44.90	39.70	42.88	43.90	36.96	59.58	59.92	60.77	37.44	34.00	51.25	46.27	63.92	65.12	36.89	65.09	71.70	70.25	58.69	53.54	55.33	67.21
10.17	13.32	8.87	9.06	8.53	9.40	9.11	8.06	11.07	10.75	10.98	7.89	7.32	10.33	9.28	11.90	12.14	7.83	11.17	13.3	12.64	11.46	9.76	10.10	13.54
3.14	3.90	3.01	2.83	2.81	3.24	3.18	2.74	3.51	3.87	3.95	2.58	2.50	3.42	2.94	3.73	4.82	2.52	3.47	4.33	3.78	3.72	3.03	3.16	5.12
8.21	11.28	7.62	7.78	7.13	8.72	8.32	7.44	9.12	8.90	9.04	7.20	7.20	9.42	7.97	9.47	10.36	6.71	9.34	10.20	9.99	9.00	7.92	7.40	12.16
1.13	1.40	1.09	1.13	1.03	1.24	1.09	1.07	1.26	1.22	1.25	1.05	1.05	1.14	1.15	1.32	1.45	1.07	1.27	1.48	1.39	1.22	1.12	1.12	1.60
6.01	7.12	5.82	6.18	5.74	6.66	6.20	5.82	6.54	6.45	6.49	5.90	5.33	7.84	6.35	6.86	7.64	5.71	6.55	7.30	7.33	6.24	6.00	5.96	8.69
1.01	1.25	1.03	1.08	1.08	1.16	1.13	1.02	1.24	1.11	1.11	1.02	1.03	1.64	1.11	1.17	1.33	1.13	1.22	1.34	1.40	1.15	1.05	1.02	1.56
2.66	3.30	2.63	2.88	2.27	3.04	2.66	2.54	2.66	2.79	2.86	2.64	2.68	3.65	2.88	2.98	3.36	2.45	2.61	3.42	3.02	2.59	2.71	2.70	4.02
0.36	0.4	0.35	0.41	0.31	0.41	0.41	0.33	0.29	0.37	0.37	0.37	0.34	0.51	0.39	0.40	0.45	0.38	0.29	0.45	0.35	0.34	0.38	0.38	0.55
2.25	2.64	2.20	2.60	1.93	2.47	2.23	2.06	2.24	2.22	2.26	2.28	1.92	3.03	2.54	2.49	2.75	2.29	2.15	2.69	2.42	2.05	2.41	2.40	3.36
0.33	0.36	0.32	0.40	0.28	0.36	0.34	0.30	0.27	0.32	0.33	0.34	0.31	0.47	0.38	0.36	0.40	0.35	0.27	0.41	0.31	0.31	0.36	0.36	0.50

				Pre-Manengouba lavas							
				Eastern old volcanic basement				North-western graben edges			
Baré	Nzoh substratum	NW Manjo Cone 749	NW Bangem	Nkongsamba	Baressoumtou	Nkongsamba	S Nkongsamba	Bakossi NW Bangem	Bakossi W Bangem	Bakossi NW Bangem	Ekomane Essom pike
CT61	NZ8	CT42	CT105	CT30	KBT5	CT33	PL5	CT103	CT14	CT101	CT107
flow	flow	flow	dome	flow	flow	flow	flow	extrusion	extrusion	extrusion	extrusion
M	M	M	Tr-Ph	H	H	M	M	Ph	Ph	Ph	Tr
54.10	53.18	53.78	60.72	47.86	48.44	51.95	53.41	54.76	54.40	53.67	64.65
1.65	1.58	1.86	1.08	2.85	2.33	1.96	1.95	0.20	0.18	0.19	0.40
16.17	17.88	17.27	17.61	16.92	16.36	17.77	17.82	20.07	20.51	20.54	15.68
9.49	8.32	8.47	3.75	11.94	13.85	9.37	8.81	4.33	3.37	3.34	3.36
0.22	0.15	0.15	0.07	0.17	0.22	0.18	0.17	0.22	0.21	0.21	0.21
1.78	2.59	3.35	1.47	5.14	3.23	3.22	3.06	0.31	0.23	0.38	0.42
5.59	5.45	4.95	3.09	7.41	6.95	6.20	6.65	1.09	0.8	0.95	1.26
5.22	5.66	5.09	6.72	4.14	4.42	4.76	5.41	9.69	10.14	8.67	4.77
2.70	2.87	3.45	4.85	2.13	1.82	2.12	2.21	5.97	5.53	5.69	5.96
0.57	0.71	0.55	0.31	0.82	1.04	0.57	0.64	0.07	0.07	0.06	0.08
2.49	1.14	1.06	0.28	0.61	1.66	1.93	-0.13	4.12	4.46	6.14	2.20
99.98	99.53	99.98	99.95	99.99	100.32	100.03	100.00	100.83	99.9	99.84	98.99
62.21	62.61	62.66	82.50	44.83	47.97	54.29	56.96	86.94	89.56	90.65	91.70
49.2	79	108.6	56.18	148	85.53	92.83	101	5.743	4.695	6.312	2.29
10.85	12	20.04	23.05	23.76	15.93	38.18	37				
9.35	14.9	19.41	7.82	30.79	24.92	19.75	15.4	0.978	0.86	1.08	0.862
6.84	15.00	25.25	14.12	36.92	15.11	23.61	23.00				
8.96	18.24	15.41	8.553	24.41	30.9	18.84	21.42				
25.9	26.71	25.47	25.67	24.25	23.00	25.32	25.99	40.85	39.54	40.18	29.31
58.20	78.00	101.30	143.50	55.32	37.05	44.42	46.00	254.1	259.5	209.7	95.99
613.0	1137.0	764.0	417.3	1099.0	900.2	692.0	726.0	33.80	32.15	36.52	115.6
41.43	33.20	30.03	50.39	33.69	33.91	35.50	34.70	26.20	26.36	26.54	48.24
399.9	537.0	587.3	684.3	494.1	350.3	306.0	301.0	1001.0	1040.0	1014.0	831.3
75.73	106.85	112.2	122.6	92.12	74.48	76.71	79.24	108.00	107.20	110.30	98.77
1147.0	830.0	681.5	544.3	634.2	526.2	1739.0	2038.0	16.73	15.3	54.7	935.6
9.02	11.04	12.21	14.23	9.93	7.68	6.83	6.36	16.24	16.55	16.15	16.95
5.48	8.05	9.17	10.87	6.50	5.28	5.30	5.3	2.59	2.621	2.62	6.95
6.02	5.00	5.55	8.12	3.46	3.41	3.34	4.71	29.61	29.5	29.49	13.60
7.97	10.15	14.88	22.98	6.25	5.83	8.10	8.73	28.77	28.09	28.01	13.21
1.89	3.09	4.03	6.38	1.64	1.59	1.65	2.45	9.06	8.60	8.98	3.22
68.95	89.26	78.96	105.00	69.64	58.99	72.96	72.16	81.00	82.33	81.75	100.10
140.80	168.00	145.6	136.8	142.00	121.20	134.7	143.00	102.4	101.00	103.20	200.40
16.63	17.73	16.32	17.55	16.61	14.4	15.77	15.54	7.41	7.55	7.49	22.56
66.44	65.20	58.06	61.67	63.77	56.94	58.84	59.30	19.12	19.30	19.49	81.18
13.41	11.18	10.40	10.81	12.04	11.05	11.14	10.43	2.78	2.79	2.80	14.13
5.14	3.53	2.94	2.51	3.75	3.52	5.19	5.04	0.73	0.75	0.74	2.62
11.74	9.22	7.95	9.75	9.87	9.27	9.77	8.76	2.70	2.68	2.81	10.94
1.56	1.28	1.16	1.44	1.35	1.29	1.36	1.20	0.48	0.47	0.47	1.66
8.48	6.65	6.18	8.08	7.02	6.94	7.25	6.51	3.20	3.26	3.20	9.36
1.53	1.28	1.06	1.53	1.18	1.19	1.27	1.21	0.76	0.76	0.75	1.72
3.95	2.85	2.79	4.27	3.04	3.11	3.33	2.56	2.60	2.66	2.56	4.89
0.55	0.36	0.40	0.62	0.39	0.42	0.44	0.28	0.46	0.47	0.46	0.72
3.35	2.51	2.59	4.20	2.46	2.67	2.75	2.12	3.43	3.54	3.47	4.82
0.49	0.34	0.39	0.66	0.35	0.40	0.40	0.23	0.54	0.56	0.54	0.76